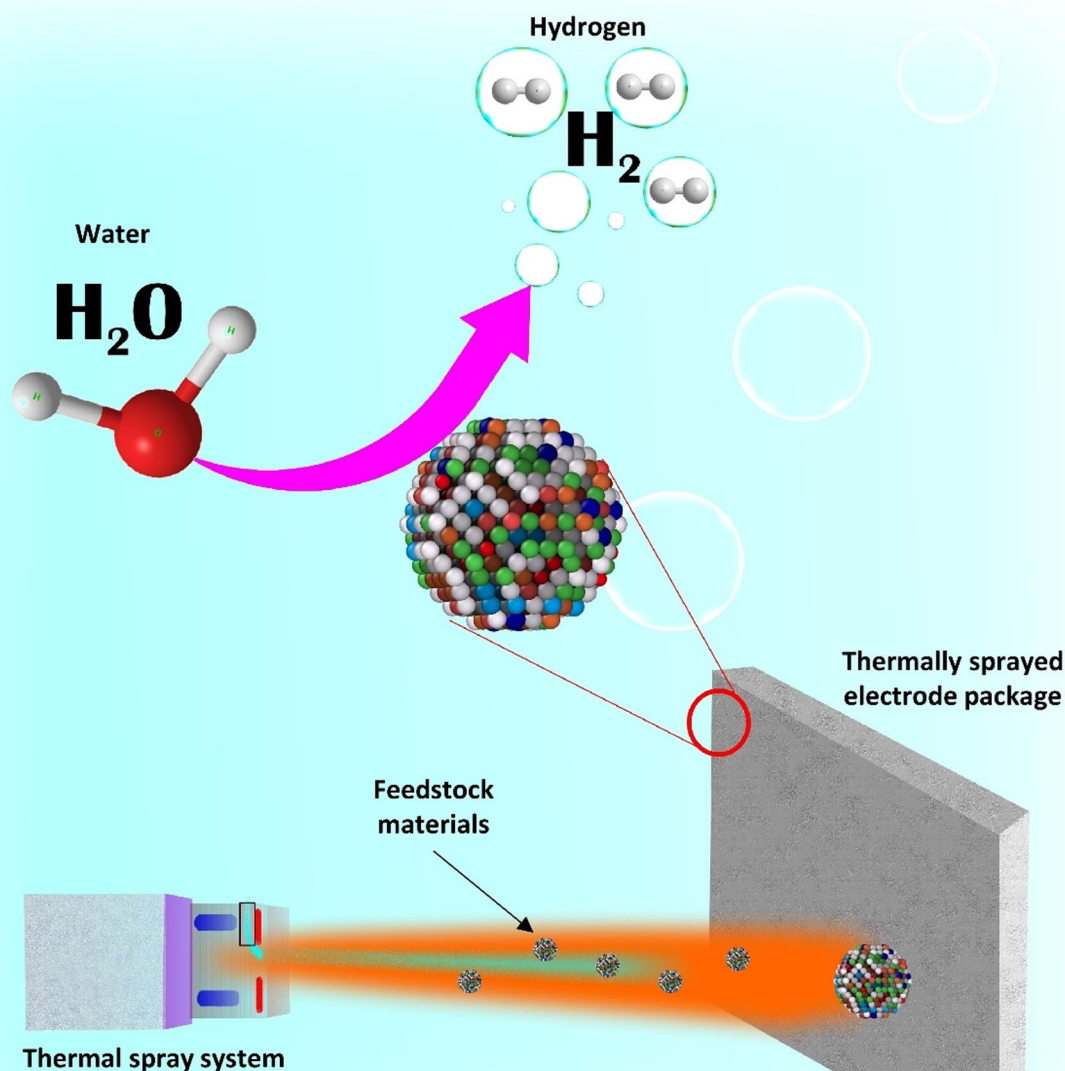


# Application of Thermal Spray Coatings in Electrolysers for Hydrogen Production: Advances, Challenges, and Opportunities

Nadimul Haque Faisal,<sup>\*,[a]</sup> Anil Prathuru,<sup>[a]</sup> Rehan Ahmed,<sup>[b]</sup> Vinooth Rajendran,<sup>[a]</sup> Mamdud Hossain,<sup>[a]</sup> Viswanathan Venkatachalapathy,<sup>[c]</sup> Nirmal Kumar Katiyar,<sup>[c]</sup> Jing Li,<sup>[d]</sup> Yuheng Liu,<sup>[d]</sup> Qiong Cai,<sup>[d]</sup> Bahman Amini Horri,<sup>[d]</sup> Dhinesh Thanganadar,<sup>[e]</sup> Gurpreet Singh Sodhi,<sup>[e]</sup> Kumar Patchigolla,<sup>[e]</sup> Carlos Fernandez,<sup>[f]</sup> Shrikant Joshi,<sup>[g]</sup> Sivakumar Govindarajan,<sup>[h]</sup> Victoria Kurushina,<sup>[a]</sup> Sai Katikaneni,<sup>[i]</sup> and Saurav Goel<sup>[c, j, k]</sup>



**Thermal spray coatings of critical and vital constituents (as catalysts (anode/cathode), solid electrolyte, and transport layer, including corrosion-prone parts such as bipolar plates**

**Abstract:** Thermal spray coatings have the advantage of providing thick and functional coatings from a range of engineering materials. The associated coating processes provide good control of coating thickness, morphology, microstructure, pore size and porosity, and residual strain in the coatings through selection of suitable process parameters for any coating material of interest. This review consolidates scarce literature on thermally sprayed components which are critical and vital constituents (e.g., catalysts (anode/cathode), solid electrolyte, and transport layer, including corrosion-prone parts such as bipolar plates) of the water splitting electrolysis process for hydrogen production. The research shows that there is a gap in thermally sprayed feedstock

material selection strategy as well as in addressing modelling needs that can be crucial to advancing applications exploiting their catalytic and corrosion-resistant properties to split water for hydrogen production. Due to readily scalable production enabled by thermal spray techniques, this manufacturing route bears potential to dominate the sustainable electrolyser technologies in the future. While the well-established thermal spray coating variants may have certain limitations in the manner they are currently practiced, deployment of both conventional and novel thermal spray approaches (suspension, solution, hybrid) is clearly promising for targeted development of electrolysers.

## 1. Introduction

The continually evolving hydrogen generation sector is expected to be a 160 billion USD market by 2026.<sup>[1]</sup> Rapid advances in this critical area of energy generation are enabled by the commitment of various governments (COP26 agreement) aiming to achieve net-zero emissions in view of the issue of climate change, the world is facing today.<sup>[2]</sup> As per a recent

report by the International Energy Agency (IEA),<sup>[3]</sup> there has been a significant expansion in the number of projects and installed electrolyser capacity (from < 1 MW in 2010 to more than 25 MW in 2019). Also, there has been a significant and steady increase in project sizes from < 0.5 MW in the early 2010s to 6 MW in 2017–19, with much larger 10 MW (in Japan) and 20-MW (in Canada) projects also currently under construction. Many other worldwide announcements targeting to develop hundreds of MWs have recently been reported.<sup>[4]</sup>

Overcoming current challenges related to production (as well as transportation and storage) are key to future rapid expansion in hydrogen value chain. As shown in Figure 1, there are seven major types of water-based electrolyser technologies that can be used for hydrogen production: (i) proton exchange membrane electrolysis (PEME), (ii) anion exchange membrane electrolysis (AEME), (iii) alkaline water electrolysis (AWE), (iv) solid oxide water electrolysis (SOWE), (v) thermochemical water splitting (TWS), (vi) photolysis water splitting (PWS), and (vii) photoelectrochemical water splitting (PEC). Generally, configuration of electrolysers contains a catalyst and transport layers. To accurately assess the suitability of any catalyst, transport layer, and housing (in electrolyser) for hydrogen production, innovation in materials and manufacturing routes for its production is vital. There is a growing pressure of not to rely only on traditional materials and methods to manufacture catalysts and electrolyser housings which offers new opportunities to investigate agile alternatives for exploring the electrode space to maximise conductivity while minimising the corrosive environment of various components within the electrolyser. Criticality assessment has been recently proposed<sup>[5]</sup> to identify materials in water electrolysers keeping in view the possible future supply constraints.

Electrodeposition, thermal decomposition, electroless plating, pressing, and sintering are some of the traditional catalyst manufacturing routes for electrolysers. However, due to considerable disadvantages associated with such traditional routes (e.g., low mechanical stability, time-consuming processes, undesired decomposition reaction, phase transformations, etc.), alternative manufacturing routes for electrolysers involving coatings offers promise on the scale of a cost-effectiveness and large-area scalability. Various coating manufacturing methods,

- [a] Prof. N. H. Faisal, Dr. A. Prathuru, V. Rajendran, Prof. M. Hossain, Dr. V. Kurushina  
School of Engineering, Robert Gordon University, Garthdee Road, Aberdeen, AB10 7GJ (UK)  
E-mail: N.H.Faisal@rgu.ac.uk
- [b] Dr. R. Ahmed  
School of Engineering and Physical Sciences, Heriot-Watt University, Edinburgh, EH14 4AS (UK)
- [c] Dr. V. Venkatachalapathy, Dr. N. K. Katiyar, Prof. S. Goel  
School of Engineering, London South Bank University, 103 Borough Road, London, SE1 0AA (UK)
- [d] J. Li, Y. Liu, Dr. Q. Cai, Dr. B. A. Horri  
Department of Chemical & Process Engineering, University of Surrey, Guildford, GU2 7XH (UK)
- [e] Dr. D. Thanganadar, Dr. G. S. Sodhi, Dr. K. Patchigolla  
School of Water, Energy and Environment, Cranfield University, Cranfield, MK43 0AL (UK)
- [f] Dr. C. Fernandez  
School of Pharmacy and Life Sciences, Robert Gordon University, Garthdee Road, Aberdeen, AB10 7GJ (UK)
- [g] Prof. S. Joshi  
Department of Engineering Science, University West, Trollhättan, 46186 (Sweden)
- [h] Dr. S. Govindarajan  
Centre for Engineered Coatings, International Advanced Research Centre for Powder Metallurgy and New Materials, Balapur, Hyderabad 500 005, Telangana (India)
- [i] Dr. S. Katikaneni  
Research and Development Centre, Saudi Aramco, Dhahran, 31311 (Saudi Arabia)
- [j] Prof. S. Goel  
Department of Mechanical Engineering, Indian Institute of Technology Guwahati, Guwahati, 781039 (India)
- [k] Prof. S. Goel  
Department of Mechanical Engineering, University of Petroleum and Energy Studies, Dehradun, 248007 (India)

© 2022 The Authors. ChemNanoMat published by Wiley-VCH GmbH. This is an open access article under the terms of the Creative Commons Attribution License, which permits use, distribution and reproduction in any medium, provided the original work is properly cited.

Nadimul Haque Faisal (PhD, CEng, MIMechE, MIMMM, FHEA) is a Professor of Surface Engineering & Micromechanics at Robert Gordon University. His interest includes micromechanical behaviour analysis of thermal spray coatings & thin films, metamaterial manufacturing using thermal spray coating techniques, sensor based instrumented mechanical testing, and acoustic emission (AE) sensor-based condition monitoring. He has over 80 peer-reviewed journals, 1 US Patent, and 4 book chapters, and over 50 conference publications. He is member of Royal Society of Edinburgh's Young Academy of Scotland, EPSRC peer review college member, and member of UK's Metamaterials Network. Total research and commercial funding obtained is over £1.25 M (as PI/Co-I). He is Principal Investigator of recently funded EPSRC grant 'METASIS' (EP/W033178/1).



Dr Anil Prathuru is a lecturer in the School of Engineering, Robert Gordon University, an early career researcher with experience in thermal spray coating development and characterisation. Before joining RGU, he worked as a mechanical engineer for EC-OG, Aberdeen, a subsea renewables company. His research interests include thermal spray coatings for energy harvesting, hydrogen energy and remote sensing applications, application of machine learning in material development. He also worked on the development of structural health monitoring based on NDT techniques and associated data processing methods. He has worked on several commercial projects related to early-stage technology development as research projects on the digitalisation of material development.



Dr Rehan Ahmed is the Associate Director of Research and Senior Programme Director for Mechanical Engineering at Heriot-Watt University. He is an internationally leading expert on surface engineering, mechanics, materials, and manufacturing and has published more than 100 refereed research papers. His research has led to patents in the design of orthopaedic implants and Solid Oxide Fuel Cells. The former patent led to an SME established in Scotland. He has successfully secured more than twenty competitive research grants with value in excess of £2.2 million from Industry and Research Councils. He is a member of the EPSRC Peer-Review college and has been the Guest Editor for special issues in the Journal of Thermal Spray Technology.



Mr Vinooth Rajendran is a PhD research student working on the research title of Nanowire-based hybrid sensors at the pipe-insulation interface for corrosion under insulation (CUI) monitoring and analysis at Robert Gordon University, Aberdeen, UK. He obtained a Master's (Materials science and engineering) and Bachelor's (Chemical and Electrochemical Engineering) from Queen's University Belfast, UK and CSIR – Central Electrochemical Research Institute, Karaikudi, India, respectively. He has experience in the Oil and Gas industry as a Cathodic protection engineer for four years and a member of the Institute of Corrosion. He is currently working as a part of various teaching/research assistantships at Robert Gordon University.



Mamdud Hossain, SFHEA, CEng, IMechE is a Professor of Future Energy Technology at Robert Gordon University. His research interests include applying computational modelling techniques to solve some of the most challenging and interesting problems related to wind energy, hydrogen fuel cell and electrolyser. He has secured funding to explore complex flows relevant to Wind Energy and Hydrogen from EPSRC, Oil and Gas Technology Centre (OGIC), net Zero Technology Centre (NZTC), Scottish Funding Council, Innovate UK and the Carnegie Trust. He has supervised 15 PhD students to completion and two postdoctoral researchers. He has published 29 journal articles, 32 conference articles and 5 book chapters. He is a Science Board member of EPSRC Hydrogen and Fuel Cell Supergen Hub, a member of EPSRC Reviewer College and an Academic Adviser to the Commonwealth Scholarship Commission and a member of board of directors of Energy Technology Partnership.



Dr Viswanathan Venkatachalapathy (Vish Venky) (PDRA, LSBU) is a materials Science graduate with a PhD in Plasma Processing for retention of nanostructures. Prior to joining LSBU, Vish has worked for the global conglomerate of General Electric and has developed Thermal spray parameters and Robot programs for Coating the Industrial Gas turbine and Land & Marine Engine Components. He is currently a post-doctoral research fellow at LSBU working on the EPSRC exploratory the future scheme project COATIN (EP/T024607/1) with Dr Goel. He has just migrated from Singapore to the UK on a Global talent VISA and will bring 15 years of top tier industrial experience in GE to perform the thermal spray experiments desired by this project. Vish has authored several journal publications and book chapters on thermal spray and bulk nano material processing. His current interests are material productivity, hybridization and digitization of processes involving thermal spray. Vish manages the thermal spray facility at LSBU working with several collaborators to obtain digital data. Scope includes hands on equipment operation and other logistics of lab day to day operations. He is also currently serving as a guest editor for a special issue titled "Newer Paradigm in Advanced Material Characterization".



Dr Nirmal Kumar Katiyar is a Newton International Post- Doctoral Fellow at London South Bank University, London, awarded by Royal society UK. He received his PhD in Materials Science and Engineering from Indian Institute of Technology Kanpur, Kanpur India. His Interest focused on nanomaterials preparation, characterization, and their functional applications, thermal spray coating, cryo-ball milling, High entropy alloy and catalysis. His devotion is towards development of nature inspired materials for eco-friendly sustainable development.





Prof Saurav Goel (FHEA, FIMMM) is a Professor of Manufacturing at London South Bank University with visiting appointments at various Universities in India, China and the UK. He is an Early Career Forum member in Manufacturing Research appointed by the UK's apex funding council EPSRC. His research interest is mainly in the direction of Sustainable precision manufacturing of free-form surfaces and using advanced simulation and digital tools to understand underlying mechanisms. He is serving as an Associate Editor for four International Journals (*Journal of Advanced Manufacturing Systems*, *Journal of Manufacturing Processes*, *BioMaterials and Polymers Horizons* and *Nanofabrication*). He has authored 100+ journal papers in various top-tier International Journals.



Jing Li received her master's degree from Chongqing University, Chongqing, China, in 2018. She is currently a PhD candidate at the chemical engineering department, University of Surrey, Guildford, U.K. Her current research interests focus on the high-performance of electrolytes for solid oxide electrolyser cells (SOEC) and Low-temperature solid oxide fuel cells (LT-SOFC).



Yuheng Liu received his master degree from the Wuhan University of Technology in 2019. He is currently working toward the PhD degree in the Department of Chemical and Process Engineering from the University of Surrey. His current research focuses on developing new solid oxide electrolysis cells for clean hydrogen generation.



Dr Qiong Cai is a Fellow of the Royal Society of Chemistry and an Associate Professor in Chemical Engineering at the University of Surrey, with 18 years' experience in multi-scale materials design for energy conversion and storage applications. Her research has been funded by UKRI EPSRC, Faraday Institution, H2FC SUPERGEN Hub, The Royal Society, and industry. Currently she leads a group of 12 researchers working on multi-scale materials design for various electrochemical energy technologies including fuel cells, hydrogen electrolyzers, and batteries, using both computational and experimental approaches. Her research has been published in over 100 peer-reviewed papers in top journals.



Dr Bahman Amini Horri is a Senior Lecturer of Chemical Engineering and the leader of the MSc programmes at the University of Surrey. He coordinates the research studies in green hydrogen, solid oxide fuel cells and electrolyzers (SOFCs/SOECs), and energy materials, holding 5 US/European patents, 50+ papers in top-tiered journals, five book chapters, and 30+ presentations in national and international conferences (most of them as an invited speaker). He received his PhD in Chemical Engineering from Monash University in 2012 (Australia). The national and international communities have recognised his research in hydrogen and fuel cell with multiple awards, including the "Leverhulme Trust Fellowship Award" (2021), IAAM Lecture Award (2020, Sweden), Innovation Award in Emerging Technologies (2018, UK), Postgraduate Publication Award (2012, Australia), FEIPRS award (2009, Australia), MGS Award (2008, Australia).



Dr Dhinesh Thanganadar is an academic fellow at Cranfield University, UK. He received his PhD from Cranfield University, UK where he investigated the performance and integration challenges of advanced power generation cycles with thermal storage and different heat sources. He has obtained Erasmus+ mobility grant and UKCCSRC early career researcher collaboration award during his PhD which facilitated him to visit Politecnico Di Bari, Italy and EPFL, Switzerland, respectively. Prior to joining PhD, he has gained eight years of industrial experience in the power generation sector including coal-fired, combined cycle and first-of-a-kind concentrated solar thermal power demonstration plants as a performance engineer. His research interest is numerical modelling and optimisation of advanced low-carbon energy systems for realising NetZero.



Dr Gurpreet Singh Sodhi is a Post-Doctoral Research Fellow at Cranfield University, Bedford, UK. He received his PhD in Thermal and Fluid Sciences from Indian Institute of Technology Guwahati, Assam, India. His interests are focused on solar thermal technologies such as solar thermal storage using phase change materials and other low carbon technologies. He was also awarded with visiting researcher fellowships such as Queen Elizabeth Advanced Scholar and MITACS Graduate Research Award to visit Simon Fraser University, Canada, where he worked on the material characterization of PCM-Expanded Graphite composites focused on electronic thermal management technology.





Dr Kumar Patchigolla is a Reader in Low Carbon Energy Systems. His research interests are in the science surrounding the wide range of application areas for the cost-effective and reliable energy systems to balance renewables and other low carbon technologies, to address the carbon targets, and to help improve the energy efficiency of dispatchable power plants. He performs experimental, theoretical and thermodynamics research into many aspects of energy systems. More recently he has been applying his knowledge in energy storage and heat recovery for these systems. Total research and commercial funding secured over £12 M from EU, EPSRC, I-UK and industry and has published 69 papers and one book.



Dr Carlos Fernandez is a Senior Lecturer in Analytical Biochemistry at Robert Gordon University, Aberdeen, UK. CF has published over 150 ( $h=26$  Scopus, 2525 Citations Scopus) peer review articles in Analytical Chemistry (Electrochemistry) and Materials Chemistry and 20 peer review conference manuscripts. His research interests focus on the use of Materials Chemistry for Energy Storage Devices and Battery Applications, and also concentrate on the utilisation of voltammetric techniques in Analytical Chemistry as an electrochemical sensor. CF has successfully secured as principal or co-investigator from a variety of organisations, including Oil and Gas Innovation Centre, Standard Voucher Scheme (Scottish Funding Council/Interface), Analytical Chemistry Trust Fund, PhD studentship and Game Changers in Collaboration with NNL (National Nuclear Laboratory) and Royal Society of Edinburgh. He holds membership of several professional bodies including The Institute of Physics (MIInstP), Royal Society of Chemistry (MRSC) and Electrochemical Society (MECS) and Fellow of The Royal Geographical Society (FRGS). CF is also Chartered in Chemistry (CChem), a Chartered Scientist (CCci) and a Fellow of The Higher Education Academy (FHEA).



Shrikant Joshi is a Professor in the Department of Engineering Science at University West, Sweden with nearly 30 years of experience in areas spanning Surface Engineering, Laser Materials Processing and now also Additive Manufacturing. He is a Chemical Engineer by academic training, having obtained his MS and PhD degrees from the Rensselaer Polytechnic Institute and University of Idaho, respectively, in USA. Prior to moving to Sweden, he has had long stints as a Scientist at a couple of premier federally funded materials' research laboratories in India. His work has led to many industrial applications, over a dozen patent submissions and more than 200 publications in peer-reviewed journals.



Dr Sivakumar Govindarajan is a Senior Scientist at the Centre for Engineered Coatings, International Advanced Research Centre for Powder Metallurgy and New Materials (ARCI), Hyderabad, India. His research interests include thermal barrier coating, development of coating solutions for diverse wear & corrosion issues and other functional applications through thermal spray processes. He has over 50 peer-reviewed journals, 3 patents and more than 30 conference publications. He has executed various Industrial sponsored and federal research projects in the capacity of PI & Co-PI worth of over \$3 M.



Dr Victoria Kurushina is a postdoctoral research fellow at the Robert Gordon University working with multiphysics simulations. She has a PhD in Engineering from the University of Aberdeen and previously worked as a research associate at Newcastle University. Her research interests include flow-induced vibrations of flexible pipelines due to internal and external fluid flows, phenomenological modelling, multiphase flows, wake oscillator, moving loads, computational fluid dynamics for a number of applications, fluid – structure interaction, optimization, oil and gas engineering, offshore systems, pipelines and risers.



Dr Sai P. Katikaneni is Research Science Consultant at R&D Center, Saudi Aramco, Dhahran. Prior to this, he worked at FuelCell Energy, Danbury, USA, as Director. He has more than 30+ years R&D experience in hydrogen, fuel processing, fuel cell and clean energy production technologies. His research interests include fuel processing, fuel cell technologies, catalysis, hydrogen production and application of catalytic materials for clean fuels and industrial chemicals. Dr Katikaneni is co-inventor of 20 patents, delivered Keynote Presentations, published 60 papers in refereed journals, presented 50 papers in international conferences and Guest edited 3 special journal issues on fuel cells.



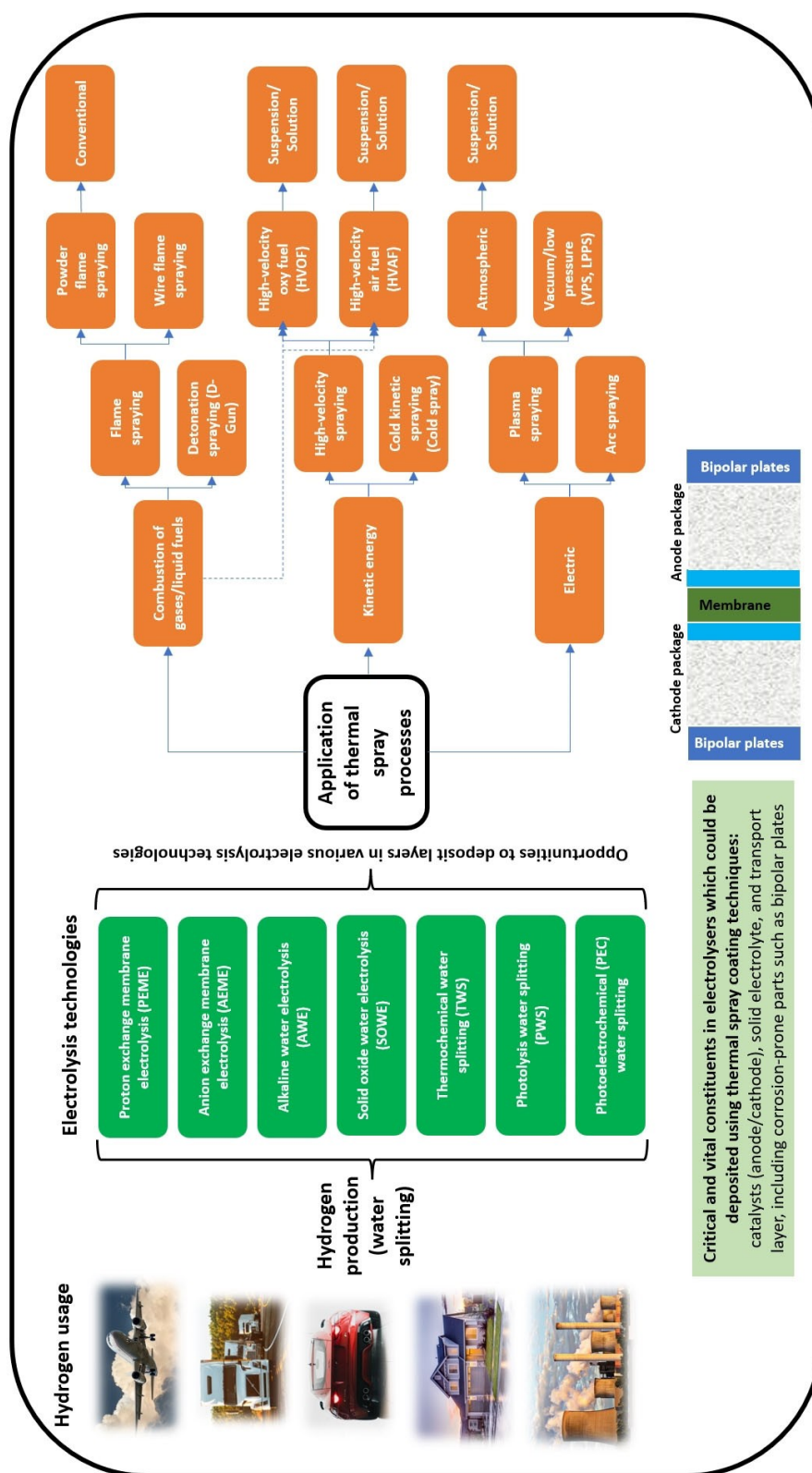


Figure 1. Applications of thermal spray coating processes to deposit layers in various electrolyser technologies which could help in water splitting leading to hydrogen production (note: there are multiple other manufacturing routes which is beyond the scope of this review, authors original image).

e.g., physical: physical vapour deposition, dip-coating, spin-coating, casting, filtration, lay-by-layer assembly, thermal spray;

and chemical: coupling agents, sol-gel method, chemical vapour deposition, surface grafting, *in-situ* growth, electroless



plating, electroplating can be used to produce functional catalytic membranes.<sup>[6]</sup> Among these coating routes, thermal spray process continues to remain a preferred industrial route for its cost advantages and reliability. Thermal spraying is a robot guided coating deposition technique where feedstock materials (in a molten or semi-molten state) are sprayed on a substrate to add/improve new functionality to the substrate. There is a desire to develop a facile manufacturing method for electrolyser components that can be scalable for affordable mass production and nearly all variants of the thermal spray technology reflected in Figure 1 meet this requirement. Within the thermal spray family, several process-related variants exist (e.g., gas temperatures and velocities that provide the driving force for heat up/melting and acceleration of the droplets/particles (3000 °C to 15000 °C at 50 m/s to 1000 m/s velocities: arc, flame, plasma, high-velocity oxy-fuel, detonation spray, cold spray, etc). While at relatively low temperature (e.g., up to 800 °C at 200 m/s to 1000 m/s velocities; cold gas dynamic spraying), wherein kinetic energy rather than thermal energy plays an important role in coating formation.<sup>[7]</sup> Thermal spray coatings are usually thicker (few microns to mm thicknesses) and can be cost-effective for a broad range of engineering materials (e.g., metal, metal alloys, metal oxides, semiconducting oxides, carbides, ceramics, cermet's, rare earth elements, carbon-based polymers, and polymeric composites). This has enabled thermal spray techniques to become an integral part of the aviation, transportation, power generation, chemical and biomedical industry of worth 7.6 billion USD.<sup>[8]</sup> Apart from the immense versatility, thermal spray technology also possess the capability to deposit structured/patterned surfaces with tailored microstructure which can enhance catalytic properties for producing hydrogen gas.

Thermal spraying technology enables maintaining the materials performance across demanding environments, for instance to enhance the service life of components as well as their performance. For example, a well-established application necessitating elevated temperature protection of the gas turbine structural parts involves deposition of a multilayered thermal barrier coating (TBC) configuration comprising of porous zirconia based ceramic top coat – dense Ni based alloy intermediate bond coat applied over super alloy substrates.<sup>[9]</sup> Over years, there has been a significant process in the way how thermal spray is performed to obtain the right micro-architecture. Inspired from these advancements, novel material combinations and composite microstructures can be explored for efficient electrolysis to produce hydrogen – which was the core remit of this review.

This review examines the potential of thermal spray to manufacture electrolyser components (mainly catalysts, transport layer, including manufacturing of protective layers against corrosion), thus summarising state-of-the-art and future directions in the area. As will be seen through this review, various properties and functional attributes of thermal spray coating materials have been investigated in the past, with a focus to achieve water splitting and corrosion resistant properties based on their microstructure as well as composition. In this review, the potential influence of coating manufacturing schemes,

microstructure and their composition on the electrolytic performance of the thermally sprayed electrodes has been assessed, with special attention paid to the considerations for future thermally sprayed materials for hydrogen production through water splitting.

## 2. Design-to-manufacture approach in thermal spray coatings

Depending on the electrolyser types and operational requirements, the design of components can be undertaken for achieving the desirable functional properties, although, the task is not straight forward. Few approaches to achieve this can be through tailoring of thick or thin layer, porous or non-porous/dense layers, electrical conductive, thermally conductive, ion conductive, pore size (nano/micro) and low environmental degradation (e.g., in alkaline), corrosion resistant, high flexibility, lightweight, high strength and cost-effective commercial feasibility. This could also include enhanced mechanical strength such as hardness, fracture toughness, ductility, and yield strength. A range of materials with desirable catalytic properties can be used (e.g., materials such as metals, metal alloys, metal oxides, semiconducting oxides, carbides, ceramics, cermets, rare earth elements, carbon-based polymers, and polymeric composites). Such materials could be deposited through thermal spray techniques on various substrate material types (e.g., metals, ceramics, polymeric and non-polymeric composites, glass, etc.).

The definition of thermal spray technology is quoted as “thermal spraying comprises a group of coating processes in which finely divided metallic or non-metallic materials are deposited in a molten or semi-molten condition to form a coating”.<sup>[10]</sup> Many industrial applications are surface engineered using spray deposition, not only for the surface coating applications but within the manufacturing of new materials with advanced functional properties. They are widely used within various industries (e.g., aerospace, agriculture, automobile, architecture, biomedical, decoration, maritime, metal working, papermaking and printing, electronics, petrochemical, geothermal, construction, space technology, nuclear, various utilities, sports, offshore, refineries, railroad, etc.) due to the fine microstructure in the finish that improves protective and aesthetic properties.

There are different methods of thermal spray techniques, with the general process involving mass and energy transfer through the spraying gun in form of gases and powders. High temperatures/high velocities allow the molten particle stream to coat the substrate as required.<sup>[11]</sup> Some methods such as flame spray or oxy/acetylene combustion spray uses a welding torch with the addition of high-velocity air streams to properly melt particles onto the surface. Plasma spray is another process where inert gas is fed past an electrode which causes the ‘plasma’ state of the gas. When this gas exits the nozzle and returns to its normal state, a large amount of heat energy is

released. Ceramic coatings are most often applied using this method due to their high melting temperatures.

High-velocity oxy-fuel (HVOF) is a well-known technique to produce coatings of metals and ceramics with better mechanical properties such as abrasion and wear resistance and electrical and thermal insulations. The maximum temperature in HVOF processes is around 3000 K while in plasma spray processes, it can reach 10000 K, however in many cases, the temperatures are often found to be between 1000 K and 1300 K.<sup>[12]</sup> High-velocity air-fuel (HVOF) is another variant of thermal spray techniques which offers improved coating characteristics coupled with increased productivity than HVOF. With further reduction in particle temperature and increased particle velocity than HVOF sprayed equivalents, HVOF technique even allows thin, dense cermet and alloy coatings that are desirable for enhanced oxidation & corrosion protection. Figure 2 shows a schematic of the thermal spray process<sup>[13]</sup> and Figure 3 shows range of spray particle temperature and velocity achievable by thermal spray processes.<sup>[14,15]</sup>

To improve the quality and efficiency of thermal spray processes, it is necessary to optimise all relevant parameters, such as gun design, fuel/oxygen ratio, gas jet formation, the position of the substrate, particle size and shape. Carrier gas flow needs to be optimized to get the correct dwelling time of the particle in the melt stream. Density, particle size and morphology of the powders would define how much of carrier gas flow is needed to get a coating with high deposition efficiency, low or no unmelts, high or low porosity. The particle characteristics depend mainly on the temperature and velocity of the spray system in use.<sup>[11]</sup> The authors also suggest that although the temperature is arguably the main factor affecting the coating, it also strongly depends on the preparation of the substrate surface, the standoff distance, the angle of impingement, the relative velocity, and the spray pattern. The surface is cleaned, roughened, and then cleaned again before spraying, otherwise, the coatings may not properly adhere to the substrate.

Though there are challenges associated with the application of finer feedstock for thermal spraying,<sup>[16,17]</sup> over the last decade, there has been desire to consider nano- or sub-micron sized powders as thermal spray feedstock materials. Principally, these nano- or sub-micron sized powders are characterized by poor flowability can be challenging to thermally spray using conventional techniques (e.g., APS, HVOF). Their relatively low momentum during spraying also precludes controlled powder delivery by the inability of the nano- or sub-micron sized powder particles to penetrate high velocity gas streams that are a hallmark of virtually all industrially exploited thermal spray variants.<sup>[18]</sup>

Meanwhile, two variants of thermal spray involving use of liquid feedstock, i.e., suspension plasma spray or SPS, and solution precursor plasma spray or SPPS have been extensively investigated recently.<sup>[8,19,20]</sup> The use of a suspension comprising of finer particles in a suitable liquid medium, or of a solution of precursor salts that can lead to particle generation *in-situ*, has been conceived primarily to address the flowability limitations.<sup>[21]</sup> Liquid feedstock based spraying has attracted greater interest due to its ability to spray fine structured coatings.<sup>[20]</sup> The process can be integrated with the conventional powder based infrastructure through appropriate choice of feedstock injection systems which allows the use of either suspension or solution precursor based feedstock. The significant advantage with both processes originates from the ability to deposit thinner lamellae that can be transformed into thin as well as thicker coatings with diverse microstructural features.<sup>[19]</sup> Suspension spraying process requires a stable suspension feedstock comprising of nano- or sub-micron sized particles formulated with a suitable solvent. Whereas, solution precursor spraying allows *in-situ* synthesis and subsequent consolidation of fine sized deposits in a single step, by employing appropriate precursors.<sup>[22]</sup> Although plasma spray is widespread spray variant for liquid feedstock, the use of HVOF based suspension spraying also shown interesting coating characteristics.<sup>[23]</sup> Further, the advent of axial injection based plasma spraying allowed more effective utilisation of suspensions at relatively

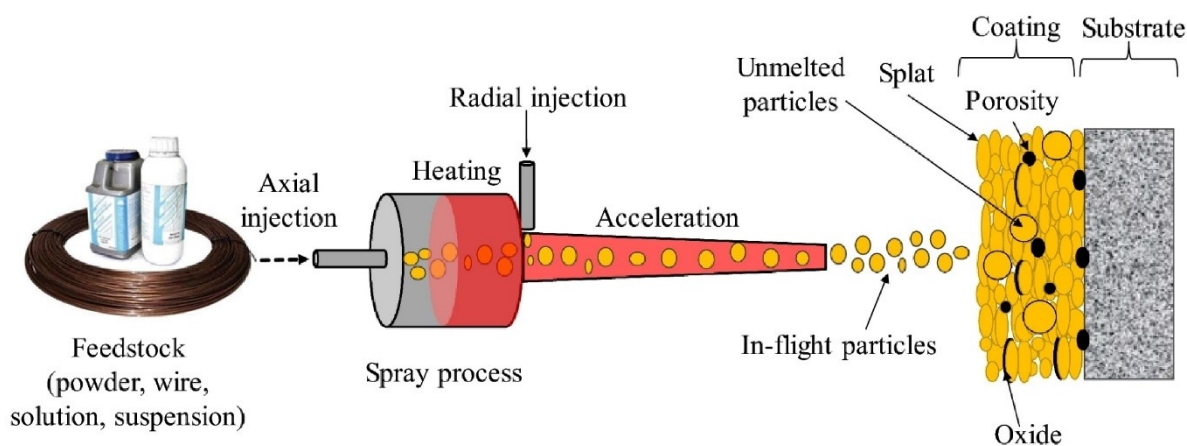


**Figure 2.** Thermal spray process schematic diagram (reproduced under the terms of the Creative Commons CC BY license).<sup>[13]</sup> Copyright (2019), Springer Nature.



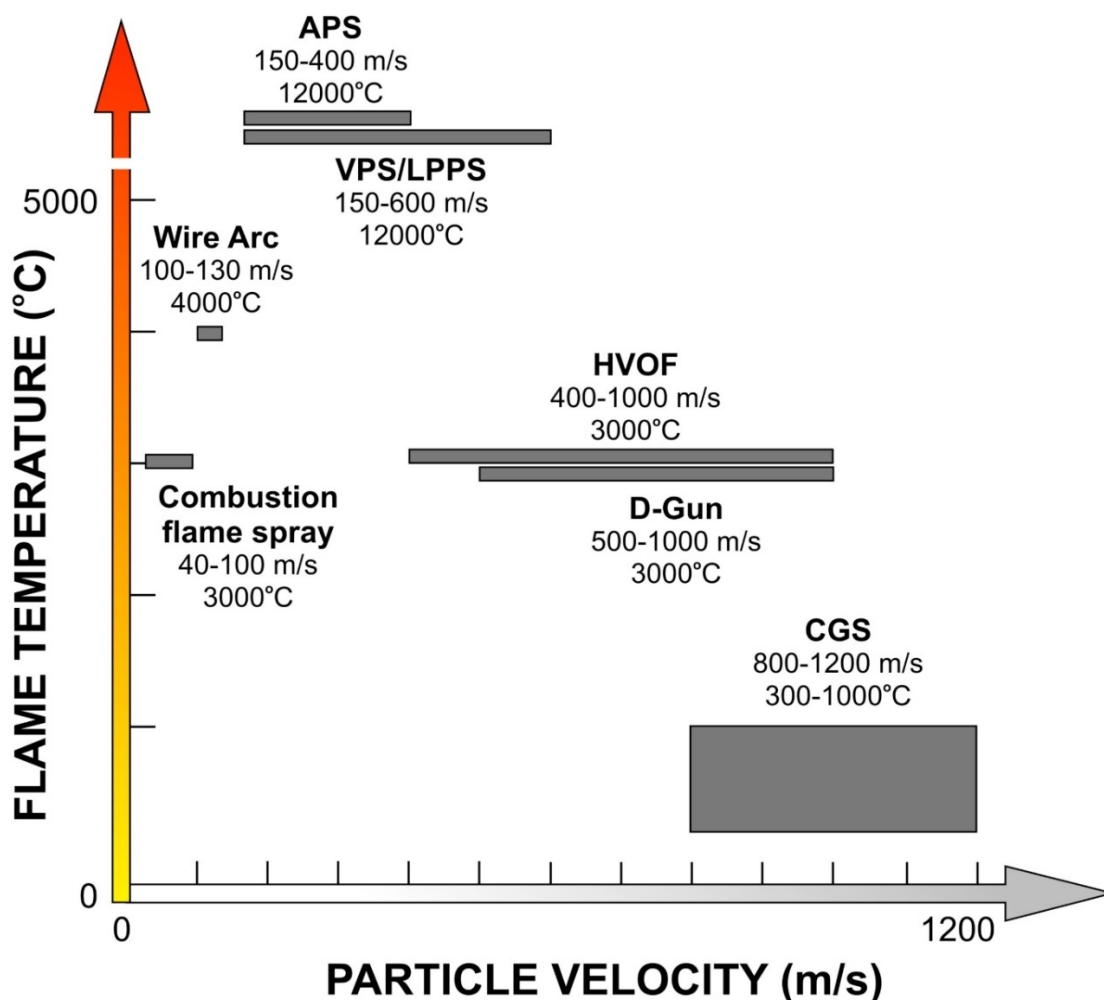


**Figure 3.** Thermal spray map based on process particle velocity and flame temperature attainable in different thermal spray techniques (note, APS: air plasma spray, VPS: vacuum plasma spray, LPPS: low pressure plasma spray, HVOF: high velocity oxygen fuel, D-gun: detonation gun, CGS: cold gas spray) (reproduced under the terms of the Creative Commons Attribution license).<sup>[14]</sup> Copyright (2011), MDPI.

higher deposition rate and tailored microstructure has generated strong academic and industrial interest.<sup>[20]</sup> Solution precursor plasma spraying (SPPS) process opens up new avenues for developing compositionally complex functional oxide coatings. In fact by means of hybridizing with powder injection system, it even allows depositing composite metal/alloy/ceramic plus ceramic films as well. Major benefits of the SPPS and hybrid APS plus SPPS process are (i) ability to create fine-sized/bi-modal type of microstructures, (ii) flexible, rapid exploration of novel precursor compositions and their combinations, (iii) better control over chemistry of the deposit. Specifically, the hybrid approach allows realisation of unique microstructural features having (i) layered architecture through alternate injection of liquid and powder feedstock, and (ii) composite coatings through simultaneous injection of liquid and powder feedstock.<sup>[19]</sup> More recently, the possibility of utilising a powder-liquid 'hybrid' feedstock has also been demonstrated and found to be an effective pathway to create unique, function-dependent coating architectures.<sup>[20,24]</sup>

The line-of-sight thermal spray coating methods are easily scalable for industrial applications. However, for coating of critical and vital constituents in electrolyzers, the thermal spray routes can also pose following potential challenges: (a) thermal spray can be a very costly technique for spraying precious noble metals as catalysts due to significant wastage of materials during spraying, (b) retention of nanostructures, which is an important consideration to improve the efficiency of catalytic reaction, can be difficult to control in low melting point materials due to overheating, (c) materials highly prone to oxidation are difficult to deposit in pristine condition due to possible alteration in the surface chemistry as a result of in flight oxygen pick up; however, this can also be advantageous as surface chemistry changes can be highly effective to alter the catalytic efficiency, and (d) retaining the core-shell morphology is difficult during thermal spraying since the high velocity impact of materials on the substrate can burst the core-shell structure.

Notwithstanding the above, the advantages of using thermal spray coatings for critical and vital constituents in

electrolysers are compelling and span the following: (a) convenient laboratory-to-industry scale up for production, (b) ability to deposit low-cost transition metal element alloy catalytic materials, (c) suitability to create nano structuring/nanopatterning over the electrode surface, and (d) enhanced catalytic activity through increased surface area by means of pores, voids and splat boundaries. Moreover, advances in thermal spray technology and their improved understanding has helped overcome some of the previously mentioned challenges, such as ability to retain nanostructures and/or suppress *in-situ* oxidation. This makes thermal spray routes apt for serious consideration for fabricating electrolyser components.

In electrolyser applications, two aspects are particularly important for component fabrication: (a) choice of material, and (b) structure of the deposited layer. There is considerable control over both of the above if using the thermal spray technique. As it is known today, the thermal spray processes could provide a cost-effective manufacturing route to deposit complex material compositions not only as an overlay coating but also as free-standing coatings.<sup>[25]</sup> This route also provides the ability to control the porosity and structure, e.g., metasurface.<sup>[26]</sup> Figure 4 show air plasma spraying (APS) on disc shaped test coupons at thermal spray booth.

### 3. Hydrogen production

#### 3.1. Hydrogen production overview

Overall, there are three ways in which hydrogen (e.g., brown hydrogen, blue hydrogen, green hydrogen) can be produced. Brown hydrogen is produced through steam methane reforming (SMR) of natural gas via an endothermic reaction.<sup>[28]</sup> Blue hydrogen is produced via a combination of SMR and carbon capture and storage (CCS), in which the carbon emissions produced are recycled by capturing and storing them. Green hydrogen is produced by electrolysis in which water molecules are splitted into hydrogen and oxygen by passing electric current.<sup>[29]</sup>

As of now, SMR is the predominant method of producing hydrogen constituting around 95% of total production with as little as 4% green hydrogen produced from electrolysis.<sup>[30]</sup> There are many barriers that presently hinder green hydrogen production, such as considerable cost associated with the electrolysis process and the colossal challenge of scaling up production and infrastructure to meet the current global demand. Furthermore, green hydrogen production has contributed only a minor part of the total production in the previous two decades largely due to the low cost of fossil fuel-based production. With the rising demand for renewables, it is likely to lead to a reduction in the cost of green hydrogen, and high level cost analysis<sup>[31,32]</sup> clearly suggests that green hydro-

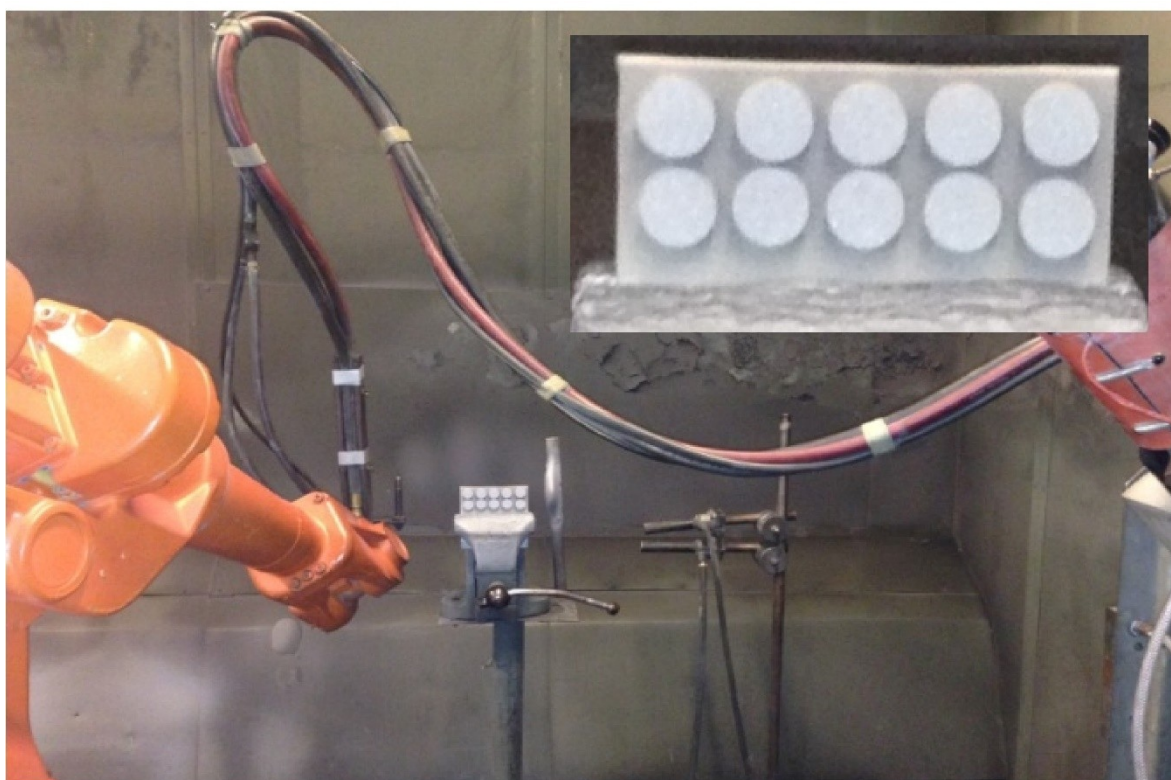


**Figure 4.** Air plasma sprayed (APS) samples getting sprayed at thermal spray booth (inset - disc shaped 10 samples, Monitor Coatings Ltd) (Faisal et al., 2015, reproduced with permission).<sup>[27]</sup> Copyright (2015), Springer Nature.



gen is expected to play a significant role in achieving net-zero emissions in the future. For the development of next-generation electrolyzers, enhancement in their efficiency and durability under various operating conditions would be among the most desirable features. Hydrogen production is expected to share 9.5% of the total final energy consumption in 2050, out of which 60% is projected to be green hydrogen and nearly 38% grey hydrogen.<sup>[32]</sup>

In view of the above and to reduce dependency on fossil fuels, there is an urgent need to make rapid progress in other hydrogen generation technologies from renewable resources such as biomass and water. In this review, the hydrogen generation technologies based on water (i.e., electrolysis processes) are considered with specific focus on the application of thermal spray coatings to manufacture catalysts and other protective layers against corrosion (of bipolar plates or housing) for the electrolyzers. Therefore, some basics about the catalysts and electrolysis process are presented below for a better perspective on the thermal spray requirements.

### 3.2. Electrolysis for hydrogen production

Figure 5 presents water splitting electrolyser technologies for hydrogen production where water is one of the feedstocks. Pure water is a limited and often valuable resource as about 96.5% of total water is seawater or brackish water, containing dissolved salts that are highly corrosive. Ultra-purified water is the main feedstock along with the catalysts for conventional electrolyzers powered by renewable electricity for producing green hydrogen. One kilogram (kg) of hydrogen requires nine kilogram of water as an input from a stoichiometric perspective.

However, this can range from 18–22 kg of water per kilogram of hydrogen when considering the desalination process using tap water<sup>[33]</sup> (which can further vary for brine/grey water or seawater feedstocks) considering the losses and the recovery rate of the purification process.

The catalyst is an agent that enhances the reaction rate (i.e., current density) without being consumed in the reaction. Electrocatalyst is a catalyst that affects the activation energy (which is related to the voltage at which a reaction occurs) of an electrochemical reaction (i.e., oxidation, reduction). As summarized by Wang et al. (2021),<sup>[34]</sup> catalysis during water-splitting electrolyser is the key to hydrogen gas (H<sub>2</sub>) and oxygen gas (O<sub>2</sub>) production in the current context. The chemical reaction of water electrolysis is divided into two half-cell reactions; namely, hydrogen evolution reaction (HER) where water is reduced at the cathode to produce hydrogen, and oxygen evolution reaction (OER) where water is oxidized at the anode to produce oxygen. Therefore, the chemical kinetics at the catalyst surface (minimizing the overpotentials) during HER and OER is critical to the production of hydrogen and oxygen. Thus, an electrolyser involves the following chemical reactions: cathode:  $2\text{H}^+ + 2\text{e}^- \rightarrow \text{H}_2$ ; anode:  $2\text{OH}^- \rightarrow \frac{1}{2}\text{O}_2 + \text{H}_2\text{O} + 2\text{e}^-$ ; overall:  $\text{H}_2\text{O} \rightarrow \frac{1}{2}\text{O}_2 + \text{H}_2$ . For an electrolysis reaction to take place, electrical (and thermal) energy is needed. As shown in the electrolyser chemical reactions, the overall energy requirement for reaction ( $\Delta\text{H}$ ) can be partly provided by heat ( $\Delta\text{Q}$ ) and other parts (i.e., Gibb's energy change,  $\Delta\text{G}$ ) can be supplied through electricity (see Figure 6).<sup>[35]</sup> With increase in temperature (0–1000 °C), the overall energy demand ( $\Delta\text{H}$ ) varies slightly (i.e., between 283.5 and 291.6 kJ/mol H<sub>2</sub>, shown with blue dash-line). However, the heat share ( $\Delta\text{Q}$ ) rises with temperature, reducing the minimum electrical energy demand ( $\Delta\text{G}$ ) (note: heat of

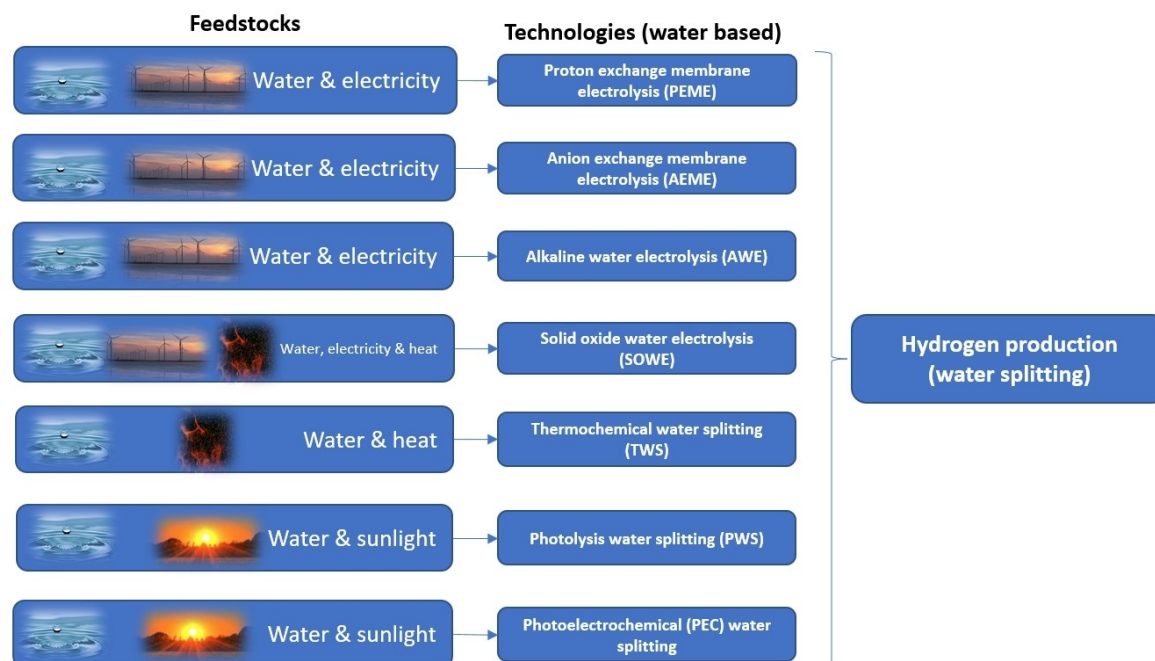
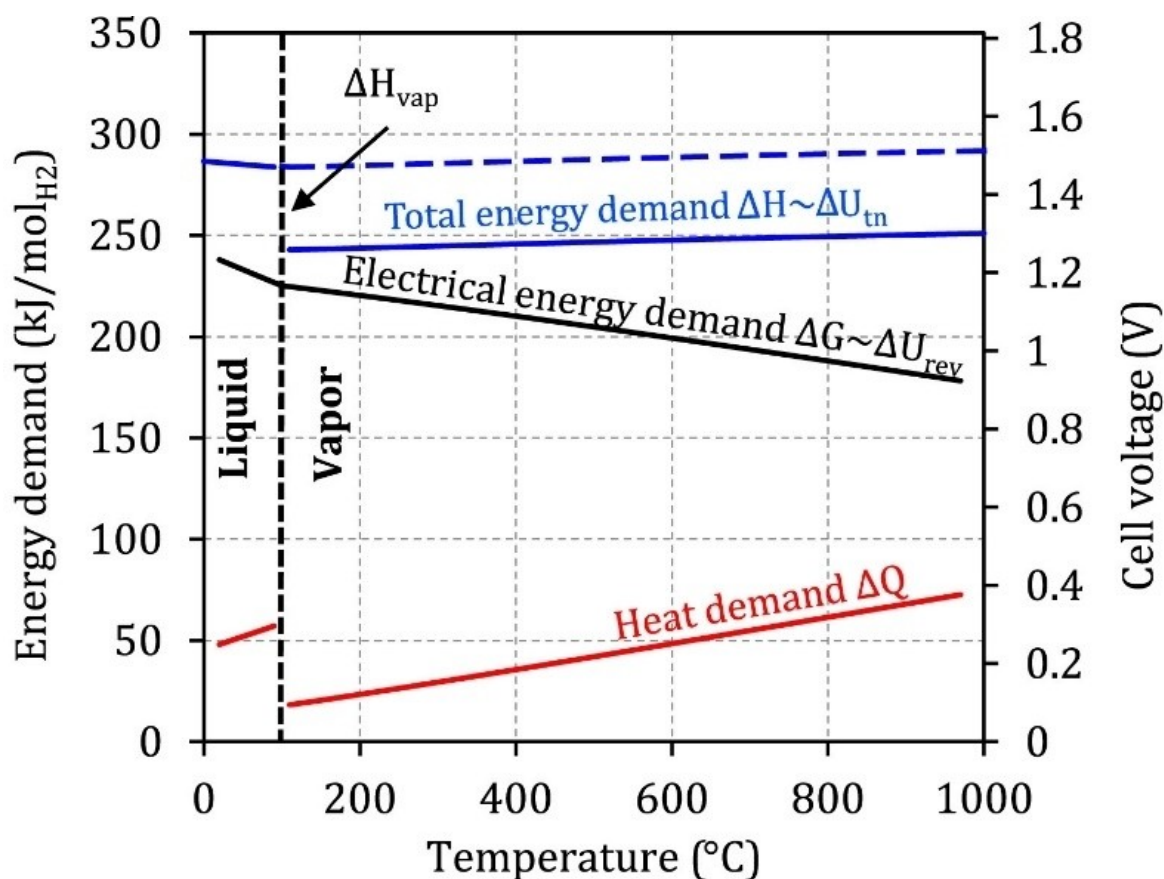


Figure 5. Water splitting electrolyser technologies for hydrogen production where water is one of the feedstocks (authors original image).



**Figure 6.** Overall energy demand ( $\Delta H$ ), electrical energy ( $\Delta G$ ) and thermal energy ( $Q$ ) demand of an ideal electrolysis process as function of the temperature (note: as known generally, the low temperature electrolyzers operate at 60–90 °C, whereas high temperature electrolyzers operate at 700–900 °C) (Buttler and Spliethoff, 2018, reproduced with permission).<sup>[35]</sup> Copyright (2018), Elsevier.

vaporisation of water is 41 kJ mol<sup>-1</sup>H<sub>2</sub>, and the electrical energy could be replaced by thermal energy in the order of 41 kJ mol<sup>-1</sup>H<sub>2</sub>.<sup>[36]</sup> This suggests that, beside improved kinetics, the high heat utilisation of internal losses is a major motivation of high-temperature electrolysis (e.g., 700–900 °C).<sup>[35]</sup> At higher temperature, the electrical potentials in the cell is typically low (indicating high ionic conductivity and low electrical resistance, leading to higher electrolysis process efficiency).

### 3.3. Operations and critical materials for water-splitting electrolyser techniques

Figure 7 presents existing electrolysis technologies based on membrane electrode assembly. Proton exchange membrane (PEM) electrolyser operates at low temperature range (50–80 °C) to generate hydrogen.<sup>[37]</sup> The PEM electrolyser includes two catalysts (i.e., anode and cathode) and a membrane. Typically, it uses platinum (Pt) black, iridium, rhodium, and ruthenium for electrode catalysts and a membrane (typically made of Nafion). Due to suitable mechanical properties and high corrosion resistance, titanium (Ti) is used as the base material for bipolar plates in PEM electrolyzers.<sup>[5]</sup> Furthermore, titanium screens, foams or felts are used for porous transport layers (PTL) in PEM

technology. As summarised by Miller et al. (2020),<sup>[37]</sup> the PEM cell operation environment which is corrosive acidic requires the use of specialised materials. To handle the high current densities at anode, these materials must sustain the high applied over voltage (2 V). Corrosion resistance applies for the catalysts, and for current collectors and separator plates. As shown in Figure 7(a),<sup>[38]</sup> in PEM electrolyzers, water is introduced at the anode catalyst which then splits into protons (H<sup>+</sup>) and oxygen (O<sub>2</sub>). The protons (H<sup>+</sup>) then go through the membrane to the cathode, where they are recombined into hydrogen. Such electrolyzers can have low ionic resistance, which means high currents of >1600 mAcm<sup>-2</sup> can be achieved while maintaining efficiencies up to 55–70%.<sup>[39]</sup> Further details about PEM electrolysis for hydrogen production can be seen elsewhere.<sup>[37,40]</sup>

Anion exchange membrane (AEM) electrolyser operates at low temperature range (50–60 °C) and works with an alkaline environment at the membrane interface provided by the immobilized positively charged functional groups on the polymer backbone or on pendant polymeric side chains.<sup>[37,41]</sup> As shown in Figure 7(b),<sup>[38]</sup> in AEM electrolyzers water is introduced at the anode catalyst. The AEM electrolyser includes two catalysts (i.e., anode and cathode) and a semipermeable membrane through which water travels from the anode half-

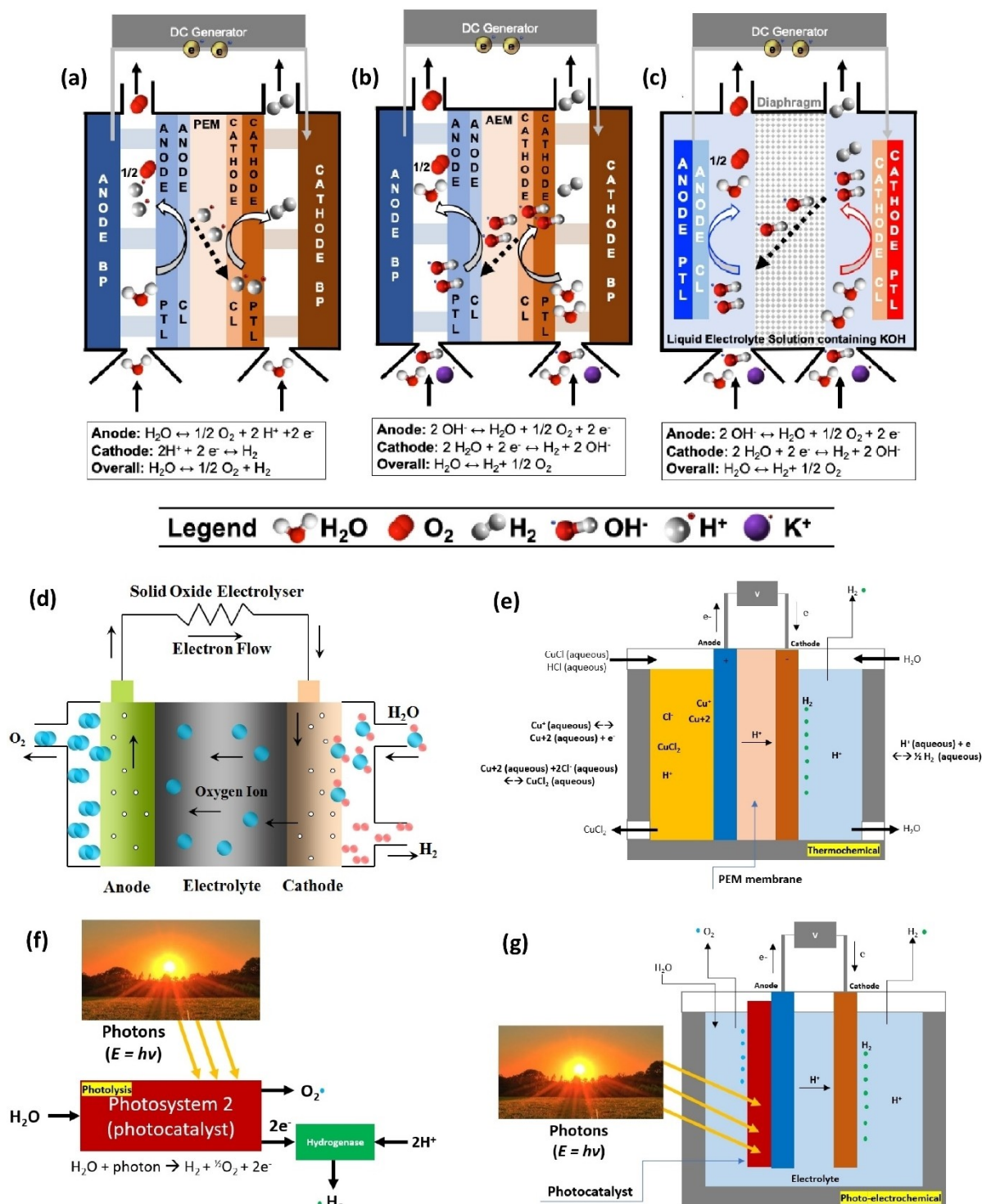


**Figure 7.** Types of water electrolysis technologies: (a) proton exchange membrane (PEM) (reproduced under the terms of the Creative Commons Attribution license),<sup>[38]</sup> Copyright (2022), Wiley, (b) anion exchange membrane (AEM) (reproduced under the terms of the Creative Commons Attribution license),<sup>[38]</sup> Copyright (2022), Wiley, (c) alkaline water electrolysis (AWE) (reproduced under the terms of the Creative Commons Attribution license),<sup>[38]</sup> Copyright (2022), Wiley, (d) high-temperature solid oxide water electrolysis (SOWE) (authors original image), (e) CuCl/HCl thermochemical water splitting (authors original image), (f) photolysis water splitting (PWS) (adapted and reproduced with permission),<sup>[39]</sup> Copyright (2009), Elsevier, and (g) photoelectrochemical water splitting (PEC) (adapted and reproduced under the terms of the Creative Commons Attribution license),<sup>[81]</sup> Copyright (2012), MDPI.

cell. Typically, it uses Ni and Ni alloys as cathode, and Ni, Fe, and Co oxides as anode.<sup>[37]</sup> Hydrogen is produced from water at the cathode and released via the gas diffusion layer (GDL).

While oxygen is produced from anion ( $\text{OH}^-$ ) at the anode and released via GDL along with the electrolyte circulation, anion ( $\text{OH}^-$ ) moves back to the anode via the membrane. There are



similarities between PEM and AEM, but the main difference is that the PEM electrolyser is less sensitive towards the drastic changes of the current loads (especially when electricity supplied is produced by renewable energy sources), it achieves higher current densities that leads to higher production rates and the system is more compact.<sup>[37]</sup> Further details about AEM electrolysis for hydrogen production can be seen elsewhere.<sup>[37,42]</sup>

As shown in Figure 7(c),<sup>[38]</sup> alkaline water electrolyzers (AWE) operates at low temperature range (60–80 °C) and are composed of two catalysts (i.e., anode and cathode), a microporous membrane, and an aqueous alkaline electrolyte of potassium hydroxide/KOH or sodium hydroxide/NaOH.<sup>[37,39]</sup> In AWE, there must be ions in the water to conduct electricity for electrolysis process. For anode, Ni, Pt, Co, Ir, Rh or Ni–Co alloy is used. For the cathode, low carbon steel mesh, Ni, Ni–Mo alloys or Ni coated low carbon steel is used. Other materials could be cobalt, zinc, lead, palladium, platinum, and gold.<sup>[43]</sup> For microporous membrane (to separate product gases and transport hydroxide ions, and nonconductive to electrons), high-polymer composites (e.g., polyphenylene-sulphide) are used, replacing traditional asbestos (silicate mineral). In AWE cell, water is introduced at the cathode where it decomposes into hydrogen (H<sub>2</sub>) and hydroxide ion (OH<sup>-</sup>). The OH<sup>-</sup> ion travels through the electrolytic (KOH or NaOH) to the anode where O<sub>2</sub> is formed. AWE current density is 100–300 mAcm<sup>-2</sup> and achieves efficiencies of about 50–60% based on the lower heating value of hydrogen.<sup>[39]</sup> Further details about the AWE electrolysis for hydrogen production can be seen elsewhere.<sup>[37,42]</sup>

Solid oxide water electrolysis (SOWE) electrolyser is based on solid oxide fuel cell (SOFC) technology which operates at high temperature between 500 °C to 850 °C.<sup>[40]</sup> The SOFC can generate electricity and can operate reversibly as a SOWE electrolyser to generate hydrogen. The SOWE electrolyser includes two catalysts (i.e., anode and cathode) and a solid oxide material (non-permeable dense layer) as electrolyte which conducts negative oxygen ions (O<sup>2-</sup>) from the cathode to the anode. Some of the popular solid oxide materials (electrolyte) include yttria-stabilized zirconia (YSZ), gadolinium doped ceria (GDC) and scandia stabilized zirconia (ScSZ). For the anode, some of the popular materials are cermets (i.e., metal mixed with ceramics) such as nickel mixed with YSZ (i.e., Ni-YSZ) or chromite (La<sub>0.8</sub>Sr<sub>0.2</sub>Cr<sub>0.5</sub>Mn<sub>0.5</sub>O<sub>3</sub> or LSCM). For the cathode, some of the popular materials are lanthanum strontium manganite (LSM) or LSM-YSZ. The operating higher temperatures increases the SOWE electrolyser efficiency by decreasing the catalysts overpotentials (i.e., anode and cathode) which causes power losses in electrolysis (Holladay et al., 2009). As shown in Figure 7(d),<sup>[44]</sup> in SOWE electrolyzers water is introduced at the cathode catalyst where it splits into hydrogen (H<sub>2</sub>) and oxygen ion (O<sup>2-</sup>). SOWE operates like the alkaline system where oxygen ion (O<sup>2-</sup>) travels through the solid electrolyte leaving the hydrogen (H<sub>2</sub>) in the unreacted steam stream and can achieve high efficiencies of 40–60%. Unlike KOH solution (electrolyte) for alkaline systems, the advantage with solid electrolyte layer is that it is non-corrosive, and it does not have flow distribution problems, however sealing issues exist. Further details about

SOWE electrolysis for hydrogen production can be seen elsewhere.<sup>[45]</sup>

As shown in Figure 7(e) (adapted from Naterer et al., 2019),<sup>[46]</sup> in thermochemical water splitting or TWS (thermolysis or thermal decomposition via high temperature electrolysis (HTE), e.g., at nuclear reactors<sup>[47]</sup>), heat is used to split water into hydrogen and oxygen<sup>[48]</sup> with overall efficiencies of about 50%.<sup>[49]</sup> The thermochemical cell (e.g., CuCl/HCl cycle) is composed of two catalysts (i.e., anode and cathode) and a PEM membrane (e.g., Nafion/polypyrrole and Nafion/polyaniline composite).<sup>[46]</sup> During thermochemical cycle, when water is heated to 2000 °C to 2500 °C, part of it decompose into OH, monatomic oxygen, monatomic hydrogen, oxygen, and hydrogen.<sup>[50]</sup> As water decomposes at such high temperatures, there could be materials stability issues as well as issues related to heat sources availability.<sup>[51]</sup> Therefore, chemical reagents have been proposed to lower the temperatures, reducing high operating temperature from 2500 °C, but typically require higher pressures.<sup>[39]</sup> Naterer et al. (2019)<sup>[46]</sup> advised that ceramics, refractory metals, Mo and Ni based alloys, graphite-based materials, and Hastelloy C can be most suitable construction materials for high temperature and corrosive environments (e.g., Cu–Cl thermochemical cycle). Alternatively, for such extreme electrolysis applications, other materials could also be considered, for example, Xie et al. (2012)<sup>[52]</sup> considered carbide/nitride materials, Wu et al. (2013)<sup>[53]</sup> considered mullite materials, Sure et al. (2012)<sup>[54]</sup> considered partially stabilized zirconia (PSZ) with graphite coatings, Kamali and Fray (2013)<sup>[55]</sup> considered graphite, Vignarooban et al. (2014)<sup>[56]</sup> considered Hastelloy C276, C-22 and N, Sellers et al. (2012)<sup>[57]</sup> considered Hastelloy N and Steel 316, and Siantar (2012)<sup>[58]</sup> considered metallic and ceramic coatings on a base metal. Various reviews on hydrogen production through thermochemical water decomposition method can be seen elsewhere.<sup>[49,59–63]</sup>

High temperature heat of nuclear reactor can be useful to split water into hydrogen and oxygen; with additional merits, such as free from carbon dioxide, large scale, and efficient hydrogen production.<sup>[47,64]</sup> Application of high-temperature steam electrolysis and cerium-iodine (Ce–I) thermochemical cycle,<sup>[65]</sup> iron-chloride (Fe–Cl) thermochemical cycle,<sup>[66]</sup> iodine-sulfur (I–S) thermochemical cycle,<sup>[64]</sup> and Cu–Cl thermochemical cycle,<sup>[46,63,67]</sup> for splitting water by using nuclear heat source has been found to be most suitable process for hydrogen production. It has been suggested that such a thermochemical cycle can also be additionally powered by solar heat to meet temperature requirements.<sup>[62]</sup> Since thermochemical cycles operates at high temperature (sources such as solar, and nuclear) with the corrosive environment, the structural components (including electrodes) require special considerations (mainly having corrosion resistant properties).

As shown in Figure 7(f) (adapted from Holladay et al., 2009),<sup>[39]</sup> in photolysis water splitting (PWS), sunlight (or any photon with sufficient energy, considering the seasonal fluctuations in surface water temperature (from 0 to 20 °C or more) at latitudes far from the equator (Furatian and Mohseni, 2018))<sup>[68]</sup> as feedstock with water, directly decomposes water into hydrogen and oxygen and uses selective photocatalyst semiconduct-

ing materials. Among many photocatalysts, heterogeneous metal oxides can be materials of interest due to their stability, endurance to photo-corrosion, and doping of nitrogen and sulfur atoms to reduce the band gap of the metal oxide semiconductor. The photocatalysts or material of interest could be solid solutions having  $\text{Ln}_{0.8}\text{Ga}_{0.2}\text{InO}_3$  (with  $\text{Ln} = \text{La, Gd, Y, Yb}$ , both undoped and doped with sulfur atoms).<sup>[69]</sup> Figure 8<sup>[70]</sup> shows a schematic of the relevant photocatalytic steps for a semiconductor photocatalyst of one-step water splitting.  $\text{TiO}_2$  is the most preferred photocatalytic material due to its appropriate valence and conduction band positions.<sup>[71]</sup> Photocatalytic process-based water splitting effect of  $\text{TiO}_2$  was discovered by Fujishima and Honda in 1972,<sup>[72]</sup> and since then photocatalysis technique has been carried out for many uses, such as water remediation, food preservation, disinfection, air treatment, and many other applications.<sup>[73,74]</sup>  $\text{TiO}_2$  photocatalysis has been extensively reported for water splitting leading to hydrogen production, including air and water purification systems, self-cleaning surfaces, sterilization, and photoelectrochemical cells.<sup>[71,75–77]</sup>

Based on the physics of semiconductor-liquid contacts discussed by Walter et al. (2010),<sup>[78]</sup> the conversion of one  $\text{H}_2\text{O}$  molecule to  $\text{H}_2$  and  $1/2 \text{O}_2$  under standard conditions, the free energy change is  $\Delta G = 237.2 \text{ kJ/mol}$ , and it corresponds to

$\Delta E^\circ = 1.23 \text{ V}$  per electron transferred (as per Nernst equation). Usually, semiconducting materials are selected as photocatalysts due to their narrow band gap, unoccupied conduction band and occupied valence band.<sup>[79]</sup> The photocatalysts absorb photons with energy equal to or larger than their bandgap, which results in electrons production in the conduction band (CB) and holes in the valence band (VB), which then accelerates oxidation-reduction reactions.<sup>[80]</sup> Therefore, the selected semiconducting materials must absorb radiant light with  $> 1.23 \text{ eV}$  photon energies (which is equal to wavelengths of about 1000 nm and shorter) and convert the energy into hydrogen and oxygen. The photocatalysis process must generate two electron-hole pairs per molecule of  $\text{H}_2$  ( $2 \times 1.23 \text{ eV} = 2.46 \text{ eV}$ ) or four electron-hole pairs per molecule of  $\text{O}_2$  ( $4 \times 1.23 \text{ eV} = 4.92 \text{ eV}$ ). To carry out hydrogen evolution reaction (HER) and oxygen evolution reaction (OER) using electron/holes generated under illumination without recombination, photoinduced free charge carriers (i.e., electrons and holes) in the semiconductor must travel to a liquid junction and must react only with solution species directly at the semiconductor surface. The electron-transfer processes at semiconductor-liquid junctions produce losses due to the concentration and kinetic overpotentials needed to drive the HER and the OER. Considering photolysis key requirements, the photo (sunlight) interaction

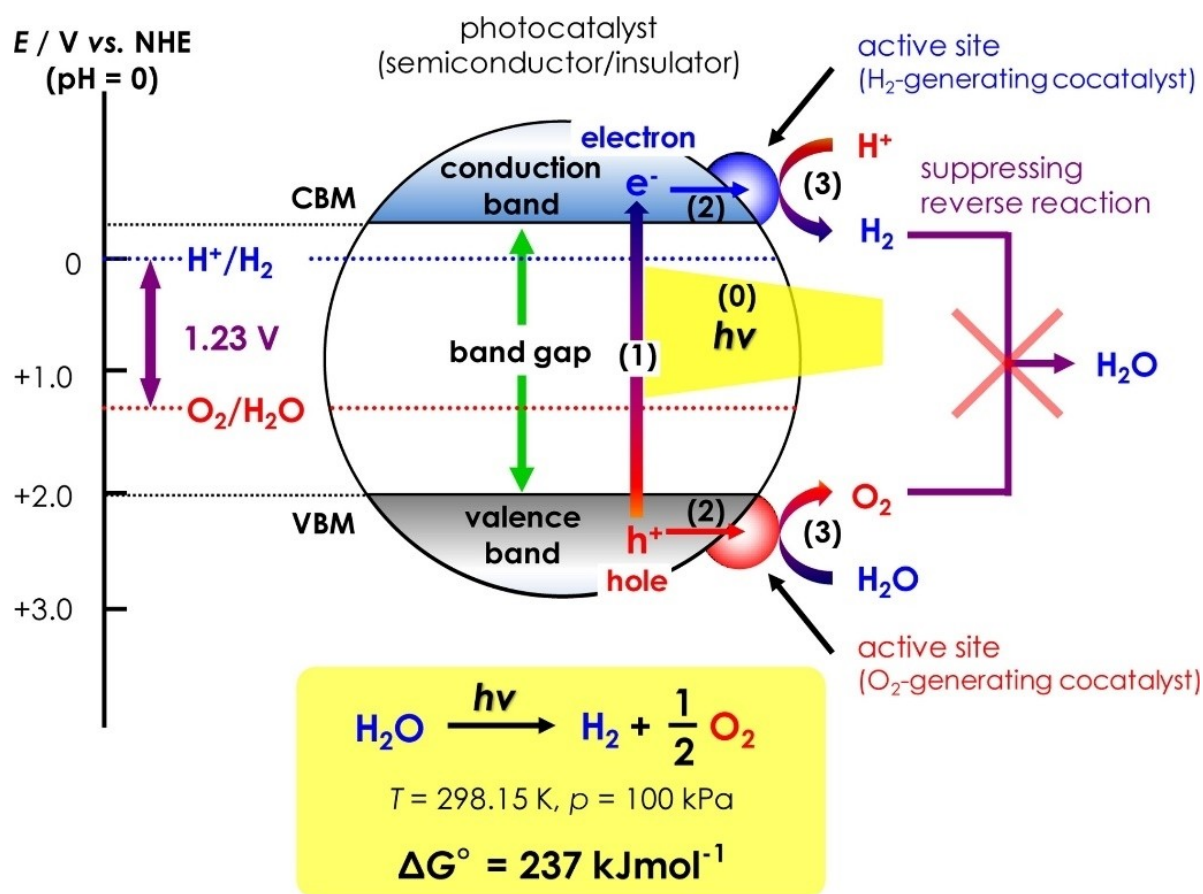


**Figure 8.** Schematic of the photocatalytic steps for a semiconductor: (1) shows that the light gets absorbed to generate electron-hole pairs; (2) migration occurs of excited carriers (i.e., electrons, holes) to the surface; (3) surface reaction occurs to produce hydrogen with electrons and oxygen with holes (reproduced with permission).<sup>[70]</sup> Copyright (2013), Elsevier.

with photocatalyst semiconducting materials with different band gaps should be enough to split water into hydrogen and oxygen. The energy required for photoelectrolysis at a semiconductor photoelectrode is around 1.6–2.4 eV per electron-hole pair generated, to account for these losses, and therefore multiple semiconductors can be selected which can drive water splitting.

As shown in Figure 7(g) (adapted from Liao et al., 2012),<sup>[81]</sup> with sunlight as feedstock with water, the photoelectrolysis (or photoelectrochemical/PEC) process split water into hydrogen and oxygen and uses semiconducting materials like those used in photovoltaics.<sup>[39,81]</sup> Basically, when a photon with energy greater than the semiconducting material's bandgap is absorbed in the p-n junction, an electron is released, and a hole is formed. With the presence of an electric field, the hole and electron move in opposite directions creating an electric current. This process is called as photoelectrolysis when a photocathode (i.e., a p-type material with excess holes), or a photoanode (i.e., an n-type of material with excess electrons), is immersed in an aqueous electrolyte, but instead of generating

an electric current, water splits to form hydrogen and oxygen.<sup>[39]</sup>

Some of the recent reviews where the electrolysis process has been described in detail can be seen elsewhere,<sup>[34,82–84]</sup> and based on high-level assessment, Table 1 presents comparison of water electrolysis technologies.

### 3.4. Carbon footprint of hydrogen production via electrolysis

Even though hydrogen is a clean fuel, its production comes at the cost of environmental consequences.<sup>[36,85,86]</sup> Presently, most of the hydrogen is produced using fossil fuels such as natural gas and used in chemical industries or refineries.<sup>[87]</sup> The carbon footprint associated with hydrogen production can be analysed based on the life cycle assessment (LCA), which is defined in internationally recognized standards ISO 14040 (ISO, 2006)<sup>[88]</sup> and ISO 14044 (ISO, 2006).<sup>[89]</sup> LCA constitutes the emissions assessment of the entire cycle of energy production/consumption processes starting from the raw products to the final

**Table 1.** Comparison of water electrolysis technologies.

Electrolysis technologies	Advantages	Challenges and opportunities
Proton exchange membrane electrolysis (PEME)	Operates at low temperature, compact design, short cold start, high purity hydrogen production, best suited for operation with fluctuating electricity from renewable sources, near-term commercialisation.	High-cost polymeric membranes, works in acidic environment (therefore be used to protect the electrodes from corrosion), electrodes made of noble or precious metals, higher investment cost, requires highly purified water to avoid electrocatalyst degradation. Innovation in flow channel design an area of further work.
Anion exchange membrane electrolysis (AEME)	Low investment cost, sustainable technology which combines the advantage of PEME and traditional AWE electrolysis systems.	Needs further research in membrane stability, main challenges with the low ion conductivity and long-term electrochemical stability of the AEMs (under highly basic conditions at elevated temperatures) remain.
Alkaline water electrolysis (AWE)	Operates at low temperature, low investment cost, does not require critical raw materials (CRM), relatively stable and long lifetime, mature technology based on the chloralkali process, currently at the commercial scale.	Corrosive electrolyte, hydrogen crossover, slow dynamics, low-pressure hydrogen production capability, and requirements to improve durability & reliability are still challenging, not as robust as PEME, long cold start (high).
Solid oxide water electrolysis (SOWE)	Enhanced kinetics, thermodynamics: lower energy demands, high efficiency (over 100% if steam is freely available from excess heat), no precious metals, ceramic proton conductors has gained attention as such materials show higher ionic conductivity and better efficiency compared to that of oxygen-ion conductors at the intermediate temperature range.	Operates at high temperature undergoing with risk of material degradation, mechanically unstable electrodes, thermal mismatching of the individual layers; (cracking), safety issues (improper sealing), microstructural issues (delamination, passivation, blocking of triple phase boundary), high investment cost, currently laboratory & demonstration scale.
Thermochemical water splitting (TWS)	Suitable for large-scale applications, High temperature electrolysis is more efficient economically than traditional room-temperature electrolysis (some of the energy is supplied as heat, which is cheaper than electricity, and also because the electrolysis reaction is more efficient at higher temperatures), no need for electricity (in pure cycles). Recent hybrid cycles can reach a high efficiency (above 90%).	Operates at high temperatures leading to structural degradation of the redox pairs, high investment cost, molten salt very corrosive for structural parts, overall operational conditions require special attention, not many research data available (in particular for nuclear thermochemical), currently laboratory scale. Significant research needed to develop materials and manufacturing of structural part which could sustain high temperature corrosion and nuclear radiation (contamination and degradation).
Photolysis water splitting (PWS)	Simpler technology which includes direct approach to generate clean hydrogen without external electric power sources, simple set-up (requires water and suitable catalysts), the chemical reaction does not involve the use of fuel-based energy sources nor involves the generation of toxic by-products.	Low water-splitting efficiency (usually below 1%), feasibility is limited by constraints regarding result reproducibility, operation factors, and process scalability; generation of gases (oxygen and hydrogen) occurs simultaneously in the same reactor and complicates the separation of gases. Potential to enhance surface area through metasurface design of electrode.
Photoelectrochemical (PEC) water splitting	Low investment cost, sustainable technology, combines the advantage of photolysis and electrochemical systems, eco-friendly and promising technology, hybridisation of semiconducting oxides with noble metals is expected to provide the enhancement of photoelectrochemical performance.	Owing to a limited light gathering, energy loss related to rapid recombination of photoinduced hole-electron pairs, as well as electrode degradation, low energy conversion efficiency, and low TRL level (not ready yet for medium to large scale applications). Potential to enhance surface area through metasurface design of electrode (anode).



output i.e., hydrogen in this case.<sup>[90]</sup> The stages for hydrogen production which contribute to the carbon emissions are as follows: (1) resources/raw materials, (2) inter-operation transportation, (3) production, (4) purification, (5) storage or compression, (6) end-use, and (7) waste treatment during hydrogen utilisation (Figure 9).

In the previously studied literature,<sup>[91–93]</sup> it has been feasible to conduct the LCA analysis of hydrogen generation starting from raw-materials to its storage or compression and is termed as cradle-to-gate system boundary. Nevertheless, aiming towards sustainable and eco-friendly hydrogen production (green hydrogen) in future, a combination of renewables (solar-PV, solar thermal, wind, hydro, nuclear and bio) and emission-free methods such as electrolysis is the most favourable choice (note: bio-resources based hydrogen production is termed green only if it is through the electrolysis route, however, bio-methane reformation still has high carbon intensity and needs carbon capture and storage (CCS) integration for emission reduction). Other methods such as steam methane reformation or SMR (using natural gas) have significant emission levels and require CCS integration for emission reduction.<sup>[39]</sup>

The wind-based electrolysis has the least global warming potential (GWP). Spath and Mann (2004)<sup>[91]</sup> estimated from the LCA of wind-electrolysis that most (~78%) of the GWP contributions come from the manufacturing and operation of wind turbines. Hydrogen storage and compression account for 17.6%, whereas 4.4% comes from the electrolysis operation. Solar technologies have a high GWP associated with the manufacturing processes. Biomass electrolysis has a higher GWP of the overall process. An important aspect while considering the GWP of green hydrogen technologies is grid integration. Without renewables, the grid-based electrolysis has an extremely high GWP (~31 kg CO<sub>2</sub>eq/kg H<sub>2</sub>). Studies suggest that up to 90% of emissions can be reduced by replacing renewable electricity with grid electricity. Steam methane reformation of natural gas which is mostly used for hydrogen production presently has a high GWP of ~10 kg CO<sub>2</sub>eq/kg H<sub>2</sub>, however, CO<sub>2</sub> emissions can be reduced by ~65% by integrating with CCS.<sup>[93]</sup> Green hydrogen is expected to become cost-competitive in the future due to rising demands stimulated by the increase in renewable electricity production. Besides carbon footprint, the green hydrogen production technologies have

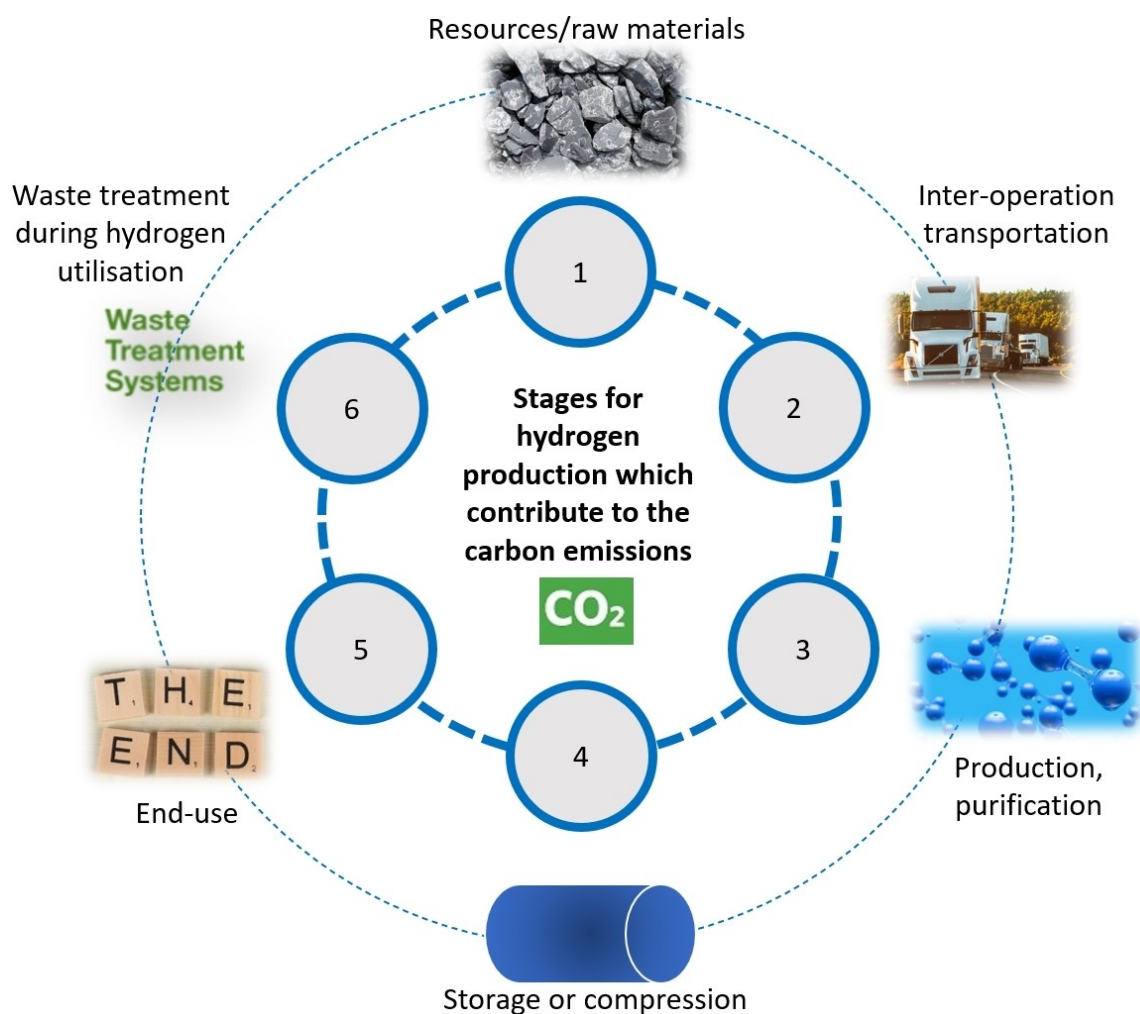


Figure 9. Stages for hydrogen production which contribute to the carbon emissions (authors original image).

other environmental degradation factors such as water consumption,<sup>[93]</sup> hazardous waste generation,<sup>[94]</sup> and acidification potential.<sup>[95]</sup>

There is a need to cut carbon footprint to manufacture electrolyser catalysts and corrosion resistant protective layers. As underlined by Viswanathan et al. (2021),<sup>[86]</sup> thermal spray techniques could lead to improved productivity compared to other manufacturing processes and could also prolong parent materials' life if appropriately designed. It has been suggested that when combined with other techniques such as additive manufacturing (AM), thermal spraying could play a key role in lowering energy consumption and feedstock material usage, thereby potentially reducing the carbon footprint which would help tackling the issue of climate change.

## 4. Thermal spray coatings for electrolysers

This section presents specific examples of catalysts, transport and corrosion resistant protective layers manufactured using thermal spray coating techniques and characterised for various catalytic and transport characteristics to produce hydrogen through electrolytic routes. Wherever relevant, limitations of specific thermal spray variants are highlighted to emphasize the fact that not all thermal spray techniques maybe suited to deposit every material of interest and vice-versa.<sup>[17]</sup>

### 4.1. Thermal spray coatings for proton exchange membrane (PEM) electrolysers

As summarised by Lettenmeier et al. (2017),<sup>[96]</sup> considering bipolar plate's key requirements in PEM electrolysers (i.e., high currents and small contact resistances), the electrical and thermal conductivities of the plates should be appropriate. On the anode and the cathode side it should separate the gases, and should transfer current from anode to cathode side. It should also transport the produced gases. The cathode should be resistant to embrittlement and oxidation, whereas the anode should be corrosion resistant against oxygen in acidic media and voltages up to 2 V. Considering porous transport layer (PTL), current collector (CC) or gas diffusion layer (GDL) key requirements in PEM electrolysers, the layer should (i) transport electrons from the catalytic layer to the bipolar plate, (ii) transport gases produced at the electrode, and (iii) distribute water towards the electrode. The layer should (i) be resistant to corrosion for voltages up to 2 V, (ii) have suitable porosity and pore size, (iii) be mechanically stable against hydrogen embrittlement from cathode cross-over, (iv) have a low thickness for optimal removal of resulting gases, and (v) have low resistance to the anode catalyst layer and bipolar plates. On the cathode side of current collector, usage of carbon paper is the state-of-the-art technique, however fine stainless steel fibers, sintered plates and meshes can also be used. Since cathode has moderate conditions during electrolysis, based on the literature the consideration has been to develop better thermal spray coating materials for the anode only. It is known that pore size

and porosity affect the electrical resistance of the current collector (i.e., with a decrease in pore size and porosity, current collector electrical resistance decreases). The porosity and pore size can be adjusted by the suitable choice of the titanium (Ti) particles with the use of sintered materials, but the possibilities for their upscaling are very limited (Lettenmeier et al., 2017).<sup>[96]</sup> On the other hand, meshes, fibers and foams are less limited in terms of thickness and shape, and also cheaper to manufacture, but pore size and porosity control are more complex.

In their pioneering work for PEM electrolyser, Gago et al. (2016)<sup>[97]</sup> and Lettenmeier et al. (2017)<sup>[96]</sup> proposed corrosion-resistant stainless steel bipolar plates (BPP) to reduce the cost of the stack. The BPP were coated with Ti/Titanium (using vacuum plasma spraying (VPS), 60  $\mu\text{m}$  thick layer), and then a new 1.8  $\mu\text{m}$  thin layer of Pt using magnetron sputtering on top of Ti was developed to prevent its passivation. Gago et al. (2016)<sup>[97]</sup> proposed that the Ti layer thickness could be further reduced to 30  $\mu\text{m}$  to minimise the overall production costs. Lettenmeier et al. (2017)<sup>[96]</sup> proposed stainless steel BPP coated with Ti (using VPS, 50–60  $\mu\text{m}$  thick layer), with a 1.5  $\mu\text{m}$  thin layer of Pt using magnetron sputtering on top of Ti and evaluated properties for more than 1000 h of electrolyser operation at 1  $\text{A cm}^{-2}$ . These preliminary works by Gago et al. (2016)<sup>[97]</sup> and Lettenmeier et al. (2017)<sup>[96]</sup> established that thermally sprayed Ti coatings can fully protect the stainless-steel substrate (or BPP) and that the Pt surface modification can allow achieving a cell performance comparable to the baseline.

In continuation to their previous work, Lettenmeier et al. (2017)<sup>[98]</sup> proposed the use of stainless-steel bipolar plates (BPP) coated with Nb/Niobium (using magnetron sputtering, 1.4  $\mu\text{m}$  thick layer) and Ti/Titanium (using vacuum plasma spraying (VPS), 50  $\mu\text{m}$  thick layer). Lettenmeier et al. (2017)<sup>[98]</sup> proposed Nb due to its superior corrosion protection properties and stable behaviour in an acid environment, including its abundance in the earth crust (like Cu, Sn or Zn). Coating analysis of the stainless-steel BPPs on the anode side of the cell indicated that the thin Nb layer can decrease the contact resistance by almost one order of magnitude (but showed cracking and delamination due to  $\text{H}_2$  embrittlement), whereas Ti coating can protect the stainless-steel substrate against corrosion, as no corrosion of the stainless-steel at the end of the test was observed. Combination of Nb/Ti-coatings onto stainless steel bipolar plates indicated promising application of such PEM electrolyser for more than 1000 h of electrolyser operation under nominal conditions (of 1  $\text{A cm}^{-2}$ ,  $6.5 \times 10^5$  Pa balanced pressure and 38  $^\circ\text{C}$ ). It was suggested by Lettenmeier et al. (2017)<sup>[98]</sup> that such dual-layer coatings could be promising for usage in harsh environments and could reduce the cost of BPP than the state-of-the-art Ti-based ones coated with Pt or Au. Lettenmeier et al. (2017)<sup>[98]</sup> also proposed that Nb dense coating using VPS is possible as magnetron sputtering requires long deposition times and consumes significant electricity for thick layer deposition. Lettenmeier et al. (2017)<sup>[96]</sup> suggested that in VPS, the absence of oxygen during the spraying facilitates and prevents the formation of high purity semi-conductive titanium oxides (i.e.,  $\text{TiO}_x$ ).

As shown in Figure 10 for the PEM electrolysis, Lettenmeier et al. (2017)<sup>[96]</sup> also developed a porous transport layer of titanium (on existing titanium microporous layer) by VPS. Overall, Lettenmeier et al. (2017)<sup>[96]</sup> found that by controlling the VPS process parameters, dense and protective layers as well porous structures for use as porous transport layers can be produced. It was also possible to produce a protective and highly conductive coating for BPP. By reducing VPS enthalpy, it was also seen possible that the powder material can be partially melted for use as the porous transport layer. It was also observed that the coatings were able to improve the long-term stability of the electrolyser.

#### 4.2. Thermal spray coatings for anion exchange membrane (AEM) electrolysers

Wang et al. (2019)<sup>[99]</sup> developed plasma-sprayed electrodes without any precious metals for an AEM electrolyser for operation at 60 °C and 1 M KOH electrolyte, as shown in Figure 11. With NiAlMo electrodes, it was observed that the electrolyser at a current density of 2 A.cm<sup>-2</sup> can achieve a potential of 2.086 V (comparable to the performances of industrial MW-size PEM electrolysers, which means a cost-effective alternative to this technology is possible). Observation also indicated that at the same current density, the cell potential with NiAl anode and NiAlMo cathode was 0.4 V higher, and it kept a stable operation for more than 150 h.

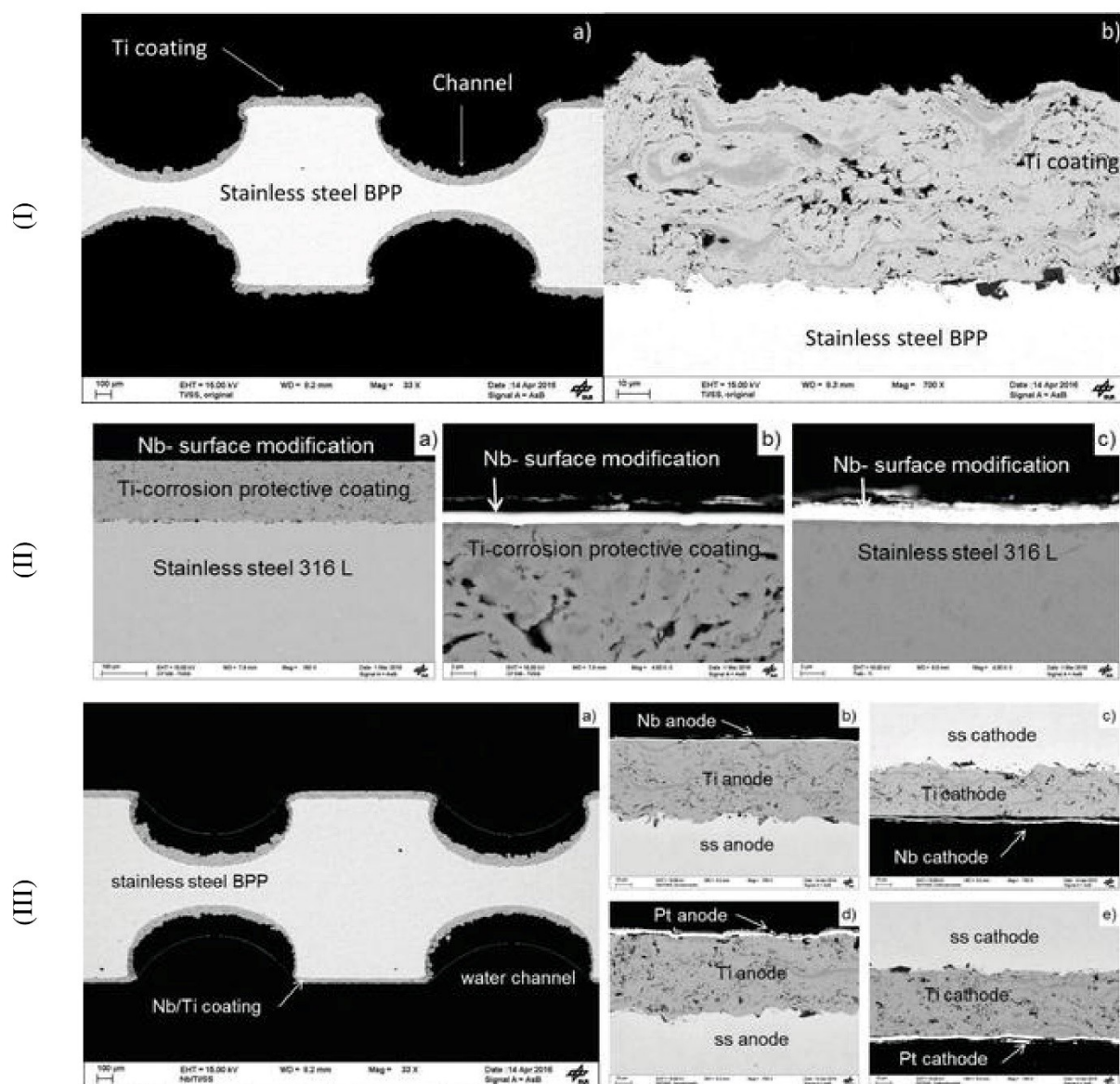


**Figure 10.** SEM images of vacuum plasma sprayed PEM electrodes: (I) (a) coated stainless steel bipolar plates with flow field channels, (b) cross-section of Ti coating, (II) (a) and (b) Nb/Ti coating on to stainless-steel, (c) Nb coating on to stainless steel, (III) post-mortem images. (a) overview, (b) Nb/Ti/ss anode, (c) Nb/Ti/ss cathode, (d) Pt anode/ss anode, (e) Pt/Ti/ss cathode (reproduced under the terms of the Creative Commons Attribution 3.0 license).<sup>[96]</sup> Copyright (2017), IntechOpen Limited.



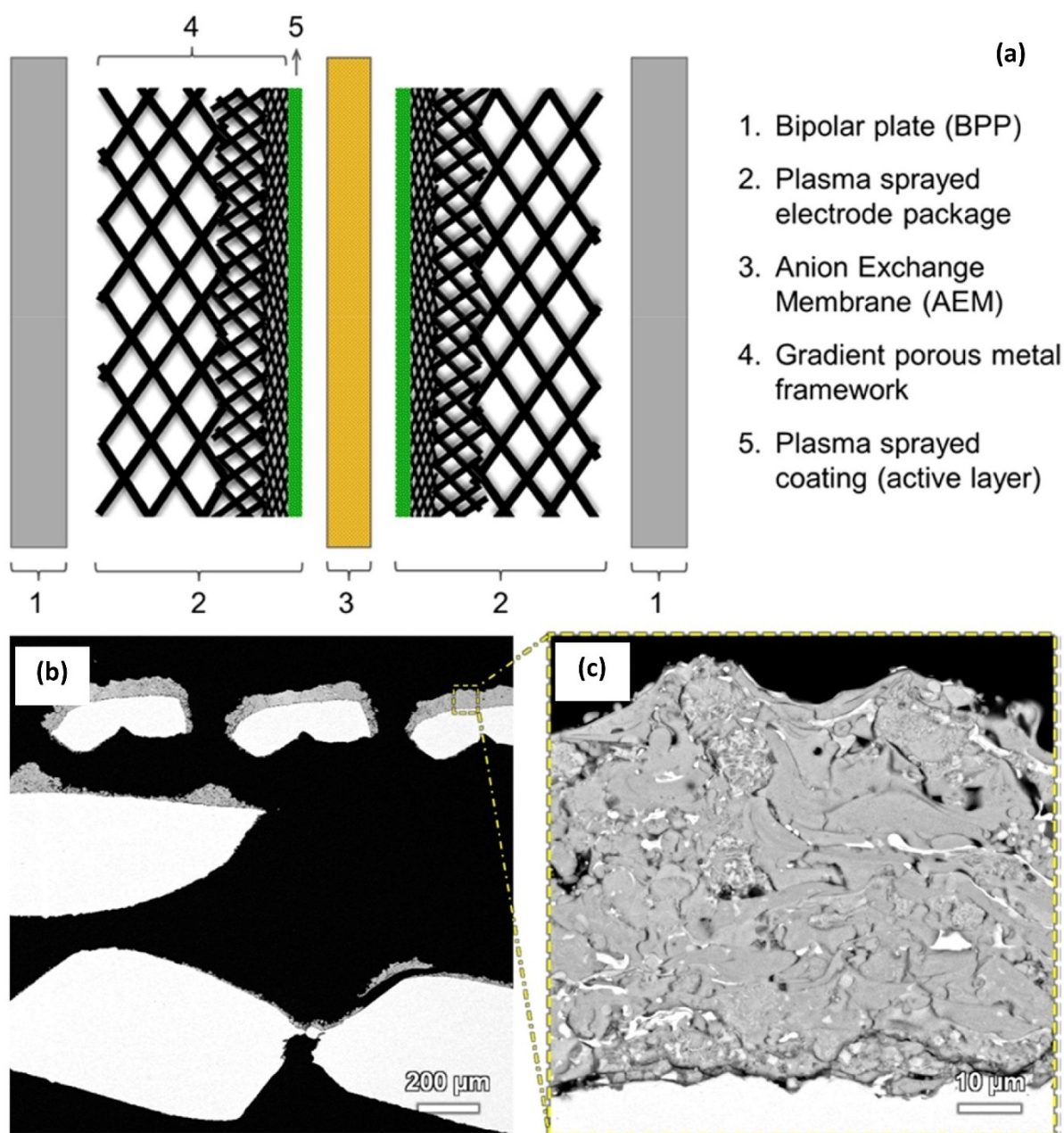


**Figure 11.** AEM electrolyser: (a) schematic diagram showing the plasma-sprayed electrode. (b) cross-section image of Ni–Al–Mo electrode (showing the catalytic layer (in grey) and the gradient porous metal framework (in white) which acts as current collector and mass transportation layer), and black region indicate the void space; (c) cross-sectional view of the catalytic layer (reproduced with permission).<sup>[99]</sup> Copyright (2019), American Chemical Society.

The operation of an AEM water electrolysis with pure water is challenging and to combat this, Razmjooei et al. (2021)<sup>[100]</sup> developed a novel approach for increasing performance in such electrolysis by introducing a backing layer on a porous transport layer (PTL), shown in Figure 12. By using the APS technique, Razmjooei et al. (2021)<sup>[100]</sup> for the first time developed the PTLs by introducing a highly porous 100  $\mu\text{m}$  thick Ni-based (Ni/C 80:20 wt%) microporous layer (or NiMPL) on top of a porous PTL made of stainless steel and observed the current density of  $0.5 \text{ A cm}^{-2}$  at a very low operating voltage of 1.90 V, which was 290 mV lower than that of uncoated bare PTL.

Analysis indicated that the combination of varied pore sizes (small, big) present in the coatings played an important role in the effective exchange of gases and water. This means, the high porosity with a large pore-size distribution and a low tortuosity, all led to a reduction of capillary pressure, which efficiently removed the gas bubbles formed at the membrane electrode assembly (MEA) surface. This means, the well-tuned NiMPL-PTL microporous layer reduced the total resistances, including both ohmic and mass transfer, leading to improved performance with pure water.

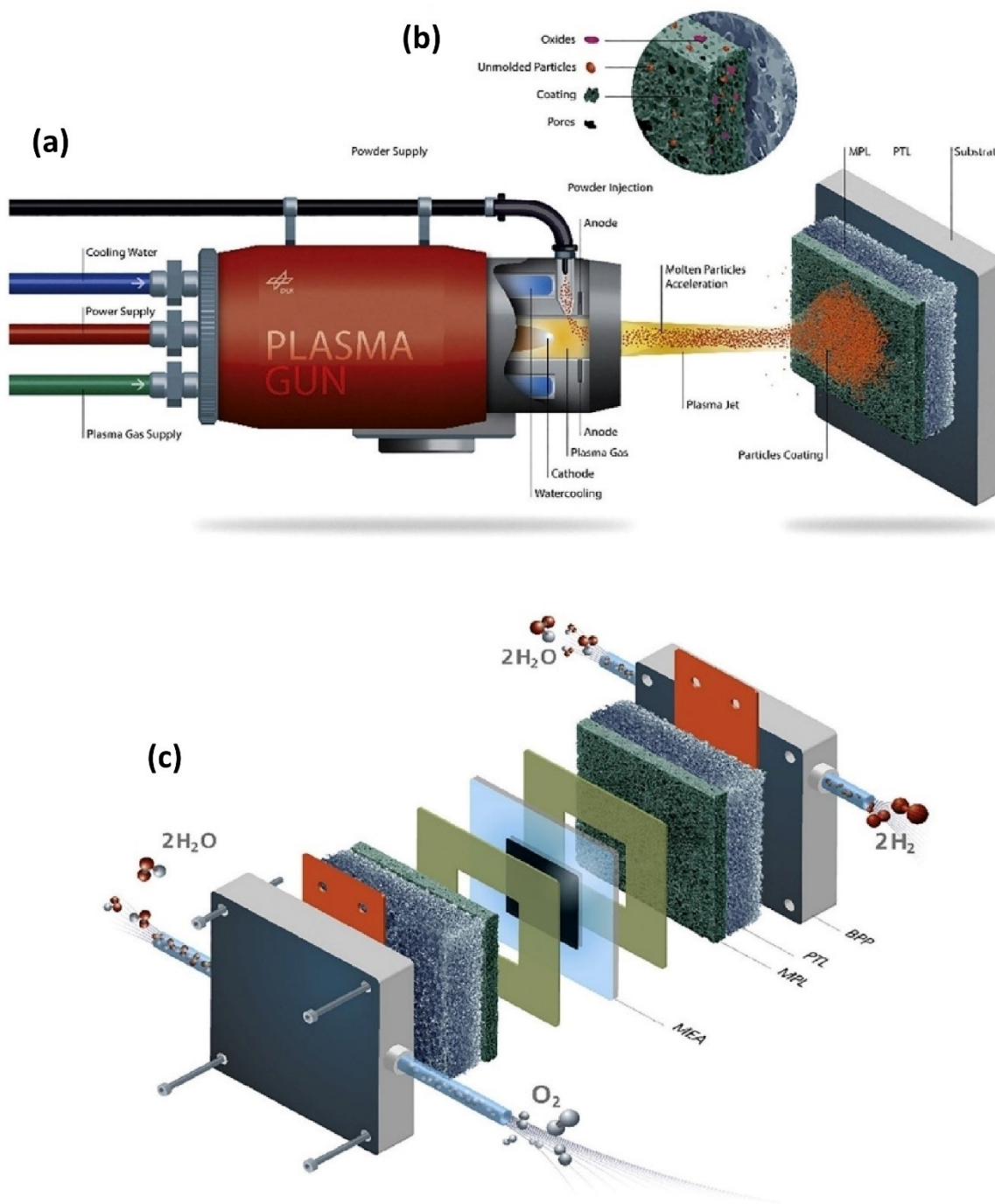


**Figure 12.** NiMPL fabrication scheme and anion exchange membrane (AEM) water electrolyser cell assembly: (a) APS coating of NiMPL on PTL, (b) a blown-up view of the plasma sprayed NiMPL, and (c) AEM cell configuration with NiMPL-PTLs (BPP: bipolar plates, PTL: porous transport layer, MPL: microporous layer, MEA: membrane electrode assembly) (reproduced under the terms of the Creative Commons CC-BY license).<sup>[100]</sup> Copyright (1969), Elsevier.

### 4.3. Thermal spray coatings for alkaline water electrolyzers (AWE)

In their pioneering work, for Chlor-alkali electrolytic cell, Coker and Argade (1977)<sup>[101]</sup> developed Ni metal coatings (using flame and plasma spraying techniques) and WC-12%Co coatings (25  $\mu\text{m}$  to 150  $\mu\text{m}$  thick) onto steel substrate (cathode) to reduce the hydrogen production overvoltage. In their cell

assembly, asbestos-deposited diaphragm or a synthetic polymeric diaphragm (i.e., chloro-substituted perfluorinated polymers, perfluorinated polymers, sulfonated polymers) were used. The improved electrocatalytic activities were related to the increased surface area of electrodes and efficient release of hydrogen bubbles were related to sprayed surface roughness or unevenness. While Coker and Argade (1977)<sup>[101]</sup> preferred Ni metal powder metal for the cathode (with criteria that the

selected metal powder is sprayable and has a lower hydrogen overvoltage than the cathode material) but indicated that other metals or alloys of these metals can be used (e.g., cobalt, nickel, platinum, molybdenum, tungsten, manganese, iron, tantalum, niobium), including the metallic compounds such as tungsten carbide and iron nitride, as well as a mixture containing graphite.

Hall (1984)<sup>[102]</sup> investigated plasma-sprayed Ni coatings for cathodes and found that it was much more efficient in alkaline electrolytes than either uncoated cathodes or cathodes with porous sintered Ni coatings. Plasma-sprayed Ni cathode coatings manufactured with fine and high surface area Ni powder produced hydrogen evolution overpotentials (0.10–0.14 V). Hall (1984)<sup>[102]</sup> indicated that the degree of coating oxidation (highly oxidised nickel surfaces) was the main factor influencing the hydrogen evolution overpotentials (i.e., efficiency improvement) at either the plasma-sprayed or sintered nickel cathode coatings, and not due to either superior coating morphology or increased surface area. Further on, for AWE applications, Henne, Schnurnberger and Weber (1984)<sup>[103]</sup> fabricated porous Raney Ni electrodes (Ni–Al alloy (50:50 weight ratio)) by low pressure plasma spraying (LPPS) technique. During electrochemical testing at a current density of 600 mAcm<sup>-2</sup> and 180 °C operating temperature, an IR-corrected decomposition potential of about 1.5 V was obtained.

Using the vacuum plasma spraying (VPS) technique, Schiller and Borck (1992)<sup>[104]</sup> developed electrode coatings for AWE. The oxide electrocatalysts Co<sub>3</sub>O<sub>4</sub> spinel and Raney Ni/Co<sub>3</sub>O<sub>4</sub> layers were coatings for anodic oxygen evolution, whereas Raney Ni and Raney Ni/Mo layers for were coatings for cathodic hydrogen evolution. While analysing using IR-free polarization curves up to 1 Acm<sup>-2</sup> current densities and long-time tests (i.e., throughout 3000 h under continuous current loading of 0.5 Acm<sup>-2</sup>). It was found that the cathode layers exhibit over voltages of 70 mV to 90 mV at 1 Acm<sup>-2</sup> and 70 °C in 25% KOH solution, whereas composite anodes (Raney nickel/Co<sub>3</sub>O<sub>4</sub>) showed overvoltage values of 290 mV at 1 Acm<sup>-2</sup>. In their further work, Schiller, Henne and Borck (1995)<sup>[105]</sup> used vacuum plasma spraying (VPS) to develop high-performing electrodes for alkaline water electrolysis. For cathodic hydrogen evolution, Mo-containing Raney Ni coatings were applied, whereas for the anodic oxygen evolution reaction, Raney nickel/Co<sub>3</sub>O<sub>4</sub> matrix composite layers were applied. For the preparation of Raney Ni coatings, a precursor Ni–Al alloy was sprayed that had to be leached subsequently in a caustic solution to remove the Al content, forming a porous, high-surface-area Ni layer. While analysing IR-free polarization curves and long-time tests (under conditions of continuous and intermittent operation), the electrocatalytic activity of the electrode coatings showed excellent electrochemical properties. In their work, Schiller and Borck (1992)<sup>[104]</sup> and Schiller, Henne and Borck (1995)<sup>[105]</sup> to spray thermally sensitive oxide electrocatalysts (i.e., Co<sub>3</sub>O<sub>4</sub>), special process conditions involving plasma-chemical effects (reactive plasma spraying) was developed. Further on, Miousse, Lasia and Borck (1995)<sup>[106]</sup> studied vacuum plasma sprayed Ni–Al and Ni–Al–Mo electrodes and compared the effect of alkaline solutions (testing in 1 M NaOH and 25% KOH at 70 °C)

and found that Ni–Al–Mo electrode was more active in 25% KOH, whereas Ni–Al electrode was more active in 1 M NaOH solutions. The alternating current impedance measurements showed two semicircles on the complex plots which indicated that the formation of the second semicircle was related to the hydrogen evolution reaction (HER).

Fournier, Miousse and Legoux (1999)<sup>[107]</sup> used the wire-arc spray technique to deposit Ni based cathode coatings of various Ni/Al ratio on to the mild steel substrate. By leaching out the Al in concentrated KOH at 70 °C, high porosity electrodes were obtained. Following leaching, the HER was studied in 1 M NaOH at 25 °C and alternating current impedance measurements were carried and observed a stable electrode with very low overvoltage values ( $\eta_{250}$  down to 179 mV at 0.25 A/cm<sup>2</sup>). Such low overvoltages were related to the high porosity of the deposited coatings.

Irissou et al. (2002)<sup>[108]</sup> used the vacuum plasma spray (VPS) technique to deposit nanocrystalline Ti–Ru–Fe–O (2-1-1-2) (on Fe, Ti (with Ti/TiH<sub>2</sub> interlayer) substrate) as cathode for hydrogen evolution, though the electrolyser types was not immediately clear. The plasma deposited coating showed a significant proportion of Ti<sub>2</sub>O<sub>3</sub> (16.3 wt.%) and TiO (13.2 wt.%), however the preliminary analysis indicated that the electrocatalytic activity for hydrogen evolution of the coating was poor. This led to modification of the coating surface by the dissolution of the superficial titanium oxide layer (by etching in HF 10% at 25 °C) and increasing the effective surface area (see Figure 13<sup>[108]</sup>). The electrochemical testing of the modified cathode in chlorate electrolysis conditions (electrolyte similar to NaClO<sub>3</sub>: 550 g/l, NaCl: 110 g/l, NaClO: 1 g/l, pH 6.5, adjusted with NaOH and HCl) showed the overpotential of  $\eta_{250} = -550$  mV to  $-575$  mV. Irissou et al. (2002) suggested that careful optimisation of the etching process could lead to the dissolution of all Ti<sub>2</sub>O<sub>3</sub>, leading to a highly porous coating.

Birry and Lasia (2004)<sup>[109]</sup> developed vacuum (high frequency) plasma sprayed Ni–Al–Mo coatings for alkaline water electrolysis. They used spray precursor alloys which were ball milled and synthesised at high temperature with stoichiometry as NiAl<sub>5</sub>Mo<sub>2</sub> (T), NiAl<sub>8</sub>Mo (G), NiAl<sub>7.5</sub>Mo<sub>1.5</sub> (H), NiAl<sub>5</sub>Mo<sub>0.67</sub> (I), 46% NiAl<sub>3</sub> + 54%Ni<sub>2</sub>Al<sub>3</sub> (B) and the mixtures 25–75% of T + B; following which the precursors were treated with an alkaline solution to leach out Al. Birry and Lasia (2004)<sup>[109]</sup> found that active stable Raney Ni–Mo electrodes can be obtained from Al rich alloys. The HER was studied in 1 M KOH at 25 °C and electrochemical impedance spectroscopy (EIS) was carried out to determine electrochemical activities. It was observed that due to an increase in the real surface area along with catalytic effect of Mo, the vacuum plasma sprayed Ni–Al–Mo coated layers were more active than those prepared by alloyed powder (heating Ni and Al powders) with similar compositions, however, the ternary phase (NiAl<sub>5</sub>Mo<sub>2</sub> (T)), which was suggested to be responsible for high activity, was not stable enough and disintegrated during leaching. However, electrodes prepared with the addition of this ternary phase (NiAl<sub>5</sub>Mo<sub>2</sub> (T)) were stable and active.

Kellenberger et al. (2007)<sup>[110]</sup> used Ni–Al and NiTi–Al wires and deployed wire arc spraying technique to fabricate electro-



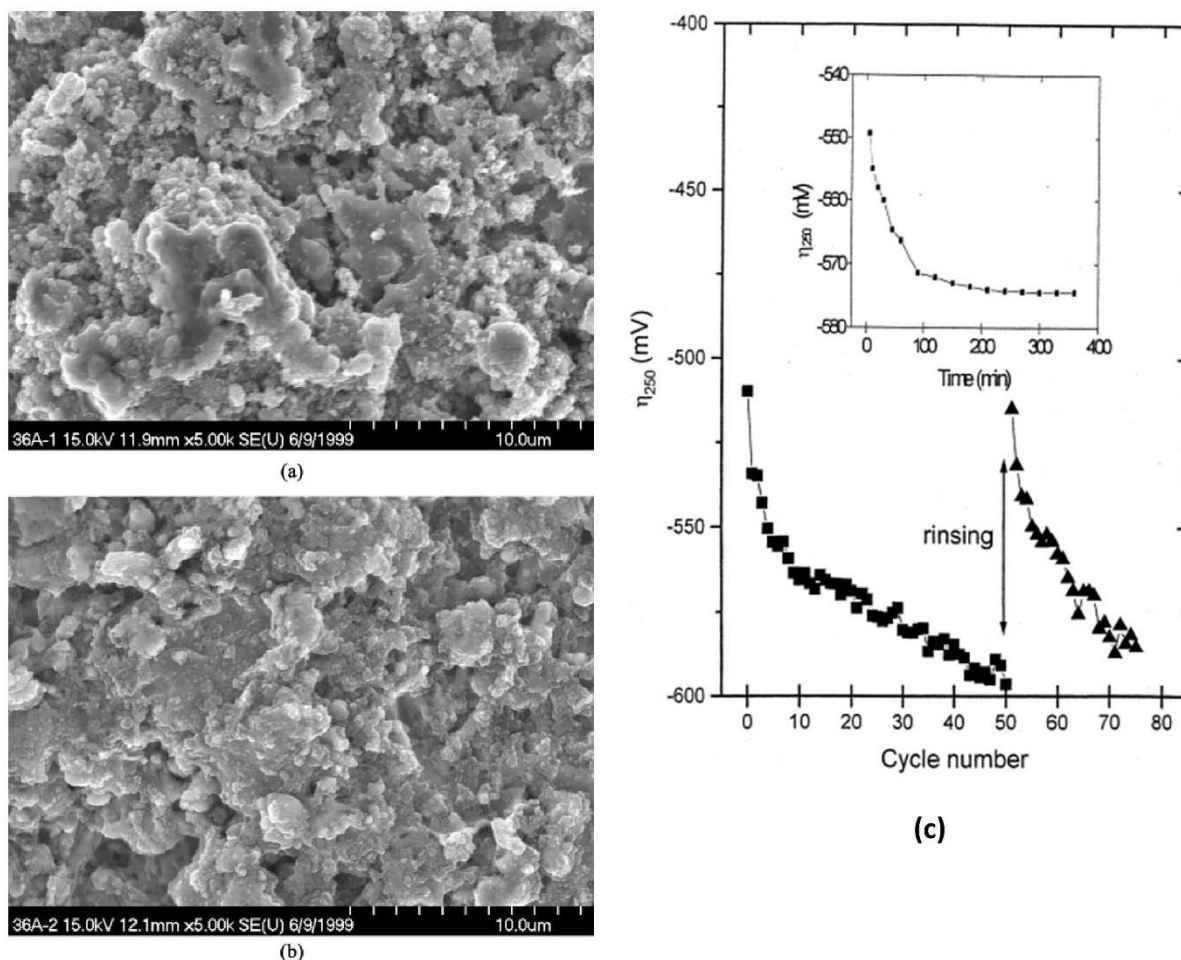


**Figure 13.** Microscopic images of vacuum plasma sprayed Ti–Ru–Fe–O (2-1-1-2): (a) as-deposited, (b) etched in HF 10% at 25 °C for 40 min, and electrochemical analysis showing (c) cathodic overpotential variation against the number of cycles (reproduced with permission).<sup>[108]</sup> Copyright (2002), Elsevier.

active coatings on steel substrates. The coatings were then treated with alkaline 1 M NaOH solution at 80 °C to leach out the Al. Electrochemical testing in 1 M NaOH solution indicated that the increased activity for the hydrogen evolution reaction (HER) is due to an increased real surface area in the case of the skeleton Ni electrodes and the catalytic effect of Ti in the case of the skeleton NiTi electrodes. The EIS indicated the presence of two potential-dependent semicircles (related to the hydrogen evolution reaction kinetics) at reduced hydrogen evolution reaction overpotentials.

As shown in Figure 14, Chade et al. (2013)<sup>[111]</sup> developed air plasma sprayed Raney Ni electrodes of three coating thicknesses 30 μm, 100 μm and 300 μm. Following electrochemical activation, the HER was studied using potentiodynamic Tafel in 30% KOH solutions over 30 °C to 80 °C and EIS was carried to determine their electrochemical activities. The best electrocatalytic activity towards HER was obtained for a 100 μm thick coated electrode, with 96% efficiency (based on the higher heating value for H<sub>2</sub>) at 300 mAcm<sup>-2</sup> current density and 70 °C, attributed to the very high electroactive area as well as enhanced kinetics on the sprayed surface.

As summarised by Aghasibeig (2015),<sup>[112]</sup> and in most of these studies above, the focus was on increasing the intrinsic activity and the real surface area of thermally sprayed electrodes by producing coatings of Raney Ni, Ni–Mo and Raney Ni–Mo alloys. Nevertheless, the effect of the other factors (e.g., thermal spray process parameters) and surface modifications on the activities of the electrodes was not always investigated. Besides additional rinsing steps and producing more waste, it is well known that the application of Raney Ni as the electrode material requires using high concentrations of hazardous caustic solutions for the leaching process at high temperatures. Also, in some of these studies above, the AWE process was conducted at high temperatures to increase the electrolyte conductivity and promote bubble detachment from the surface, which gives rise to a higher operating cost (if correlated with the electricity consumption) as well a reduction in the lifetime of the electrolyser components due to a potential corrosion. Additionally, Aghasibeig (2015)<sup>[112]</sup> proposed that the issue related to the gas bubble resistances at the electrode surface could be resolved by modifying surface profiles which can be

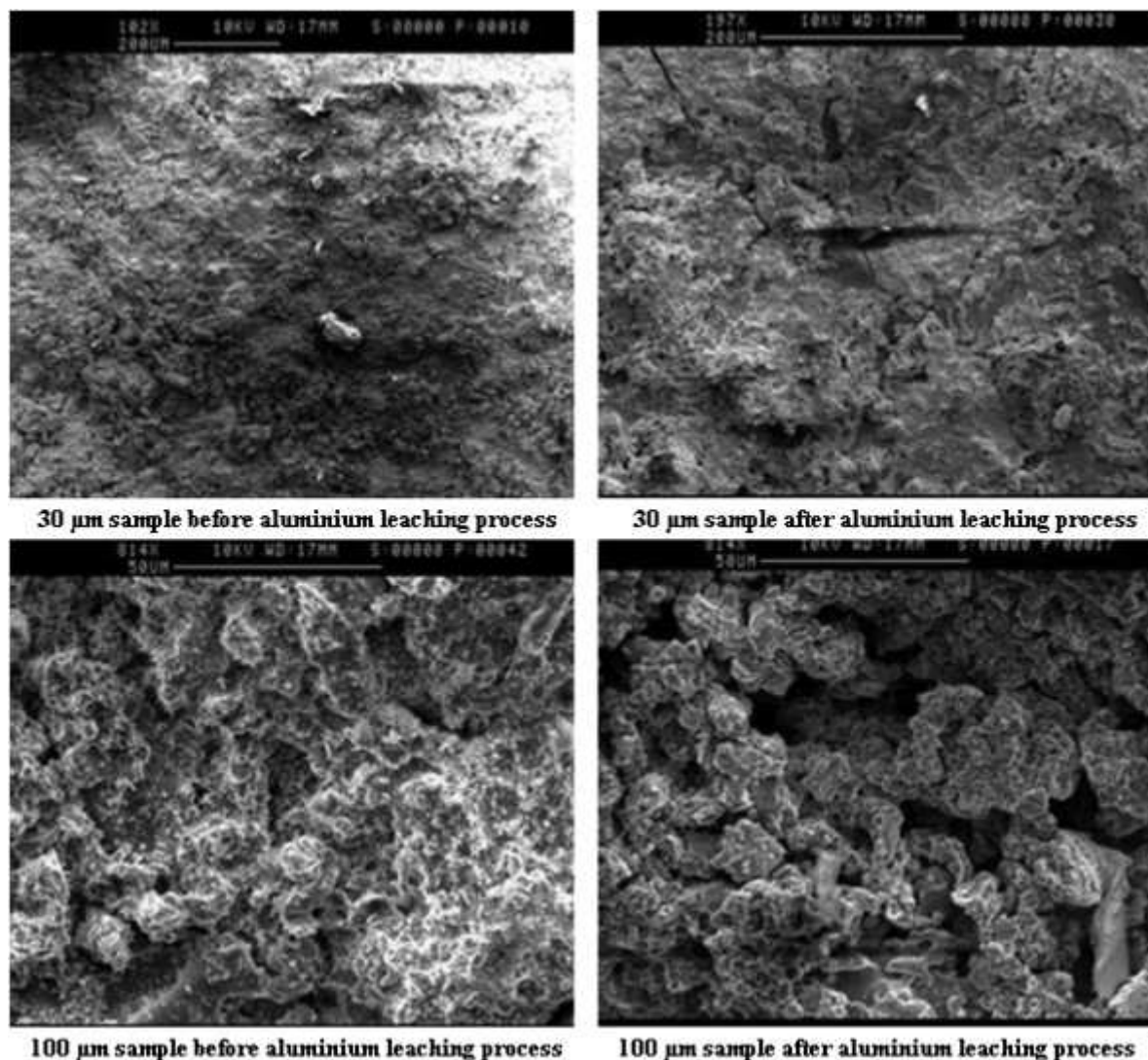


**Figure 14.** Microscopic images of 30 μm and 100 μm thick Raney Ni electrodes before (left) and after (right) chemical activation (reproduced with permission).<sup>[111]</sup> Copyright (2013), Elsevier.

possible by optimisation of the thermal spray coating processes.

Therefore, the objectives of Aghasibeig et al. (2014)<sup>[113]</sup> and Aghasibeig et al. (2016)<sup>[114]</sup> work were to develop Ni-based electrode coatings with enhanced surface areas for the HER using thermal spray techniques. Aghasibeig et al. (2014)<sup>[113]</sup> and Aghasibeig et al. (2016)<sup>[114]</sup> used atmospheric plasma spray (APS) and suspension plasma spray (SPS) techniques, where the effect of process parameters on the electrochemical active surface areas of the coated electrodes was investigated. Analysis by Aghasibeig et al. (2014)<sup>[113]</sup> demonstrated that coatings deposited by SPS exhibited a larger electric double layer capacitance (ECDLC) compared to those deposited by APS. Higher surface areas were also observed for all SPS deposits compared to those deposited using APS, attributed to the formation of fine porous agglomerates on the surface of the SPS coatings. Also, the most significant processing factors affecting the electrochemically active surface areas of the

coatings were standoff distance in APS and current in SPS techniques. Microstructurally, the development of larger surface areas was related to the deposition of semi-molten and re-solidified particles and formation of more porous structures during thermal spraying.

Applying the know-how from their previous work, in a novel application of combined APS and SPS technique to deposit Ni as cathode for AWE (i.e., SPS layer deposited on top of APS layer), Aghasibeig et al. (2016)<sup>[114]</sup> observed the highest electrocatalytic activity for electrode coated by the combined method with the exchange current density and overpotential ( $\eta_{250}$ ) values of  $6.2 \times 10^{-4}$  A/cm<sup>2</sup> and  $-386$  mV, respectively. The high electrocatalytic activity was attributed to its large specific surface area with a high surface roughness which comprised a multiscale micron/submicron-sized surface structure. Aghasibeig et al. (2016)<sup>[114]</sup> suggested that the dual microstructure of cathode and its super-hydrophilic behaviour enhanced the activity by providing more reaction sites for hydrogen adsorp-

tion, promoting the diffusive mass transport of the reactants, and facilitating hydrogen bubble ascension from the pores. It was clear from their investigation that the application of such combined APS-SPS method could be useful for materials with higher activities such as Raney Ni or Ni–Mo alloys, to increase the efficiency of the electrolysis process.

Kim et al. (2018)<sup>[115]</sup> and Kim et al., (2019)<sup>[116]</sup> fabricated the Raney Ni electrode using the APS method on to Ni-disc substrate (20 mm dia., 0.6 mm thick), and the Ni–Al alloy (50:50 weight ratio) sprayed coating contained a NiAl phase. Electrochemical measurements using 3-electrode system (counter electrode: Ni, reference electrode: Hg/HgO) were made in a 1 M KOH alkaline electrolyte. In the alkaline solution it had very slow Al leaching rate or did not leach. Through hydrogen and temperature heat treatment of the electrode, an enhancement in the uniformity of Al distribution, as well as adhesion of the coating to the substrate, was observed. Through heat treatment, the electrode becomes structurally vulnerable to deactivation (carried at a constant current density of  $-400 \text{ mA/cm}^2$  for 12 h) and the performance of HER did not increase (Tafel slope of 54 mV/dec and overvoltage of 108 mV at  $300 \text{ mA/cm}^2$  was observed). By increasing the operating temperature, the electrolyte ionic conductivity increased as well as enhanced the electrode surface kinetics; thus, the overpotential for HER decreased.<sup>[116]</sup>

#### 4.4. Thermal spray coatings for solid oxide water electrolyzers (SOWE)

Considering key requirements, in SOWE electrolyzers, the two electrodes (anode, cathode) and solid oxide electrolytes should be able to operate at high temperatures and split water to produce hydrogen. Some of the earlier work<sup>[59,117]</sup> provide an overview about how hydrogen production could be made possible by using nuclear heat (high temperature electrolysis of steam or HTES) which was at that time limited to the field of electric generation.

For tubular cell design, Hino et al. (1997)<sup>[117]</sup> fabricated gas tight  $\text{Al}_2\text{O}_3$  layers of  $100 \mu\text{m}$  thickness (for sealing at interconnecting areas and prevent oxidation during cell operation) on the support tube using plasma spraying. The porous cathode of Ni cermet ( $80 \mu\text{m}$  to  $110 \mu\text{m}$  thick) was coated on the support tube by an acetylene flame spraying. Following the gas-tight electrolyte layer of  $\text{Y}_2\text{O}_3$ -stabilized (8 mol%)  $\text{ZrO}_2$  ( $100 \mu\text{m}$  to  $150 \mu\text{m}$  thick) was plasma sprayed at low-pressure on the cathode. The anode layer (calcium or strontium-doped  $\text{LaCoO}_3$  or strontium-doped  $\text{LaMnO}_3$ ) was deposited on the electrolyte and interconnection layers up to  $200 \mu\text{m}$  thick by the acetylene flame spraying. The interconnection (i.e., Ni–Al layer of  $250 \mu\text{m}$  thickness) at both ends of the support was fabricated by the plasma spraying. In such earlier fabrication and testing up to  $950^\circ\text{C}$ , Hino et al. (1997)<sup>[117]</sup> found that the electrolysis tube served only one thermal cycle and observed that a large part of anode layers was detached from the electrolyte layers. This failure at the interface indicated that thermal spray processing

needed improvement for enhanced adhesion of layers against thermal expansion difference of multi-layers structure.

Some other research includes, for example, Ansar et al. (2008)<sup>[118]</sup> where air plasma spraying (APS) was applied to develop perovskite-type LSM ( $\text{La}_{0.8}\text{Sr}_{0.2}\text{MnO}_3$ ) and LSCF ( $\text{La}_{0.6}\text{Sr}_{0.4}\text{Co}_{0.4}\text{Fe}_{0.6}\text{O}_3$ ) cathodes. The coatings were sprayed on pre-sprayed half cells consisting of plasma sprayed  $50 \mu\text{m}$  NiO + YSZ fuel electrode and  $40 \mu\text{m}$  9 mol% YSZ electrolyte fabricated on FeCrMnTi substrates (48 mm in diameter). While testing at a current density of  $1 \text{ A/cm}^2$ , water splitting voltage was reduced to 1.4 V at an operating temperature of  $800^\circ\text{C}$  and 1.28 V at  $850^\circ\text{C}$ . Considering the degradation behaviour, long-term electrolysis tests for 1500 hours were performed by monitoring the LSCF cell voltage change against time at  $800^\circ\text{C}$  and varied between  $750^\circ\text{C}$  and  $850^\circ\text{C}$  during V–I analysis, exhibited 3.2%/1000 h degradation rates.

As shown in Figure 15, Schiller et al. (2009)<sup>[119]</sup> developed metal supported cells by applying plasma deposition technologies (APS, VPS) for use as solid oxide electrolyser cells (SOEC) for high temperature steam electrolysis. The cell included a porous ferritic steel support, a diffusion barrier layer, a porous Ni/YSZ hydrogen electrode ( $50 \mu\text{m}$  thick coating) sprayed using APS, a solid YSZ electrolyte ( $40 \mu\text{m}$  thick coating) sprayed using VPS and a porous LSCF oxygen electrode ( $30 \mu\text{m}$  thick coating) sprayed using APS. The as-made cell was electrochemically characterised including a long-term test over 2000 h. The cell voltage during electrolysis operation at a current density of  $-1.0 \text{ A cm}^{-2}$  was 1.28 V at an operating temperature of  $850^\circ\text{C}$  and 1.4 V at  $800^\circ\text{C}$ . A long-term test run over 2000 h with a steam content of 43% at  $800^\circ\text{C}$  and a current density of  $-0.3 \text{ A cm}^{-2}$  showed a degradation rate of 3.2% per 1000 h.

O'Brien et al. (2010)<sup>[59]</sup> provided a detailed state-of-the-art about high temperature (e.g., via nuclear reactor) electrolysis using solid oxide cell component design, material, and assembly. O'Brien et al. (2010)<sup>[59]</sup> demonstrated straightforward scalability of the high temperature electrolysis for long term operation and hydrogen production. For small-scale tests at  $800\text{--}850^\circ\text{C}$ , the cell included interconnecting plates made from ferritic stainless steel. The steam/hydrogen flow fields were fabricated from Ni-foil, whereas the air-side flow fields were ferritic stainless steel. To improve cell performance, the air-side separator plates and flow fields were pre-surface-treated to form a rare-earth stable conductive oxide scale, and a perovskite rare-earth coating was considered as a bond layer to the separator-plate oxide scale by either plasma spraying (or screen printing). On the steam/hydrogen side of the separator plate, a thin ( $\sim 10 \mu\text{m}$ ) Ni-metal coating was applied as a bond layer. The stack electrolytes were scandia-stabilized zirconia ( $\sim 140 \mu\text{m}$  thick). The air-side electrodes (anode in the electrolysis mode) were a strontium-doped manganite. The electrodes were graded, with an inner layer of manganite/zirconia ( $\sim 13 \mu\text{m}$ ) immediately adjacent to the electrolyte, a middle layer of pure manganite ( $\sim 18 \mu\text{m}$ ), and an outer bond layer of cobaltite. The steam/hydrogen electrodes (cathode in the electrolysis mode) were also graded, with a nickel-zirconia cermet layer ( $\sim 13 \mu\text{m}$ ) immediately adjacent to the electrolyte and a pure nickel outer layer ( $\sim 10 \mu\text{m}$ ).



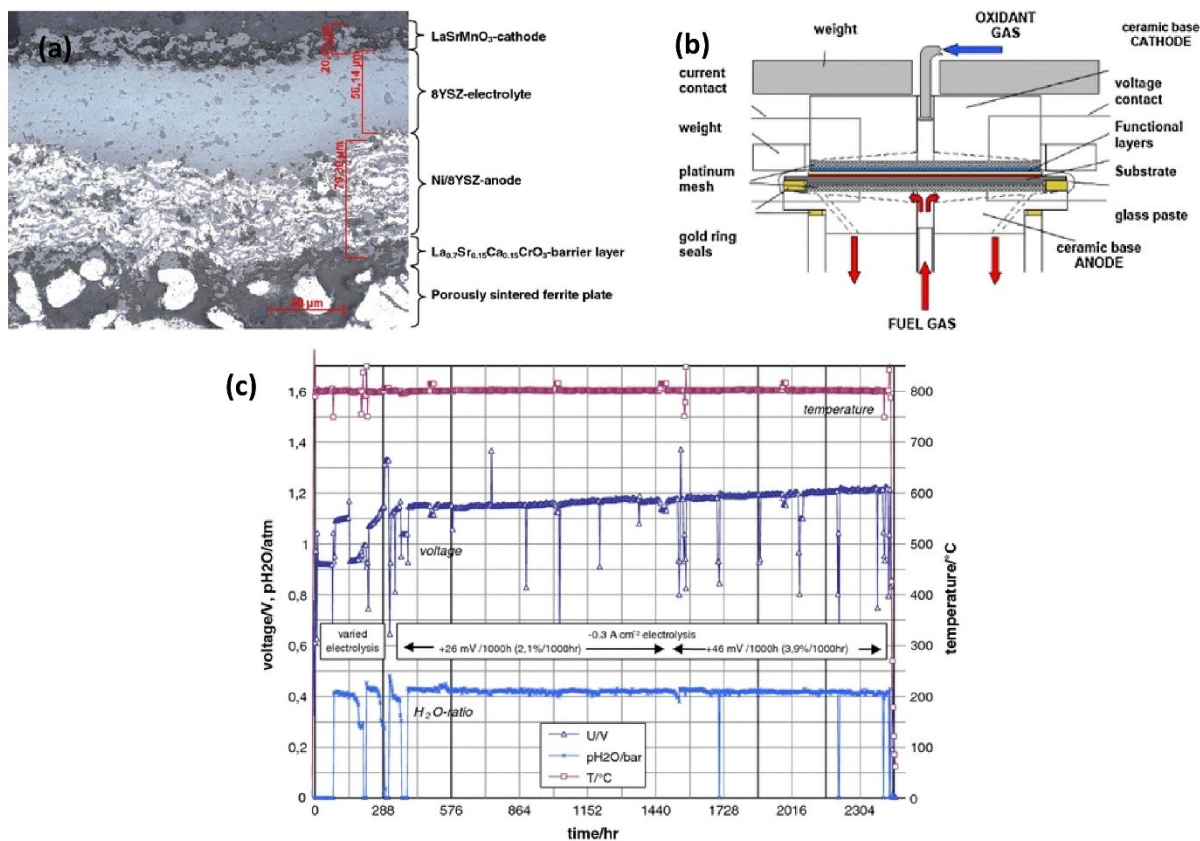


**Figure 15.** (a) Cross-section view of plasma sprayed SOWE cell, where diffusion barrier layer  $\text{La}_{0.7}\text{Sr}_{0.15}\text{Ca}_{0.15}\text{CrO}_3$  were deposited using plasma spraying or PVD process onto 1 mm thick ferritic steel plate,  $\text{H}_2$ -electrode (Ni/8YSZ layer) and  $\text{O}_2$ -electrode (LSCF layer) were deposited using air plasma (APS), whereas electrolyte (8YSZ layer) was deposited using vacuum plasma (VPS) technique, (b) set-up cross sectional view, and (c) long-term test run of cell with a continuous load of  $-0.3 \text{ A cm}^{-2}$  in electrolysis mode over 2000 h of operation (reproduced with permission).<sup>[119]</sup> Copyright (2008), Springer Nature.

As shown in Figure 16, Vardavoulis et al. (2021)<sup>[120]</sup> proposed the fabrication of free-standing solid oxide cells exclusively by APS thermal spray without the need of using any porous metallic support nor the need for a post-process heating treatment. Overall, five layers were deposited, which included spraying of the solid oxide cell layers on a porous metallic support, and then detachment of the solid oxide cell from the substrate. The layers were as follows (support electrode: composition Ni/NiO 50%-YSZ 50%, thickness 300–350  $\mu\text{m}$ , porosity 25–30%; support electrode/electrolyte transition layer: composition Ni/NiO 25%-YSZ 75%, thickness 100–120  $\mu\text{m}$ , porosity 20–25%; electrolyte: composition YSZ 100%, thickness 100–120  $\mu\text{m}$ , porosity < 5%, not connected; electrolyte/end electrode transition layer: composition 50% YSZ-50% LSM, thickness 80–100  $\mu\text{m}$ , porosity 20–25%; and end electrode: composition LSM 100%, thickness 70–90  $\mu\text{m}$ , porosity 25–30%). While the electrodes with adequate porosity were obtained, the purpose of intercalation of the transition layers was to facilitate the ionic motion and also to eliminate thermal expansion mismatches.

#### 4.5. Thermal spray coatings for thermochemical water splitting (TWS)

Though there may be many industrial examples, only a few works (mainly for nuclear Cu–Cl thermochemical cycle) have been reported or published where the application of thermal spray coatings for structural components has been deployed in such thermochemical water splitting for hydrogen production.

As an example, Siantar (2012)<sup>[58]</sup> used HVOF and APS methods to develop coatings (e.g., Diamalloy 4006 using HVOF method with thickness unknown, yttria stabilized zirconia/70  $\mu\text{m}$  thick & alumina/170  $\mu\text{m}$  thick using APS method) and investigated the immersion performance of coatings deposited on to substrates (i.e., Ni based super-alloy or Inconel 625, super austenitic stainless steel or AL6XN) exposed to molten CuCl at 500 °C up to 100 hours. Post-immersion test analysis indicated that the coatings were significantly damaged (in the form of delamination and cracks), and the cracks and pores provided pathways for the molten CuCl to penetrate under the coating-substrate interface leading to significant corrosion, dissolutions of metals and reduction of copper. In terms of materials immersion performance, the Inconel 625 substrate performed better than stainless steel AL6XN substrate, whereas, both Diamalloy 4006 and YSZ ( $\text{ZrO}_2$  18TiO<sub>2</sub> 10Y<sub>2</sub>O<sub>3</sub>) coatings provided

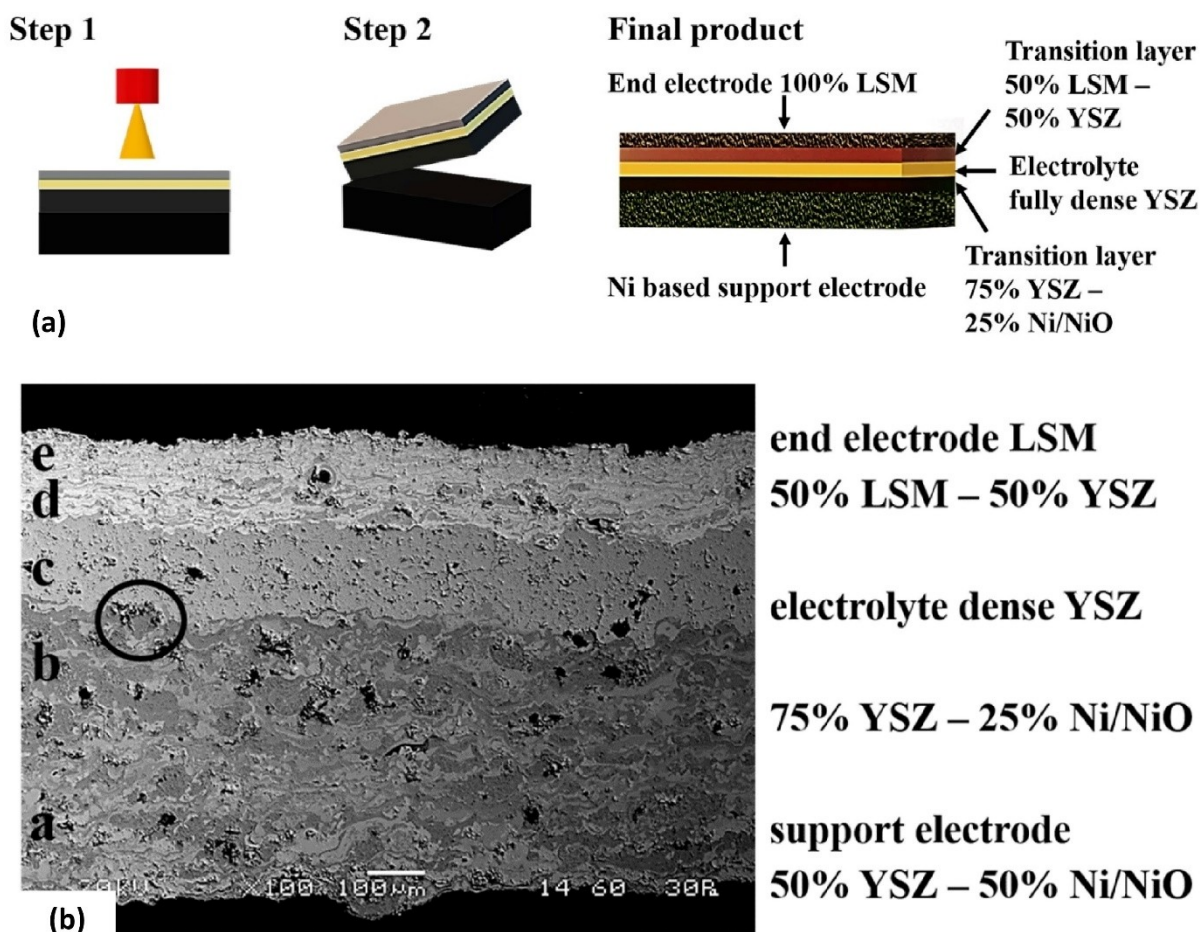


**Figure 16.** Fabrication of free-standing solid oxide cells by APS without the need of using any metallic porous support in final product: (a) step 1 shows net shape spray-forming which includes spraying of the solid oxide layers on a porous metallic support, and step 2 shows detachment of the solid oxide cell from the substrate, whereas final product shows five-layer structure of the solid oxide cell, and (b) microscopic image of the coatings cross-section (reproduced under the terms of the Creative Commons Attribution license).<sup>[120]</sup> Copyright (2021), MDPI.

better protection to the underlying base metal than alumina ( $\text{Al}_2\text{O}_3$  3TiO<sub>2</sub>) coating.

For Cu–Cl cycle electrolysis applications, using the HVOF technique, Azarbayjani, Rizvi and Foroutan (2016)<sup>[121]</sup> developed Ni-based alloy (i.e., Diamalloy 4006 or Ni-20Cr-10W-9Mo-4Cu-1B-1C-1Fe) metallic interlayer coating (and insulating YSZ top-coat, coating method not specified) which was deposited onto medium carbon steel 1045 substrate to evaluate coated sample integrity via immersion test in molten CuCl at 500 °C for a prolonged time. Characterisation and analysis demonstrated that medium carbon steel coated with only the YSZ layer is not suitable to survive even short exposure of 5-hour exposure to molten CuCl (means corrode immediately). However, YSZ coating with Diamalloy 4006 bond coat can provide better protection to the underlying base metal than only YSZ layer, as shown in Figure 17 (when tested for 48 hrs and 100 hrs), i.e., no deep cracks or corrosion observed. It was indicated that the complex mix of factors (e.g., the difference in the thermal expansion coefficient of different layers and substrate, thermal stress induced due to molten CuCl and some post-testing sample preparation) could have been the causes of coating

debonding and Diamalloy 4006 bond coat clearly helps protect the substrate and improved the adhesion between the ceramic topcoat and the metallic substrate.

Some detailed investigation can be seen elsewhere where various corrosion resistant thermally sprayed coatings were evaluated by immersion test in molten CuCl. Azhar (2016)<sup>[122]</sup> demonstrated that the bond coat of Diamalloy 4006 performed much better than the bond coat of super hard steel 9172, and that the alumina ceramic coat seemed to perform better than YSZ, but also indicated that the thermally sprayed method (HVOF, APS) may not be always suitable for molten CuCl corrosion application because of high porosity. In continuation to address the porosity related issues, Dsouza (2018)<sup>[123]</sup> proposed that better coating methods with porosities less than 1% should be tested in order to shield the substrate from the harsh molten CuCl environment and suggested that HVOF and APS coatings should be improved to reduce porosity in order to obtain a uniform and dense coating, including consideration of alternate material for their corrosion resistance capabilities.

Naterer et al. (2019)<sup>[46]</sup> tested the immersion corrosion properties (in CuCl at 500 °C) of coated medium carbon steel



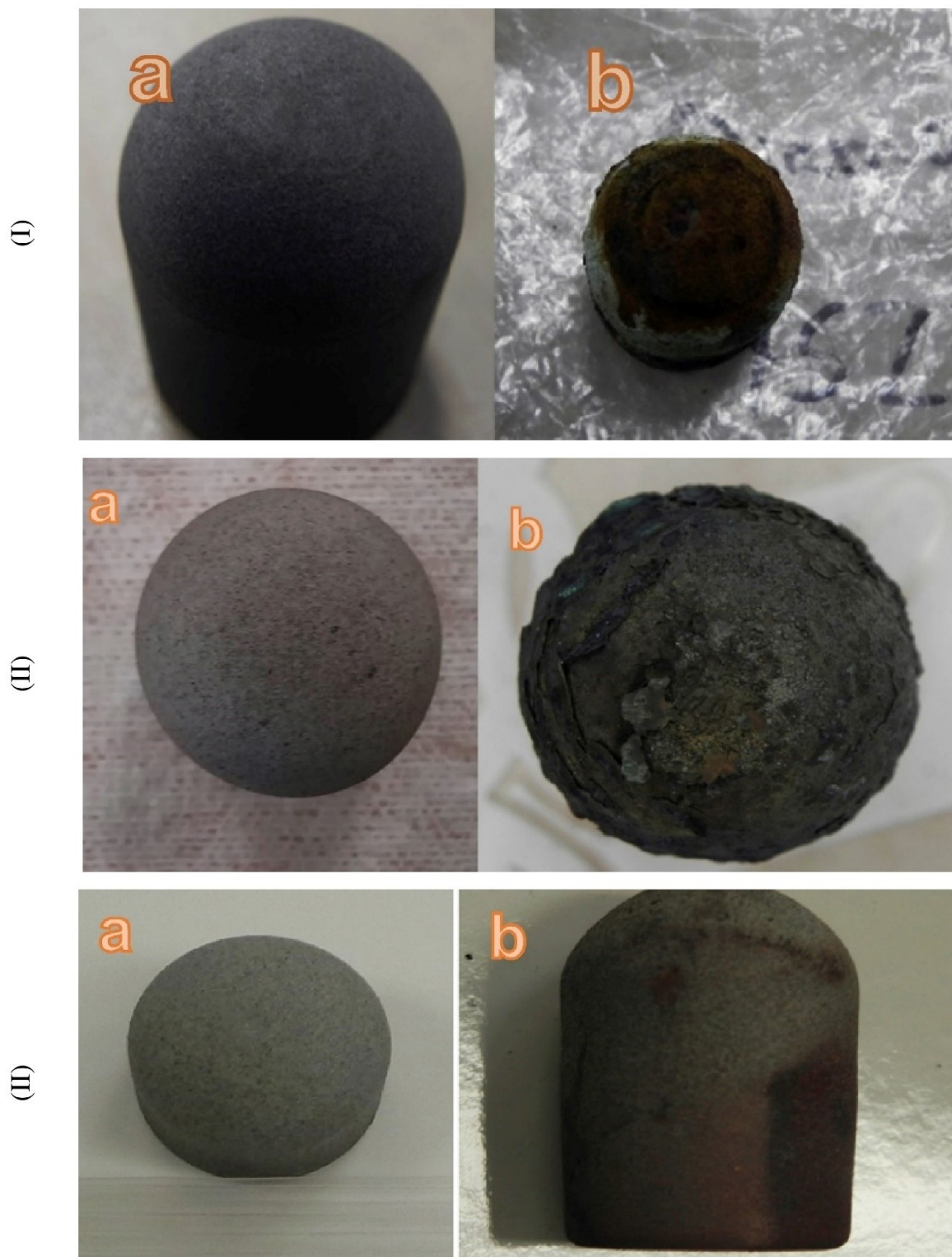


**Figure 17.** Bullet shaped coated sample before and after exposure to molten CuCl at 500 °C (a,b) sample before and after immersion test: (I) YSZ coating only (5 hrs immersion test), (II) YSZ + Diamalloy 4006 coating (48 hrs immersion test), and (III) YSZ + Diamalloy 4006 coating (100 hrs immersion test) (reproduced with permission).<sup>[121]</sup> Copyright (2016), Elsevier.

(1045). The coatings considered were YSZ as ceramic coating (coating method not specified), Diamalloy 4006 coating using HVOF technique, metal coated with Diamalloy 4006 + YSZ

(note: Ni based amorphous alloy Diamalloy 4006 (Ni 20Cr10W9Mo 4Cu 1C 1B 1Fe) coatings contained glassy (amorphous/microcrystalline) phases). While analysing corrosion



behaviour of YSZ (Zirconia,  $\text{ZrO}_2$  8% $\text{Y}_2\text{O}_3$ ) coatings, the Cu deposits were observed (indicating severe corrosion copper diffusion through the coating), a layer of YSZ on the base metal and a layer of copper (chloride) deposits were also observed on the base metal. This means the YSZ coating (without bond layer) thickness was not sufficient to resist the CuCl attack, leading to delamination of the coating. However, when the YSZ coating was applied to the base metal with a bond layer, the performance was better off but showed corrosion and erosion within its layers. While analysing corrosion behaviour of Diamalloy 4006 and YSZ coatings, factors related to mismatch of thermal expansion coefficient of the coating and substrate as well as stress or attack from the CuCl led to coating delamination in some regions, however, no cracks or corrosion were observed. While analysing corrosion behaviour of Diamalloy 4006 coatings, it was observed that the exposure to molten CuCl led to its splitting to form copper deposits on the sample, however, this coating showed promising results compared to other coatings. Additionally, though no further details were provided, Diamalloy 4006 with an  $\text{Al}_2\text{O}_3$  top coating survived longer exposure to molten CuCl. Naterer et al. (2019)<sup>[46]</sup> also proposed other alloys for future testing, such as Hastelloy, quartz glass coating, Udimet 500, IN718, nickel-based superalloy Nimonic105, etc. Previously, Naterer et al. (2015)<sup>[124]</sup> investigated various processes in the thermochemical Cu–Cl cycle for hydrogen production and proposed a predictive model to simulate the physical processes of bubble transport in a vertical liquid column, as it occurs in water splitting processes such as oxygen generation and electrolysis processes in the Cu–Cl cycle.

#### 4.6. Thermal spray coatings for photolysis water splitting (PWS)

The light absorbing ability of any material within a range (i.e., Ultraviolet (UV) – Visible (Vis) - Near InfraRed (NIR)) is a factor that is important for the improved photocatalytic property. As an example,  $\text{TiO}_2$  (n-type semiconductor most frequently used) coating's photocatalytic property can be triggered when exposed to the UV light, and there are a number of investigations on such coatings deposited using thermal spray techniques. There are numerous examples (Figure 18) where thermally sprayed photocatalyst semiconducting material for various photocatalytic uses were developed, e.g.,  $\text{TiO}_2$  coatings,<sup>[125–132]</sup> and ZnO coatings.<sup>[80]</sup> In all such investigations, the research has been more on enhancing the absorption capability of the material (possible through varied process parameters of thermal spray), which could potentially enhance sunlight-driven pure water splitting to split water into hydrogen and oxygen.

From literature observation, it can be concluded that there are more research examples where  $\text{TiO}_2$  semiconductors as photocatalysts are investigated for enhanced absorption capability (for non-hydrogen production applications, e.g., self-cleaning surfaces, air and water purification systems, sterilization (Toma et al., 2014)),<sup>[71]</sup> and very few examples on direct

investigation (or characterisation) for water splitting based hydrogen production. As numerous efforts have been made over the last decade within thermal spray techniques and control of phase transformation of feedstock materials during spraying (e.g., APS, HVOF, and cold spray (Toma et al., 2014)),<sup>[71]</sup> there is an opportunity where various other semiconductors (including  $\text{TiO}_2$ ) could be explored and investigated using thermal spray techniques for water splitting based hydrogen production.

#### 4.7. Thermal spray coatings for photoelectrochemical (PEC) water splitting

Using solution precursor plasma spraying (SPPS), Dom et al. (2013)<sup>[133]</sup> developed a 10  $\mu\text{m}$  thick ferrite nanocomposite ( $\text{ZnFe}_2\text{O}_4$ : $\text{Fe}_2\text{O}_3$ ) photoelectrode coating onto stainless steel substrate for photoelectrochemical based hydrogen production under simulated solar light. The photoelectrochemical measurements were performed using a 3-electrode cell (in 1 M NaOH (pH ~ 13.6) electrolyte) with a reference electrode (saturated calomel electrode (SCE)), a platinum electrode as the counter electrode and the ferrite nanocomposite as the working electrode. With a low band gap of 1.94 eV (band edges suitable for water splitting as well as its eco-friendly nature), the spinel oxide electrode yielded a solar-to-hydrogen conversion efficiency of 1.25% under simulated solar radiation with a hydrogen evolution rate of 99  $\mu\text{mol h}^{-1}$ . The EIS of the electrode revealed a significantly improved charge transfer characteristic compared to  $\text{ZnFe}_2\text{O}_4$ . An enhanced photoactivity for the oxidation of water from the electrode was attributed to its improved optical absorption and better charge transfer properties induced by the existence of  $\text{Fe}_2\text{O}_3$  in  $\text{ZnFe}_2\text{O}_4$ .

Unlike metal oxides (e.g.,  $\text{TiO}_2$ , ZnO,  $\text{Fe}_2\text{O}_3$ , and  $\text{WO}_3$ ) which are used in photoelectrochemical water splitting, copper oxide (CuO) is nontoxic, abundant, inexpensive, and an efficient light absorber in the visible region of the spectrum.<sup>[134]</sup> CuO material is a relatively good electrical conductor (with band gap range of 0.7–1.6 eV),<sup>[135]</sup> which means it can facilitate the extraction of photogenerated charge carriers. Alternately, the limited stability of  $\text{Cu}_2\text{O}$  (with band gap range of 2.0–2.2 eV (Basnet and Zhao, 2016)<sup>[136]</sup> which remains in the visible (Vis) light range, and which is larger than the required minimum water oxidation potential of 1.23 eV) under photoelectrochemical water splitting conditions is still an issue. Exploring these band gap features, stability, as well as low-cost mass production, Lee et al. (2016)<sup>[134]</sup> used cold spraying to deposit  $\text{Cu}_2\text{O}$  nanoparticles onto indium tin oxide (ITO)-coated soda lime glass (SLG) substrate for the fabrication of photocathodes for use in solar radiation based water splitting. To convert  $\text{Cu}_2\text{O}$  to CuO and improve their crystallinity, the coatings were sintered at various annealing temperatures (Figure 19), and it was observed by Lee et al. (2016)<sup>[134]</sup> that the optimal annealing temperature was 600 °C, producing a useful crystal (i.e., the high surface area of small crystals and better charge carrier transport in larger crystals). The photoelectrochemical measurements were performed using a 3-electrode cell (in 1 M KOH (pH ~ 14)

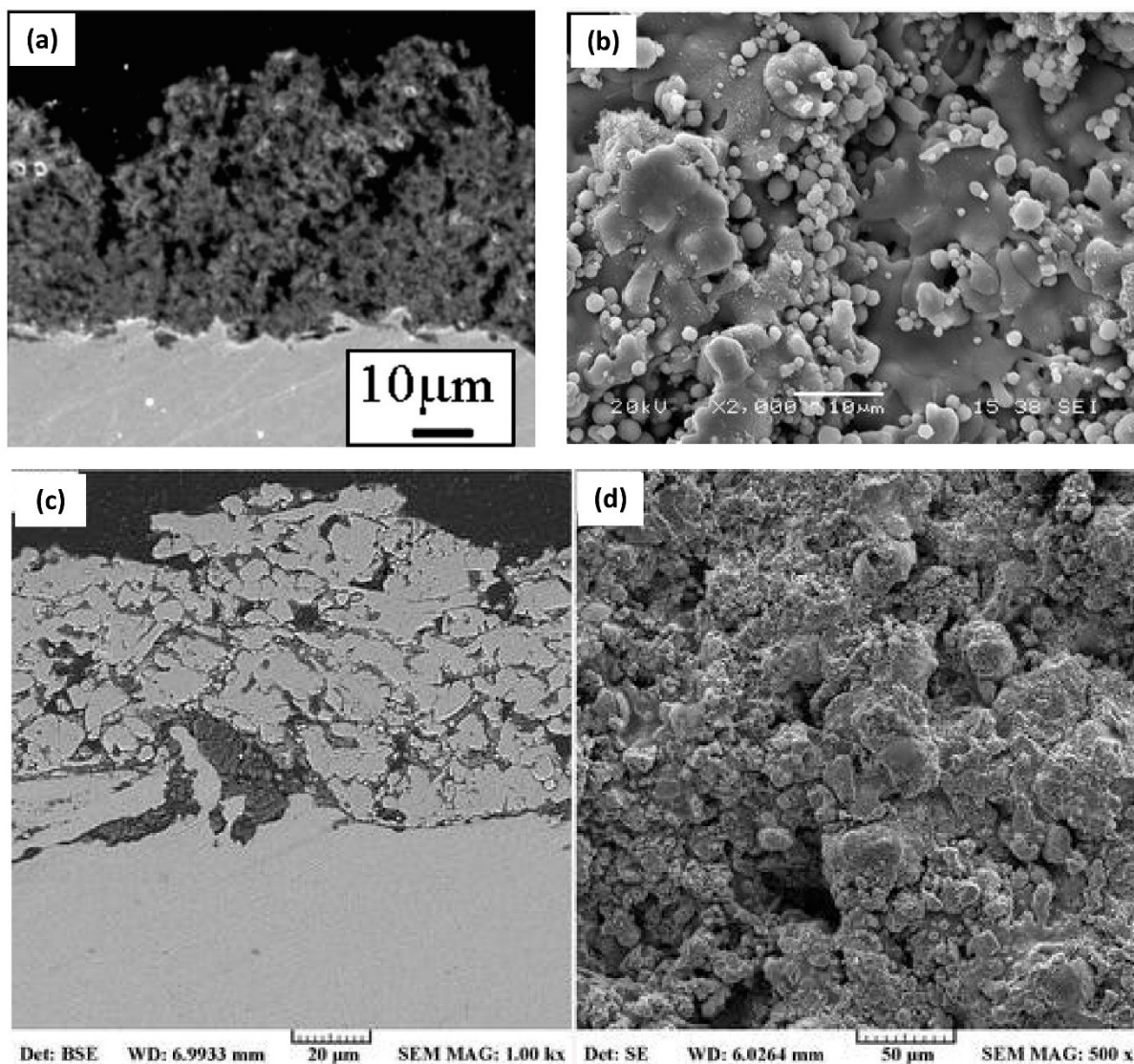


**Figure 18.** Microscopic images of thermally sprayed semiconducting materials deposited onto stainless steel substrates: (a) SPPS deposited  $\text{TiO}_2$  coating cross-section (reproduced with permission),<sup>[125]</sup> Copyright (2008), Elsevier, (b) APS deposited  $\text{TiO}_2$  coating surface, showing number of unmelted particles and porosity (reproduced with permission),<sup>[127]</sup> Copyright (2013), Springer Nature, and (c, d) APS deposited  $\text{ZnO}$  coating cross-section and surface (reproduced with permission).<sup>[80]</sup> Copyright (2017), Springer Nature.

electrolyte) with a reference electrode (Ag/AgCl rod), a platinum electrode as the counter electrode and the CuO films as the working electrode. Under simulated solar radiation, the CuO films when investigated as hydrogen evolution photocathodes, produced photocurrent densities (PCD) of up to  $3.1 \text{ mA/cm}^2$ , without the use of a co-catalyst or any additional heterojunction layers.

Haisch et al. (2017)<sup>[137]</sup> in Figure 20 showed how cold spray method can be utilised to fabricate large-scale electrode (with superior mechanical stability) for photoelectrochemical applications. They developed cold sprayed photoelectrodes (anodes) onto titanium metal substrates for electrochemical water splitting and wastewater purification. The coatings  $\text{WO}_3$  (active under visible wavelength) and  $\text{TiO}_2$  (active under UV wavelength) were investigated as photoanodes for the oxidation of

water and methanol, respectively. Methanol was chosen as an organic model pollutant in acidic electrolytes. Three-electrode based electrochemical measurements were carried out (consisting of a working (photo-) electrode (WE), an Ag/AgCl reference electrode (RE), and a Pt wire counter electrode (CE) and). Electrochemical testing was carried in 0.1 M KCl electrolyte, whereas photoelectrochemical testing was carried in 0.5 M acid ( $\text{H}_2\text{SO}_4$ ) electrolyte.

Concerning the photoelectrochemically water oxidation activity of the photoanodes, the highest photocurrents were observed for  $\text{WO}_3$  photoelectrodes in the potential range of 0.6–1.6 V, whereas for  $\text{TiO}_2$  photoelectrodes in the low potential range from 0.0–0.6 V (both vs. normal hydrogen electrode). While testing with the incident photon, it was revealed that the cold sprayed coatings (i.e.,  $\text{TiO}_2/\text{WO}_3$  photoanodes which did



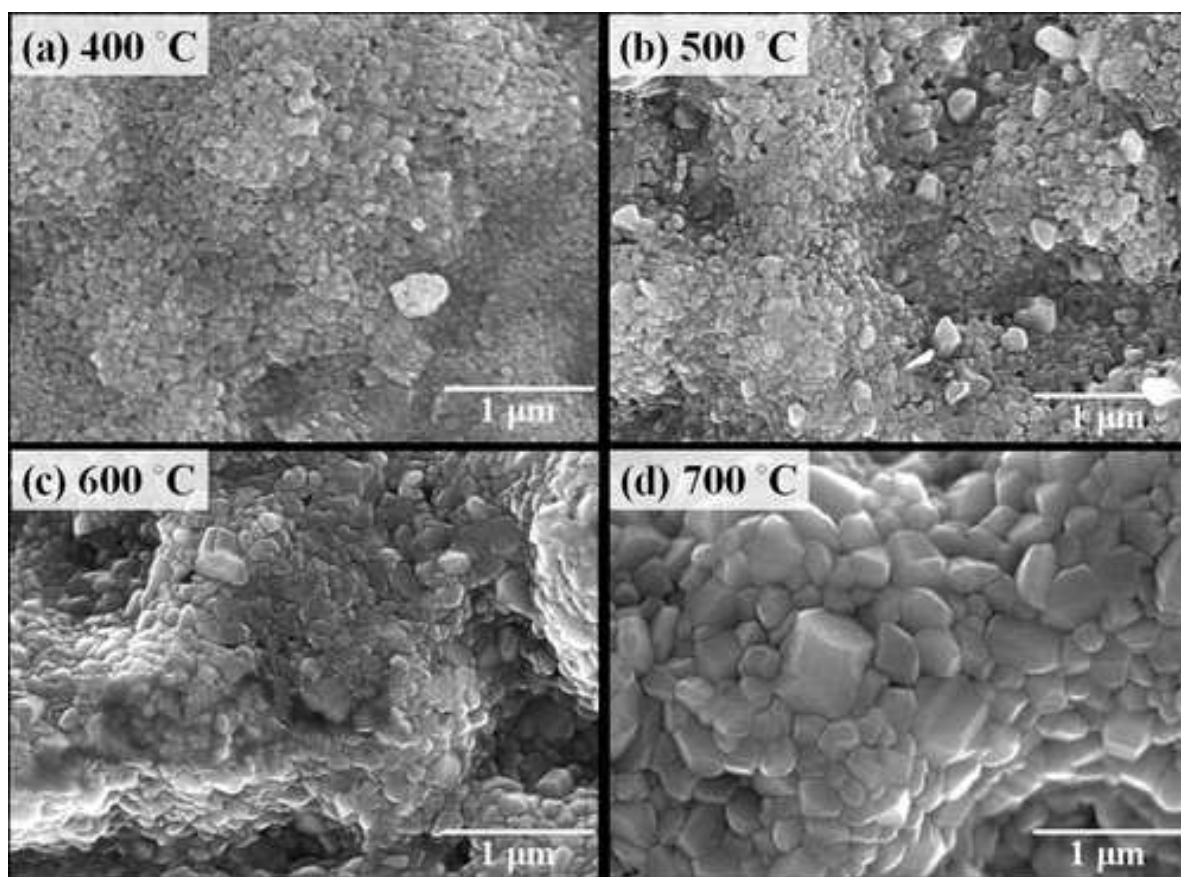


**Figure 19.** Microscopic images of surface of cold sprayed  $\text{Cu}_2\text{O}$  and then conversion to  $\text{CuO}$  by sintering at annealing temperatures: (a)  $400^\circ\text{C}$ , (b)  $500^\circ\text{C}$ , (c)  $600^\circ\text{C}$ , and (d)  $700^\circ\text{C}$  (reproduced with permission).<sup>[134]</sup> Copyright (2016), American Chemical Society.

not need any additive or binder like screen printing method) exhibited the best photoelectrochemical properties with regard to the water and methanol oxidation reactions in comparison with the benchmark photocatalyst Aeroxide  $\text{TiO}_2$  P25 (fabricated using screen printing method). This is due to more efficient harvesting of the total solar light irradiation related to their smaller band gap energies.

$\text{Fe}_2\text{O}_3$  is a nontoxic and abundant metal oxide with a bandgap of 2.1 eV (note: 1.8–2.2 eV is desirable to allow absorbance of visible sunlight spectrum above the minimum energy required for water splitting) (Kim et al., 2019).<sup>[138]</sup> However, the short lifetimes of the photogenerated electrons and holes in  $\text{Fe}_2\text{O}_3$  is an issue, as well as poor hole diffusion kinetics limit its photoanode performance for photoelectrochemical water splitting. Therefore, as demonstrated by Kim et al. (2019),<sup>[138]</sup> an overlayer coating to passivate the  $\text{Fe}_2\text{O}_3$  surface is essential for ensuring that it exhibits a high photocurrent density (PCD). Materials like thin overlayers of  $\text{Al}_2\text{O}_3$ ,  $\text{Ga}_2\text{O}_3$ , or  $\text{TiO}_2$  can be an option as passivation layers, as well as co-catalysts including  $\text{IrO}_2$ ,  $\text{Co-Pi}$ ,  $\text{Co(OH)}_2/\text{Co}_3\text{O}_4$ ,  $\text{Ni(OH)}_2$ , and  $\text{NiFeO}_x$  can be used on the surface of  $\text{Fe}_2\text{O}_3$  to improve its photocurrent density (PCD) and Faradaic efficiency, however, many of these materials are toxic, rare, or expensive. Therefore, Kim et al. (2019)<sup>[138]</sup> used the cold spraying technique for

deposition of photoresponsive  $\text{Fe}_2\text{O}_3$  particles onto ITO substrate (followed by coating with  $\text{ZnO}$  and then  $\text{TiO}_2$  overlayers using atomic layer deposition technique) for applications such as photoanodes for photoelectrochemical water splitting. While the valence band of  $\text{ZnO}$  (sandwiched layer) can facilitate the generation of photoexcited holes, but this material can undergo photo-corrosion in aqueous electrolytes, therefore,  $\text{TiO}_2$  was overlaid as a passivation layer. The photoelectrochemical measurements were performed using a 3-electrode cell (in 1 M  $\text{NaOH}$  ( $\text{pH} \sim 14$ ) electrolyte) with a reference electrode ( $\text{Ag/AgCl}$  rod), a platinum electrode as the counter electrode and the  $\text{Fe}_2\text{O}_3/\text{ITO}$  as the working electrode. Under simulated solar radiation, the films when investigated showed that the photocurrent of  $\text{Fe}_2\text{O}_3$  films ( $0.5 \text{ mA}\cdot\text{cm}^{-2}$ ) improves significantly to  $4.25 \text{ mA}\cdot\text{cm}^{-2}$  after their surface modification with an ultrathin ALD-based  $\text{ZnO/TiO}_2$  coating.

## 5. Considerations for enhanced hydrogen production

As seen from aforementioned examples, thermally sprayed materials are promising to help achieve materials' micro-



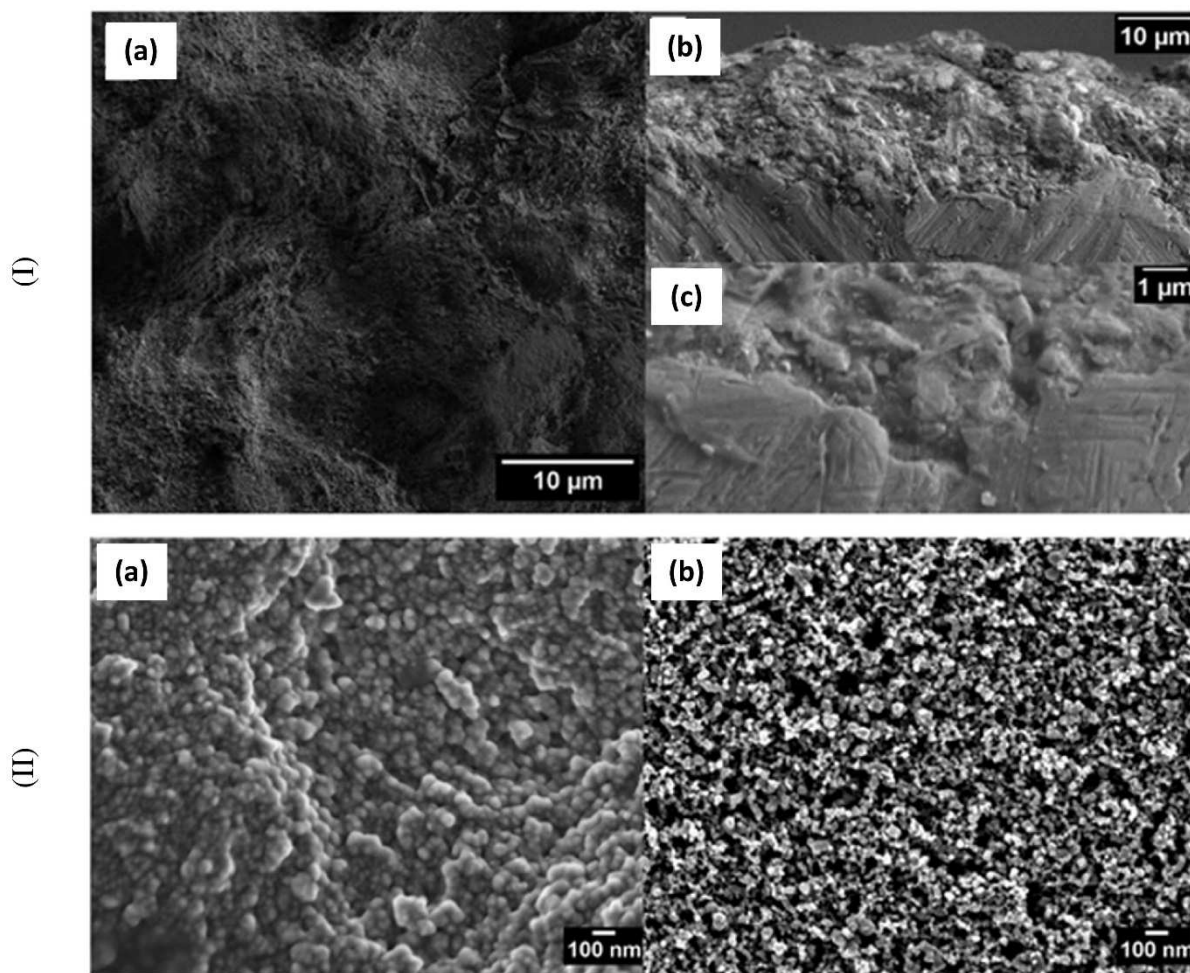


**Figure 20.** Microscopic image (I) (a) cold sprayed  $\text{TiO}_2$  film surface, (b) cross-section of cold sprayed  $\text{WO}_3$  film on a titanium substrate, and (c) cross-section of the interface region between the cold sprayed  $\text{WO}_3$  film and the titanium substrate, and (II) (a) cold sprayed  $\text{TiO}_2$  (P25/20) film on Ti metal substrate, (b) screen printed  $\text{TiO}_2$  (P25) film on FTO substrate, where images reveal that the particle sizes of the  $\text{TiO}_2$  particles in the screen-printed film are smaller than the particle sizes in the cold sprayed  $\text{TiO}_2$  film (reproduced under the terms of the Creative Commons Attribution-NonCommercial 3.0 Unported license).<sup>[137]</sup> Copyright (2017), Royal Society of Chemistry.

structures and properties which can help produce hydrogen through various water electrolysis based processes. The selection of feedstock materials requires understanding of the properties, functions, manufacturing route and overall electrolysis requirements. This section provides an overview about some direct considerations warranted which can further enhance hydrogen production.

### 5.1. Traditional feedstock materials, coating design, and post-processing

The selection of suitable feedstock materials (for thermal spraying various layers of interest) requires an understanding of the particular electrolyser type and the operational requirements expected from the deposited layer. The feedstock materials and their shape/size should be appropriate for the specific thermal spray technique being considered. As previously discussed and summarised later in Table 2, a majority of

the existing reports on thermally sprayed layers relevant to water electrolysis processes have employed relatively well-established deposition routes like APS, VPS, HVOF and Cold Spray. These generally utilize traditional spray-grade powder feedstock with particle sizes typically of the order of tens of microns. While the nature of the material (whether relatively low melting metals & alloys or high melting point ceramics) and type of process (whether plasma-based, combustion-based or kinetic energy driven) usually dictate the upper limit on the particle size, the lower limit (of approximately 5 microns) is governed by the inability to reliably feed finer powders.

Overall, from the examples discussed above, it is amply evident that thermally sprayed layers can deliver nearly tailored microstructures that can range from porous to almost fully dense to be impermeable to gases, depending on the requirements of the specific electrolyser type. Combined with an appropriate choice of the sprayed material, this can result in electronically/ionically conducting or thermochemically/electrochemically active layers with high surface areas, minimal

**Table 2.** Reported examples of thermal spray feedstock materials and spraying routes explored to fabricate coatings relevant for water-splitting leading to hydrogen production.

Thermal spray process	Feedstock materials	Remarks	Coating thickness	Substrate	Ref.
Proton exchange membrane (PEM) electrolyser VPS	Ti (coating for bipolar plates) and thin layer of Pt using magnetron sputtering on top of Ti	Ti coatings can fully protect the stainless-steel bipolar plates, Pt layer can allow achieving a cell performance comparable to the baseline	Ti: 60 µm, Pt: 1.8 µm	Stainless-steel	Gago et al. (2016) <sup>[97]</sup>
	Ti (coating for bipolar plates) and thin layer of Pt using magnetron sputtering on top of Ti	Ti coatings can fully protect the stainless-steel bipolar plates, Pt layer can allow achieving a cell performance comparable to the baseline	Ti: 50–60 µm, Pt: 1.5 µm	Stainless-steel	Lettenmeier et al. (2017) <sup>[96]</sup>
	Ti (coating for bipolar plates) and thin layer of Nb using magnetron sputtering on top of Ti	Ti coatings can fully protect the stainless-steel bipolar plates, Nb layer with superior corrosion protecting properties and stable behaviour in acid environment. Nb dense coating using VPS is possible; cell temperature: 38 °C	Ti: 50 µm, Nb: 1.4 µm	Stainless-steel	Lettenmeier et al. (2017) <sup>[98]</sup>
Anion exchange membrane (AEM) electrolyser APS	NiAlMo (cathode), NiAl (anode)	Electrolyser can achieve a potential of 2.086 V at a current density of 2 A cm <sup>-2</sup> ; cell temperature: 60 °C; electrolyte: 1 M KOH	–	–	Wang et al. (2019) <sup>[99]</sup>
APS	Ni/C 80:20 wt% (porous transport layer)	Novel approach for increasing performance in electrolysis by introducing a backing layer on a porous transport layer. Current density of 0.5 A cm <sup>-2</sup> at operating voltage of 1.90 V	Ni/C 80:20 wt%: 100 µm	Coated on top of a porous PTL made of stainless steel	Razmjooei et al. (2021) <sup>[100]</sup>
Alkaline water electrolyser (AWE) Flame spray, PS	Ni, WC-12%Co	Improved electrocatalytic activities were related to increased surface area of electrodes and efficient release of hydrogen bubbles were related to sprayed surface roughness or unevenness	25–150 µm	Steel (cathode)	Coker and Argade (1977) <sup>[101]</sup>
	Ni	The degree of coating oxidation was the main factor influencing the hydrogen evolution overpotentials at either the plasma-sprayed or sintered nickel cathode coatings; cell temperature: 80 °C; electrolyte: 30% KOH Decomposition potential of about 1.5 V was obtained; cell temperature: 180 °C	–	–	Hall (1984) <sup>[102]</sup>
APS	Ni	Cathode layers exhibited over voltages of 70 mV to 90 mV at 1 A cm <sup>-2</sup> and 70 °C in 25% KOH solution, whereas composite anodes (Raney nickel/Co <sub>3</sub> O <sub>4</sub> ) showed overvoltage values of 290 mV at 1 A cm <sup>-2</sup>	–	–	Henne, Schnumberger and Weber (1984) <sup>[103]</sup>
LPPS	Ni–Al	For the preparation of Raney Ni coatings, a precursor Ni–Al alloy was sprayed that had to be leached subsequently in caustic solution to remove the Al content, forming a porous, high-surface-area Ni layer	–	–	Schiller and Borck (1992) <sup>[104]</sup>
VPS	Co <sub>3</sub> O <sub>4</sub> spinel and Raney Ni/Co <sub>3</sub> O <sub>4</sub> (for anodic oxygen evolution), Raney Ni and Raney Ni/Mo (for cathodic hydrogen evolution)	Ni–Al electrode was more active in 25% KOH, Ni–Al electrode was more active in 1 M NaOH; cell temperature: 70 °C; electrolyte: 1 M NaOH and 25% KOH	–	–	Schiller, Henne and Borck (1995) <sup>[105]</sup>
VPS	Mo-containing Raney Ni (for cathodic hydrogen evolution), Raney nickel/Co <sub>3</sub> O <sub>4</sub> (for anodic oxygen evolution)	Low over voltages were related to the high porosity of the deposited coatings; cell temperature: 25 °C; electrolyte: 1 M NaOH	–	–	Miousse, Lasia and Borck (1995) <sup>[106]</sup>
Wire arc spray	Various Ni/Al ratios	Low over voltages were related to the high porosity of the deposited coatings; cell temperature: 25 °C; electrolyte: 1 M NaOH	–	Mild carbon steel	Fournier, Miousse and Legoux (1999) <sup>[107]</sup>

Table 2. continued

Thermal spray process	Feedstock materials	Remarks	Coating thickness	Substrate	Ref.
VPS	Ti–Ru–Fe–O (2-1-1-2) (i.e., mixing by ball milling of Ti, TiO, Ru and Fe <sub>2</sub> O <sub>3</sub> )	Careful optimisation of the etching process could lead to the dissolution of all Ti <sub>2</sub> O <sub>3</sub> , leading to a high porous coating and can enhance electrochemical activity; cell temperature: 70 °C; electrolyte: Chlorate: NaClO <sub>3</sub> : 550 g/l, NaCl: 110 g/l, NaClO: 1 g/l, pH 6.5, adjusted with NaOH and HCl	–	Fe, Ti (with Ti/TiH <sub>2</sub> interlayer)	Irissou et al (2002) <sup>(108)</sup>
VPS (high-frequency)	Ni–Al–Mo (NiAl <sub>3</sub> Mo <sub>2</sub> (T), NiAl <sub>8</sub> Mo (G), NiAl <sub>7.5</sub> Mo <sub>1.5</sub> (H), NiAl <sub>5</sub> Mo <sub>0.67</sub> (I), 46%NiAl <sub>3</sub> + 54%Ni <sub>2</sub> Al <sub>3</sub> (B) and the mixtures 25–75% of T + B)	Increase in real surface area along with catalytic effect of Mo, the Ni–Al–Mo coated layers were more active than those prepared by alloyed powder (heating Ni and Al powders) with similar compositions; cell temperature: 25 °C; electrolyte: 1 M KOH	–	–	Birry and Lasia (2004) <sup>(109)</sup>
Wire arc spray	Ni–Al, NiTi–Al	Increased activity for the hydrogen evolution reaction is due to an increased real surface area in case of the skeleton Ni electrodes and to the catalytic effect of Ti in case of the skeleton NiTi electrodes; cell temperature: 25 °C; electrolyte: 1 M NaOH	–	Steel	Kellenberger et al (2007) <sup>(110)</sup>
APS	Raney Ni (Ni–Al (50:50))	Best electrocatalytic activity towards HER was obtained for 100 μm thick coated electrode, with 96% efficiency at 300 mA cm <sup>-2</sup> current density and 70 °C, attributed to very high electroactive area and enhanced kinetics on sprayed surface; cell temperature: 30–80 °C; electrolyte: 30% KOH	30, 100, 300 μm	Raney nickel	Chade et al (2013) <sup>(111)</sup>
APS (Ni), SPS (NiO)	Ni, NiO	Higher surface areas were observed for all SPS deposits compared to those deposited using APS, attributed to the formation of fine porous agglomerates on the surface of the SPS coatings; electrolyte: 0.5 M NaOH	–	Carbon steel	Aghasiibeig et al (2014) <sup>(113)</sup>
APS (Ni), SPS (NiO)	Ni, NiO	Addition of submicron-sized cauliflower-like aggregates by SPS on the rough and porous surface of the APS deposited coatings significantly increased the exchange current density and improved the electrocatalytic activity of the electrodes; electrolyte: 1 M NaOH	100 μm (APS); 10–40 μm (SPS)	Inconel	Aghasiibeig et al (2016) <sup>(114)</sup>
APS	Raney Ni, Ni–Al	Through hydrogen and temperature heat treatment of the electrode, an enhancement in the uniformity of Al distribution as well as adhesion of the coating to the substrate was observed; electrolyte: 1 M KOH	–	Ni	Kim et al. (2018) <sup>(115)</sup> , Kim et al. (2019) <sup>(116)</sup>
<b>Solid oxide water electrolyser (SOWE)</b> APS (Al <sub>2</sub> O <sub>3</sub> ), Flame spray (Ni), Low pressure APS (YSZ), flame spray (Calcium or strontium-doped LaCoO <sub>3</sub> or strontium-doped LaCoO <sub>3</sub> or strontium-doped LaMnO <sub>3</sub> ), APS (Ni–Al)	Al <sub>2</sub> O <sub>3</sub> (for sealing & preventing oxidation), Ni (cathode), YSZ (electrolyte), calcium or strontium-doped LaCoO <sub>3</sub> or strontium-doped LaMnO <sub>3</sub> (anode), Ni–Al (interconnect)	Tubular cell design; cell temperature: 950 °C; electrolyte: YSZ	Al <sub>2</sub> O <sub>3</sub> : 100 μm, Ni: 80 μm to 110 μm, YSZ: 100 μm, calcium or strontium-doped LaCoO <sub>3</sub> or strontium-doped LaMnO <sub>3</sub> : 200 μm to 150 μm, Ni–Al: 250 μm	–	Hino et al. (1997) <sup>(117)</sup>



Table 2. continued

Thermal spray process	Feedstock materials	Remarks	Coating thickness	Substrate	Ref.
APS	LSM ( $\text{La}_{0.8}\text{Sr}_{0.2}\text{MnO}_3$ ) and LSCF ( $\text{La}_{0.5}\text{Sr}_{0.4}\text{Co}_{0.4}\text{Fe}_{0.6}\text{O}_3$ ) (cathodes), NiO + YSZ (fuel electrode), 9 mol% YSZ (electrolyte)	LSCF showed enhanced electrochemical performance compared to cells with LSM. Water splitting voltage was reduced to 1.4 V at an operating temperature of 800 °C and to 1.28 V at 850 °C; cell temperature: 800 °C; electrolyte: 9 mol% YSZ	NiO + YSZ: 50 $\mu\text{m}$ , 9 mol% YSZ (40 $\mu\text{m}$ ),	FeCrMnTi	Ansar et al. (2008) <sup>[118]</sup>
APS (anode, cathode), VPS (electrolyte)	Ni/YSZ (cathode), YSZ (electrolyte), LSCF (anode)	Cell voltage during electrolysis operation at a current density of $-1.0 \text{ A cm}^{-2}$ was 1.28 V at an operating temperature of 850 °C and 1.4 V at 800 °C; cell temperature: 800–850 °C; electrolyte: YSZ	Ni/YSZ: 50 $\mu\text{m}$ , YSZ: 40 $\mu\text{m}$ , LSCF: 30 $\mu\text{m}$	Porous ferritic steel	Schiller et al. (2009) <sup>[119]</sup>
APS, screen printing	Ni (bond layer) (steam/hydrogen side of separator plate), scandia-stabilized zirconia (electrolyte), strontium-doped manganite (anode), manganese-zirconia (inner layer), pure manganese (middle layer), cobaltite (outer bond layer), nickel-zirconia (cathode)	Demonstrated straightforward scalability of the high temperature electrolysis for long term operation and hydrogen production; cell temperature: 800–850 °C; electrolyte: scandia-stabilized zirconia	Ni: 10 $\mu\text{m}$ , Scandia-stabilized zirconia: 140 $\mu\text{m}$ , manganite-zirconia: 13 $\mu\text{m}$ , pure manganese: 18 $\mu\text{m}$ , nickel-zirconia (13 $\mu\text{m}$ )	Stainless steel (interconnect)	O'Brien et al. (2010) <sup>[89]</sup>
APS	Ni/NiO 50%-YSZ 50% (support electrode layer), Ni/NiO 25%-YSZ 75% (electrolyte transition layer), YSZ 100% (electrolyte), 50% YSZ-50% LSM (electrolyte-end transition layer), LSM 100% (end electrode)	Fabrication of free-standing solid oxide cells exclusively by APS thermal spray without the need of using any porous metallic support; electrolyte: YSZ	Ni/NiO 50%-YSZ 50%: 300–350 $\mu\text{m}$ , Ni/NiO 25%-YSZ 75%: 100–120 $\mu\text{m}$ , YSZ 100%: 100–120 $\mu\text{m}$ , 50% YSZ-50% LSM: 80–100 $\mu\text{m}$ , LSM 100%: 70–90 $\mu\text{m}$	–	Vardavoulias et al. (2021) <sup>[120]</sup>
<b>Thermochemical water splitting (TWS)</b> HVOF	YSZ, $\text{Al}_2\text{O}_3$ , Diamalloy 4006 (bond coat)	Inconel 625 substrate performed better than stainless steel AL6XN substrates; electrolyte: molten CuCl	70 $\mu\text{m}$ (YSZ); 70 $\mu\text{m}$ ( $\text{Al}_2\text{O}_3$ )	Inconel 625, super austenitic stainless steel or AL6XN	Siantar (2012) <sup>[88]</sup>
HVOF (for Diamalloy 4006)	YSZ, Diamalloy 4006 (bond coat)	YSZ coating with Diamalloy 4006 bond coat can provide better protection to the underlying base metal than only YSZ layer; electrolyte: molten CuCl	–	Medium carbon steel (1045)	Azarbayjani, Rizvi and Foroutan (2016) <sup>[121]</sup>
HVOF, APS	Diamalloy 4006 (bond coat), super hard steel 9172 (bond coat), $\text{Al}_2\text{O}_3$ , YSZ	Porosities less than 1% should be tested in order to shield the substrate from the harsh CuCl environment; electrolyte: molten CuCl	–	–	Azhar (2016) <sup>[122]</sup>
HVOF (for Diamalloy 4006)	YSZ, Diamalloy 4006 (bond coat) + YSZ	Diamalloy 4006 with YSZ or $\text{Al}_2\text{O}_3$ top coating survived longer exposure to molten CuCl; electrolyte: molten CuCl	–	Medium carbon steel (1045)	Naterer et al. (2019) <sup>[46]</sup>
<b>Photolysis water splitting (PWS)</b> APS, HVOF	$\text{TiO}_2$	–	–	–	Chen, Jordan and Gell (2008); <sup>[125]</sup> Mauer, Guignard and Vaßen (2013); <sup>[126]</sup> Zhang et al. (2013); <sup>[127]</sup> Dosta et al. (2016); <sup>[128]</sup> Wang et al.

Table 2. continued

Thermal spray process	Feedstock materials	Remarks	Coating thickness	Substrate	Ref.
APS	ZnO	–	–	–	(2015), <sup>[129]</sup> Robinson et al. 92015, <sup>[130]</sup> Kumar et al. (2016), <sup>[131]</sup> Khatibnezhad et al. (2021), <sup>[132]</sup> Navidpour et al. (2017) <sup>[80]</sup>
Photoelectrochemical (PEC) water splitting APS	ZnFe <sub>2</sub> O <sub>4</sub> ; Fe <sub>2</sub> O <sub>3</sub>	Solar-to-hydrogen conversion efficiency of 1.25% under simulated solar radiation with a hydrogen evolution rate of 99 μmol h <sup>-1</sup> ; electrolyte: 1 M NaOH	10 μm	Stainless steel	Dom et al. (2013) <sup>[133]</sup>
Cold spray	Cu <sub>2</sub> O, CuO	Photocurrent densities of up to 3.1 mA/cm <sup>2</sup> ; electrolyte: 1 M KOH	–	Indium tin oxide (ITO)-coated soda lime glass	Lee et al. (2016) <sup>[134]</sup>
Cold spray	WO <sub>3</sub> , TiO <sub>2</sub>	Highest photocurrents were observed for WO <sub>3</sub> photoelectrodes in the potential range of 0.6–1.6 V, for TiO <sub>2</sub> photoelectrodes in the low potential range from 0.0–0.6 V; electrolyte: electrochemical testing: 0.1 M KCl; Photoelectrochemical testing: 0.5 M (H <sub>2</sub> SO <sub>4</sub> )	–	Ti	Haisch et al. (2017) <sup>[137]</sup>
Cold spray	Fe <sub>2</sub> O <sub>3</sub> (followed by coating with ZnO and then TiO <sub>2</sub> overlayers using atomic layer deposition technique)	Photocurrent of Fe <sub>2</sub> O <sub>3</sub> films (0.5 mA cm <sup>-2</sup> ) improves significantly, to 4.25 mA cm <sup>-2</sup> , after their surface modification with an ultrathin ALD-based ZnO/TiO <sub>2</sub> coating; electrolyte: 1 M NaOH	–	Indium tin oxide (ITO)	Kim et al. (2019) <sup>[138]</sup>

mismatch in expansion coefficient with substrates and electrolytes. Such materials can also be electronically resistive and chemically resistive (corrosion resistant) while exhibiting sufficient mechanical and chemical integrity. An assessment of feedstock materials shows that much effort has also been devoted to exploiting composite materials (more frequently in SOWE and AWE electrolyser types) to obtain desirable catalytic characteristics.

Among the various microstructural features of interest, the porosity, pore size distribution, pore volume and pore shape are particularly critical in the context of the electrolysers, as they can directly influence the performance of corresponding thermal spray fabricated constituents (i.e., catalysts (anode/cathode), solid electrolyte, and transport layer, etc). There is no single thermal spray method that can be considered to be either universally or exclusively applicable, because of the varied materials that are of interest for current and future electrolyser applications, as well as the very wide range of porosity-related needs (from few nanometers to micrometers) in catalysts (anode/cathode), solid electrolytes, and transport layers. Traditionally, control over the pore structure and its distribution has been realized in conventional thermal spray methods (such as plasma-spray) through manipulation of one or more among various process parameters which could be either thermal spray 'gun' or feedstock related. The origin of porosity in the coating has often been related to the state of the particle at the moment of impact with the substrate, with unmolten particles leading to poor splat formation or 'bounce off' of the solid core and contribute to pore formation. Pores can also be formed due to other reasons such as enclosed gases or inherent pre-existing porosity in the powder feedstock and shrinking of splats during fast solidification. With the use of advanced thermal spray methods (for example, suspension and solution precursor spraying), enhanced control over porosity and its distribution is possible, although the fine-scale porosities can be challenging to reliably measure.<sup>[19,20,22,24]</sup> In summary, the advantage of thermal spraying methods is that it enables an appropriate combination of powder particle size, their residence time as governed by the gas velocity, and the process temperature to generate coatings with a desired level of porosity, depending on the type of coating material, parameters of the spraying process and the spraying gun system. In some cases, pore-formers are also used to intentionally introduce porosity, particularly in thermal sprayed ceramic coatings.<sup>[17]</sup>

Table 2 seeks to provide a detailed summary of the numerous examples of thermal spray feedstock materials and spraying routes used to manufacture coatings for water-splitting leading to hydrogen production. Details are also condensed in a graphical form in Figure 21 for all the seven electrolyser types that have been reviewed herein. Based on the reported literature, the following observations can be made. For PEM electrolysers, the application of Ti coatings on bipolar plates using VPS technique has been the main focus. The choice of VPS could have been due to the propensity for Ti to oxidize *in-situ* if it were to be plasma sprayed in ambient conditions. However, cold spray deposition could also be a plausible alternative due to a combination of low process temperature

and short residence time that can suppress oxygen pick-up (Wathanyu et al., 2022).<sup>[139]</sup> In case of AEM electrolysers, APS deposition of Ni based feedstocks such as NiAl and NiAlMo for anode and cathode, respectively, and of Ni-C for the porous transport layer has been evaluated. For AWE electrolysers, Ni-based materials have continued to be the main contenders, with layers being mostly deposited using APS, flame spray, LPPS, VPS and wire arc spray techniques. Preliminary studies utilizing SPS have also been reported and found to expectedly yield higher surface area by virtue of the finer particle size of the Ni-based powder used in the feedstock. Other materials such as Mo-containing Raney nickel cathodes and Raney nickel/Co<sub>3</sub>O<sub>4</sub> matrix composite anodes have also been studied. In comparison to the above types of electrolysers, the range of thermally sprayed materials evaluated in case of SOWEs has been much wider. These have included among others thermally sprayed porous Ni-cermet cathodes, a range of partially stabilized zirconia electrolytes (with yttria and scandia as stabilizers) and calcium or strontium-doped LaCoO<sub>3</sub> or strontium-doped LaMnO<sub>3</sub> as anodes. The few reports on thermal spraying for thermochemical water splitting have all involved use of a usually HVOF-sprayed Ni-based superalloy as a bond coat with a APS-deposited ceramic (YSZ or alumina) top coat. For photolysis electrolysers, the application of TiO<sub>2</sub> and ZnO coatings using APS and HVOF has been the main focus while, for photoelectrochemical electrolysers, the utility of metal oxide coatings (e.g., ZnFe<sub>2</sub>O<sub>4</sub>:Fe<sub>2</sub>O<sub>3</sub>, Cu<sub>2</sub>O, CuO, WO<sub>3</sub>, TiO<sub>2</sub>, and Fe<sub>2</sub>O<sub>3</sub>, etc.) using APS and cold spray has been evaluated.

The efforts summarized in Table 2 notwithstanding, there can be many other composite feedstock materials suitable for thermal spraying which have not been investigated yet but can potentially be considered for further investigations. For example, numerous materials and derivatives including semiconductor photocatalysts suitable for photolysis and photoelectrochemical electrolysers have been developed so far and can be deemed to be promising candidates. One such example is CuO–Al<sub>2</sub>O<sub>3</sub>–ZnO composite films for microreformers showing improved catalyst performance that can be integrated with the proposed design philosophy for enhanced photocatalytic activity.<sup>[140]</sup> Considering strategies for coating design potentially in the form of metasurface<sup>[26]</sup> for enhanced catalytic performance could be yet another approach suitable for photolysis as well as photoelectrochemical electrolysers. Such metasurfaces can lead to high catalytic activity and consequently increased hydrogen production rates through electrolysis. This can also address prominent current challenges in the field of electrode (catalyst layer) manufacturing by enabling both large-scale and structurally stable hierarchical length scale production. Availability of a robust and scalable manufacturing method with precision control over the material microstructure during scalable fabrication of catalysts represents an important current need, and the thermal spray route may be a way forward in this context.

Considering that post-processing of thermally sprayed layers is known to lead to changes in microstructure, phase constitution, etc.,<sup>[141–143]</sup> some of which could be relevant for enhancing the attributes of a few of the coatings discussed



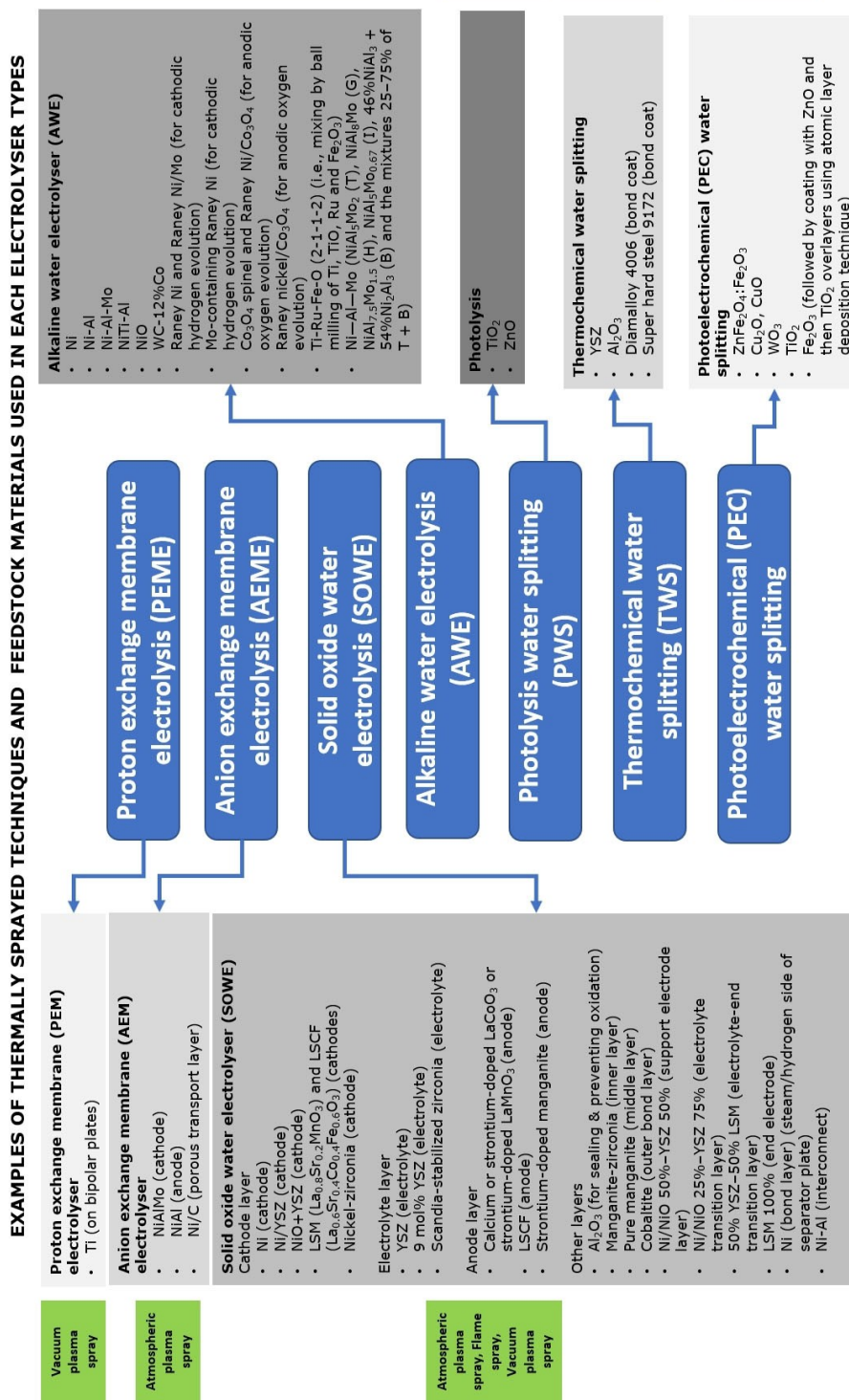


Figure 21. Mapping the thermal spray methods and feedstock materials used in various electrolyser types (authors original image).

above, not much work has been reported on this aspect in the context of coatings for electrolyzers. Most commonly, thermal post-treatment (including laser irradiation) of coatings to refine

microstructure and potentially enhance properties has been explored. Laser glazing of ceramic coatings has also been widely studied and demonstrated to yield a completely

solidified, dense top layer with segmented cracks,<sup>[144]</sup> which could be suitable for SOWE and thermochemical electrolyzers. This has the potential to enhance properties such as thermal shock behaviour and wear performance, as shown in the case of thermal barrier coatings.<sup>[145,146]</sup>

## 5.2. Advanced thermal spray methods

Due to the pivotal role that they play across virtually all industry segments, either in extending longevity of components operating in aggressive environments, enabling use of cheaper substrates or imparting specific key functionalities (as in case of electrolyser applications being discussed herein), cost-effective coatings have always been considered strategic and consequently been the subject of incessant development. The explicit advantages of thermally sprayed coatings over other methods, such as ability to be deposited over a wide range of thickness (from tens to hundreds of microns) onto complex component geometries without the constraints typical of in-chamber processes, and at comparatively lower costs, have been widely acknowledged. As a result, thermal spray variants like HVOF and APS are already entrenched on many production shop-floors. The resulting familiarity of industries with thermal spraying makes these methods well-suited for exploring new applications. In this context, the past couple of decades have seen particularly noteworthy advancements in terms of thermal spray equipment/ processing as well as new feedstocks for coating that could be gainfully harnessed for water-splitting electrolysis applications. Some of the prominent developments are discussed below.

In APS and HVOF coatings, the *in-situ* thermal 'degradation' of feedstock in the form of oxidation, decarburization, etc. is detrimental for many applications. There is also the possibility to vary porosity by other routes. The relatively recent emergence of supersonic high-velocity air-fuel (HVAF) spray process is an important development in this context.<sup>[147]</sup> HVAF involves much lower gas temperatures and considerably higher gas velocities compared to HVOF. Consequently, it causes negligible thermal degradation of feedstock while also being capable of yielding nearly fully dense and extremely well-adherent coatings because of the high particle velocities at impact. Thus, it appears capable of overcoming certain key limitations of APS, HVOF and cold spray methods, thereby offering new opportunities with both technical as well as economic merits.<sup>[148]</sup> HVAF spraying can utilize different nozzle configurations to obtain optimum coating properties. A process like HVAF is clearly promising to be explored for all metallic coatings considered appropriate for electrolyser applications, such as Ti, Ni, NiAl and Ni–Al–Mo mentioned in Table 2.

Examples in Table 2 already suggest the ability to use suspensions as feedstock has opened prospects for spraying nano- and sub-micron sized powders by suspending them in a suitable medium, most often water or alcohol. As elimination of the solvent from the injected suspension constitutes an added step involving additional thermal energy, nearly all initial efforts utilizing suspensions involved use of plasma spraying and

hence the term suspension plasma spraying (SPS) has been more common. The SPS approach can yield many different almost tailored coating microstructures ranging from porous, dense vertically cracked, columnar or nearly fully dense.<sup>[149,150]</sup> Prior work has also demonstrated that the suspension route can lead to refined coating microstructures and improved performance.<sup>[151]</sup> The refined coating structure is attributable to the fact that very fine powders (100 nm–2 μm particle size) are utilized to prepare suspensions while conventional 'coarse' spray grade powders used for APS and HVOF are typically 10–100 μm in size. This leads to splats in case of SPS being nearly two orders of magnitude smaller than in traditional powder-derived coatings and, since the splats are the building blocks for coating formation in thermal spraying, to a refined microstructure.

Another variant of plasma spraying using liquid feedstock is solution precursor plasma spraying (SPPS), in which suitable precursors that can form the desired particles *in-situ* are prepared using metal salts.<sup>[21]</sup> In this technique, precursors involving solutions of metal salts such as acetates, nitrates, butoxides, isopropoxides, etc., in an appropriate solvent (usually water or alcohol, as in the case of suspensions) have been typically used.<sup>[152,153]</sup> Various steps, such as break-up of injected droplets, evaporation of solvent, precipitation of solute, gelation, pyrolysis, sintering and melting, are postulated to be involved in eventual coating formation starting with an injected precursor droplet.<sup>[154]</sup> Apart from circumventing the problems associated with feeding of fine and typically expensive powders, a specific benefit of this route lies in its immense flexibility to rapidly evaluate novel precursor compositions and their combinations. Good control over deposit chemistries utilizing SPPS has also been demonstrated.

A vast majority of early research involving use of suspensions and solution precursors was focused on thermal barrier coatings and involved plasma spraying. However, greater process understanding and growing realization of the unique coating microstructures and superior properties that can accrue has led to a spurt particularly in suspension thermal spray research. SPS research has led to successful deposition of different chemistries apart from yttria stabilized zirconia (YSZ), such as hexaaluminates, garnets (e.g., yttrium aluminum garnet), zirconate based perovskites and rare earth zirconate based pyrochlores, with some multi-layer architectures also being explored.<sup>[155–157]</sup> These and other research efforts have contributed to generating new knowledge that allows for considerable control over SPS-derived coating microstructures. By virtue of enhanced process familiarity, the SPS route has also been used to explore a host of other material chemistries mainly spanning oxides and carbides, sometimes with incorporation of a second phase in the form of carbon nanotubes or graphene.<sup>[158–161]</sup>

Similarly, SPPS too has been explored beyond the domain of TBCs and shown to provide a facile route for producing a wide array of functional oxide ceramic coatings. This has included a wide range of oxide like TiO<sub>2</sub>-based photocatalytic coatings<sup>[125,131]</sup> as well as many others such as ZnFe<sub>2</sub>O<sub>4</sub>,<sup>[133]</sup> ZnO,<sup>[162]</sup> and Dy:YAG,<sup>[163]</sup> CeO<sub>2</sub>,<sup>[164]</sup> CuO–Al<sub>2</sub>O<sub>3</sub>–ZnO,<sup>[140]</sup>

LaSrMnO<sub>3</sub>,<sup>[165]</sup> NiO–YSZ,<sup>[166]</sup> Ce-doped Ba(Zr<sub>0.2</sub>Ti<sub>0.8</sub>)O<sub>3</sub>,<sup>[167]</sup> etc. are all considered as potentially candidate coatings for catalysts in electrolysis applications. Some other SPPS studies relevant in the present context have involved deposition of a catalytic CuO/ZnO/Al<sub>2</sub>O<sub>3</sub> layers for PEM fuel cells,<sup>[140]</sup> SOFC anode and cathode coatings of Ni–YSZ and LaSrMnO<sub>3</sub>,<sup>[165,166]</sup> as well as others such as Co<sub>3</sub>O<sub>4</sub>,<sup>[168]</sup> V<sub>2</sub>O<sub>5</sub>,<sup>[169]</sup> etc. All of the above chemistries are also amenable for SPS deposition. Additionally, there is a growing interest to explore emerging materials such as high entropy oxides, composite pyrochlore oxides and fluorite structured oxides, which exhibit high chemical stability and also exhibit catalytic activity at high temperatures.<sup>[170–174]</sup>

The above examples suggests that the new liquid feedstock route could open new vistas for electrolyser-relevant coatings. In the context of liquid feedstock thermal spraying, it is also relevant to point out that a growing number of reports on suspension and solution precursor spraying using HVOF torches (termed s-HVOF) present further possibilities to create novel coatings with unique microstructures.<sup>[175–177]</sup> While the utility of liquid feedstock thermal spraying for niche applications was always evident, the recent availability of axial-feed capable plasma spray systems in particular can be seen as a game-changer for these coatings. The significant enhancement in

deposition efficiency and throughput made possible by the improved thermal exchange between the plasma plume and the axially-fed liquid feedstock has served to largely eliminate prior concerns regarding relevance of this route for large scale production by demonstrating the ability to attain deposition rates comparable with traditional powder-derived coatings.

More recently, use of a 'hybrid' feedstock combining a suspension or a solution precursor with a conventional spray-grade powder has also been proposed and found to be a novel method for realizing coatings with unusual microstructures. The above approach enables distinct constituents with vastly different relative length scales (usually 10–100 μm in case of powder feedstock, and approximately 100 nm–2 μm in case of suspensions or in flight formed particles derived from solution precursors) to be conveniently combined. The unique microstructures are a consequence of powder and liquid feedstock derived splats differing by more than an order of magnitude in size, leading to a combination of coarse-fine features. One possible arrangement for independently controllable feeding of powder and liquid feedstocks, with possibility to also completely shut off either feed, is illustrated in Figure 22. Suitable variations in the depicted arrangement to permit both the powder and the liquid to be fed radially, or one axially and the

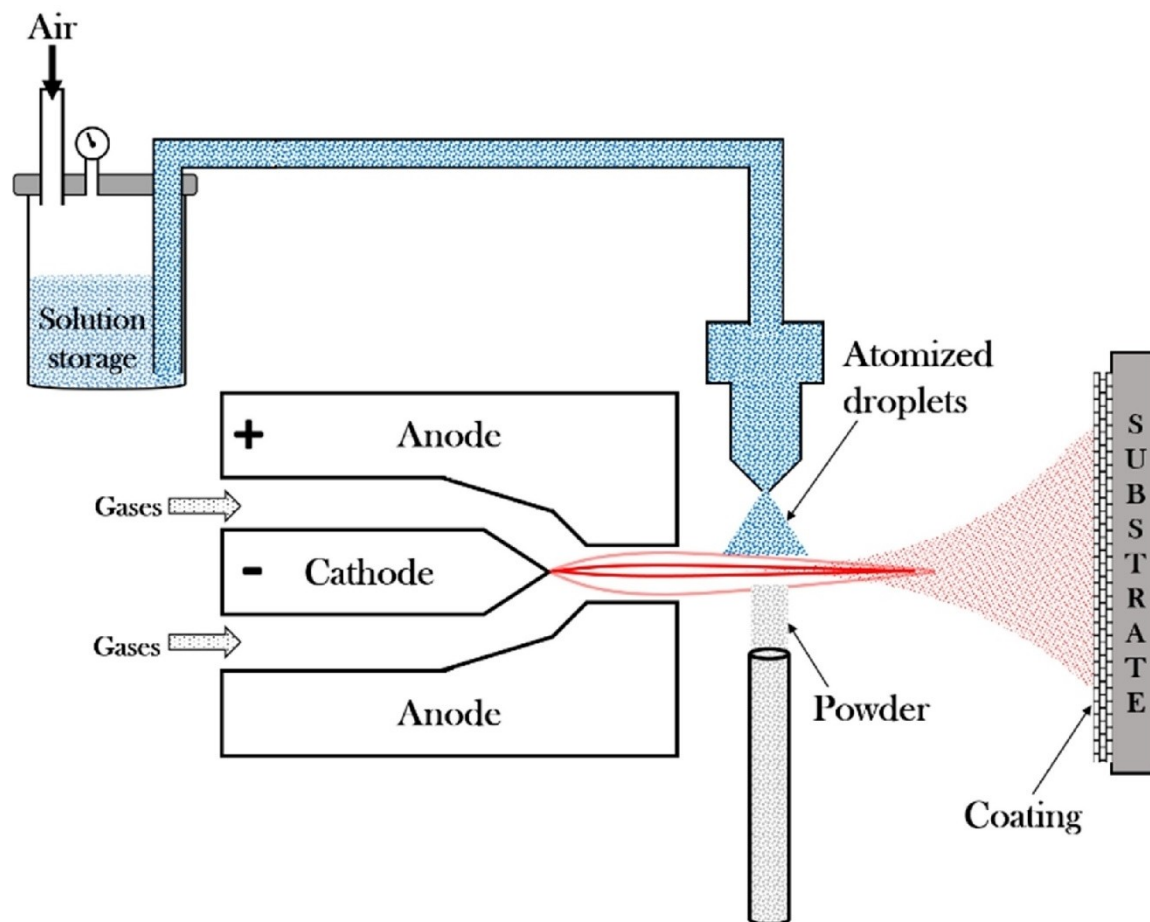


**Figure 22.** Schematic representation for depositing composite coating through hybrid powder plus solution precursor based feedstock (note: removing the powder injector will allow solution precursor driven deposits) (authors original image).



other radially, are conveniently possible. Both suspensions<sup>[24]</sup> and solution precursors<sup>[19]</sup> can be utilized with equal ease in such a hybrid configuration. Depending upon how the powder and liquid feedstocks are introduced during such 'hybrid' spraying, varied coating architectures can be realized such as layered (with sequential feeding), composite (with simultaneous feeding with constant feed rates) or functionally graded (with simultaneous feeding, involving progressively varying relative feed rates), as desired for the targeted application.<sup>[24]</sup> Deposition of coatings utilizing suspensions as well as solution precursors in tandem with conventional spray powders has been demonstrated in separate studies.<sup>[178–180]</sup> Recently, the possibility of extending such a hybrid deposition approach to HVAF process has also been demonstrated.<sup>[181–183]</sup> Thus, it is apparent that the above approach offers immense flexibility and can be conveniently utilized to spray unique material combinations without relying on commercial availability of such chemistries to be commercially available as spray-grade feedstocks. This can be particularly relevant while exploring new coating systems for potential electrolyser applications.

### 5.3. Designing advanced catalytic materials and effect of their dimensionality

The catalyst material's design is the core technology of hydrogen production by electrolysis to reduce energy consumption and increase production yield. It is to be noted that the catalyst materials dimensions are highly effective to enhance the rate of reactions and selection of reaction (selectivity) under mild conditions.<sup>[184]</sup> There are many aspects like catalytic material surface, materials support, and the electron transfer between the catalytic surface and an adsorbed molecule, which tailored the Fermi energy level of catalyst materials. The researchers are modulating the properties of catalyst materials by additive mixing of other materials, which directly affect the Fermi energy level, stability, and surface structure. Except for additive mixing, the nano-dimensions are also playing a major role in catalytic activity such as 0D (nanodots or nanoparticles), 1D (nanotubes or nanorods), 2D (nanosheets) and 3D (bulk materials). The materials having at least one dimension lying in the range of 1–100 nm differ in the properties compared to their counterparts. The spatial confinement directly affects their properties by virtue of quantum confinement which can tune the optical/catalytic and other related material properties.<sup>[185]</sup> The energy level vs density of state (DOS) for different structures (1D, 2D, 3D and bulk) are shown in Figure 23.<sup>[186]</sup> As the structural dimension decreases, carrier (electron/holes) movement is

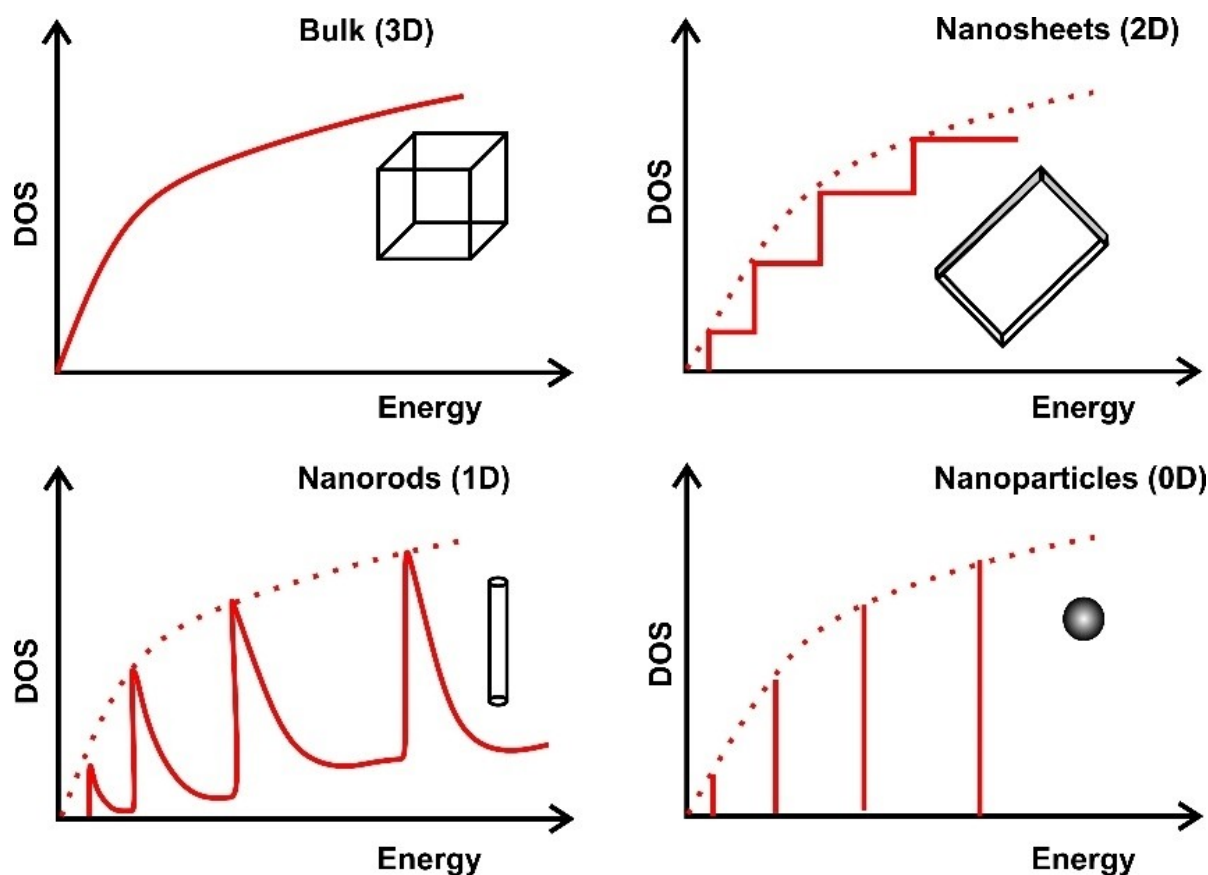


Figure 23. Density of state (DOS) vs energy variation of a material with different dimensionality (authors original image).

restricted in the corresponding directions. The bulk materials show continuous energy band. However, the nanomaterials show discretisation of energy levels, which is the cause of different behaviour of nanomaterials compared to their bulk materials. The facet of a crystal also has different catalytic properties because each facet has different dangling bonds and atomic terminations, and thus different electron densities. Consequently, the interaction of facet surface with adsorbed molecules is different. Modern catalytic science by combining with nanoscience has pushed the boundaries of bulk catalysis to single atom catalysis.<sup>[187]</sup> In the context of thermal spray, retaining nanomaterials/nanostructure during spray is a challenging task due to the presence of high temperature and kinetic energy. However, the post processing (after thermal spray coating) like dealloying can create nanoporosity, which directly affect the catalytic activity due to surface area enhancement.

The Fermi energy level of catalyst materials is an essential factor for the interaction of catalyst materials and adsorbate. It can be tailored by the addition of different dopants, different catalyst support, etc. The catalyst support changes the catalyst material's Fermi energy level due to charge re-distribution. A higher Fermi energy level support can make catalyst negatively charged, and lower Fermi energy level support can make positively charged catalyst to facilitate the reactions. Therefore, the binding energy of the adsorbate is tailored for every catalyst material. Suppose the pure materials planar surface have similar binding energy and similar active sites all over the surface (each atom have similar neighbours).<sup>[188]</sup>

On the other hand, the binary alloy has a planar surface with two types of active sites due to two different metallic

elements and the third one at both elements interfaces. However, the increasing number of elements, increases the active sites along with their binding energy of each site (as shown in Figure 24(a)).<sup>[188]</sup> For example, quinary concentrated solid solution (high entropy alloy (HEA)) has different number of active sites with different binding energy. The addition of multielement creates the favourable/unfavourable synergetic active sites for catalytic reaction (Figure 24(b)), and a catalytic material can be used for multi-catalytic reactions.<sup>[189]</sup>

The pure noble metals such as Pt, Au, Ag, and Rh are good catalyst materials but due to their high-cost, researchers have devoted themselves to finding alternatives such as transition metals and their alloys (binary, ternary, quinary and high entropy alloys (more than or five elements and each contribution  $< 5 = < 35$  atom %). Most transition metal catalyst alone suffer from electrochemical dissolution in acidic/alkaline media.<sup>[190]</sup> Nevertheless, metallic materials can be deposited by thermal spray coating techniques on a large scale/industrial scale.<sup>[191]</sup> Some metals are known for the lower efficiency of hydrogen evolution, but their alloy works better. For example, Ti and Cu are known as poor catalyst for hydrogen evolution reactions, but their combination works better at mild overpotentials.<sup>[192]</sup> The porosity in the catalyst materials enhances catalytic efficiency due to increased surface area. The dealloying process can be used to make electrodes porous after depositing by thermal spray techniques.

Lu et al. (2015)<sup>[192]</sup> have prepared bi-metallic catalyst Cu–Ti by arc melting followed by melt spinning. The hierarchical nano-porosity was created by the selective dealloying process, as shown in Figure 25(a–b). The hierarchical nano-porosity played a significant role to increase the catalytic activity

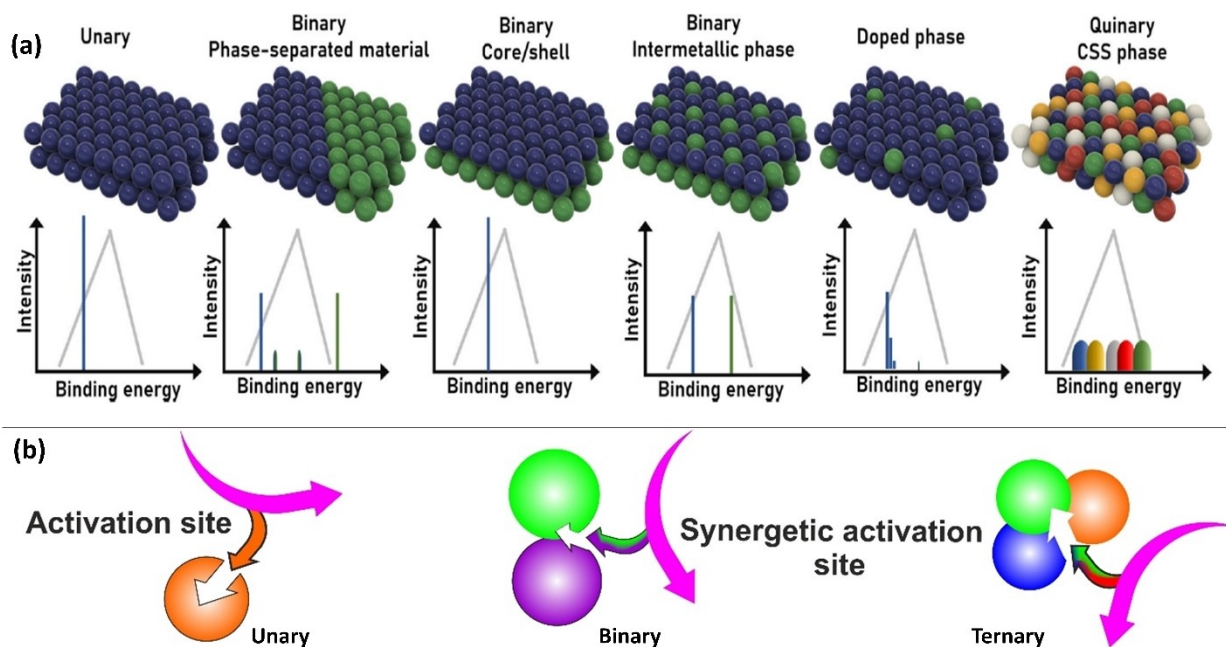


**Figure 24.** (a) Variation in the binding energy of the active sites with the addition of the number of elements (reproduced under the terms of the Creative Commons Attribution-NonCommercial-NoDerivs license),<sup>[188]</sup> Copyright (2021), Wiley, and (b) different synergetic sites with an increasing number of elements (reproduced with permission).<sup>[189]</sup> Copyright (2021), Elsevier.

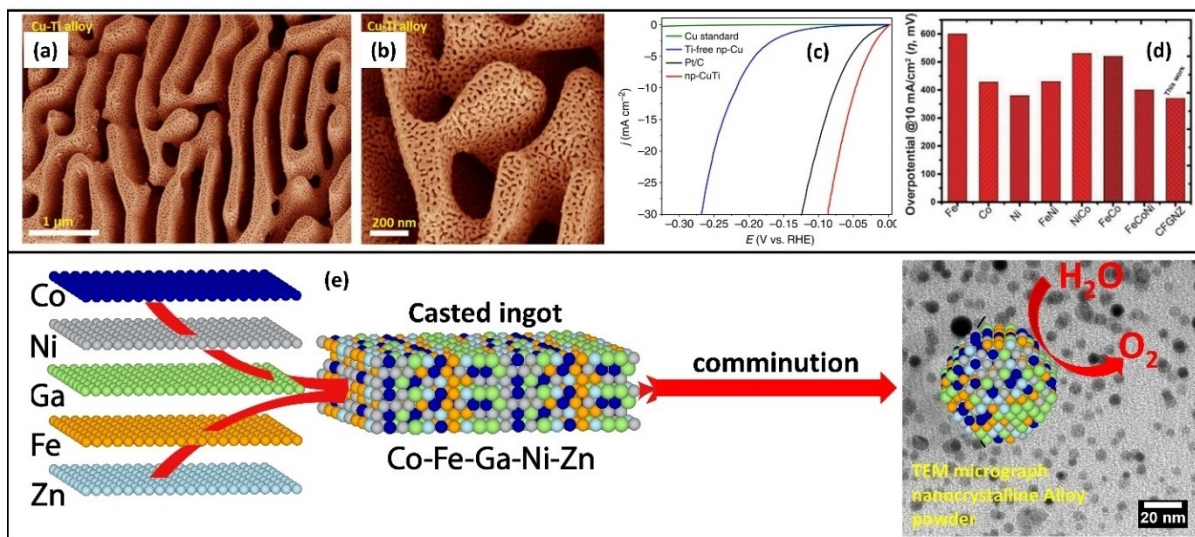


**Figure 25.** (a) Hierarchical nano-porous Cu–Ti alloy (reproduced under the terms of the Creative Commons CC-BY license),<sup>[192]</sup> Copyright (2015), Springer Nature, (b) higher magnification of Hierarchical nano-porous Cu–Ti alloy (reproduced under the terms of the Creative Commons CC-BY license),<sup>[192]</sup> Copyright (2015), Springer Nature, (c) comparison of hierarchical nano-porous Cu–Ti alloy with other catalyst materials (reproduced under the terms of the Creative Commons CC-BY license),<sup>[192]</sup> Copyright (2015), Springer Nature, (d) overpotential comparison of pure, binary, ternary and HEA alloys for the OER reaction (reproduced with permission),<sup>[201]</sup> Copyright (2021), Springer Nature, and (e) a schematic nanocrystalline HEA powder preparation for OER reaction (reproduced with permission).<sup>[201]</sup> Copyright (2021), Springer Nature.

compared to bulk Cu and alloy, as shown in Figure 25(c) by Lu et al. (2015).<sup>[192]</sup> The new concept of high entropy stabilized alloys as catalytic materials has gained prominence. They are under the wide area of designing and exploration on the laboratory scale for many catalytic reactions.<sup>[193–197]</sup> The unique feature of HEA is that the atomic mixing of many metals, can tune the catalyst for different reactions or one catalyst can work for many responses because several atoms over the surface presents wider possibilities of different active sites for the adsorbate.<sup>[189]</sup> Another unique feature of the high entropy alloys is that they are highly corrosion resistant. Therefore, it is also stable in a harsh environment or during the electrolysis of water.<sup>[198]</sup>

Cai et al. (2021)<sup>[199]</sup> designed ultra-high entropy nano-porous alloy catalyst for water splitting using Al, Ag, Au, Co, Cu, Fe, Ir, Mo, Ni, Pd, Pt, Rh, Ru, and Ti by dealloying method (i.e.,  $\text{Al}_{0.8}\text{Ag}_1\text{Au}_1\text{Co}_1\text{Cu}_1\text{Fe}_1\text{Ir}_1\text{Mo}_1\text{Ni}_1\text{Pd}_1\text{Pt}_1\text{Rh}_1\text{Ru}_1\text{Ti}_1$ ) and claimed this to be superior to  $\text{IrO}_2$  and Pt/graphene. There are some obstacles in powder preparation techniques of such catalyst, as thermal spray requires a metallic powder to be sprayed over the electrode to be deposited, but this type of catalyst suffers from phase separation or intermetallic formation during atomization (during powder preparation). Nevertheless, preparation of HEA by mechanical alloying provides the nano powder of the catalyst and overcome such phase separation.<sup>[200]</sup>

Sharma et al. (2021)<sup>[201]</sup> designed a low-cost catalyst, easily scalable material for oxygen evolution reaction using transition metal elements and it worked at a reduced overpotential of 370 mV at a current density of 10 mA/cm<sup>2</sup> (Figure 25(d)). The metallic powder was prepared by mechanical milling at extremely low temperature as per the scheme shown in Figure 25(e). Cryomilling or milling at an extremely low temper-

ature provides ultrapure nanocrystalline powder, as it protects the materials from oxidation and minimize the debris from the milling tools.<sup>[202–204]</sup> The Ir metal is known for the best catalyst of water splitting but it is a costly material. Jin et al. (2019)<sup>[205]</sup> designed Ir based HEA catalyst to replace the Ir metal (pure) and diluted Ir content by mixing high abundance transition elements which is better for oxygen evolution reaction activity compared to well know Pt/C– $\text{IrO}_2$  catalyst. The designed HEA metallic catalyst material with nano-porosity  $\text{AlNiCoIrMo}$  is highly stable under an acidic environment. As summarised above, there are many different catalytic materials that have been designed and to be designed using different metallic elements and some examples have been presented to illustrate the concept and their suitability for thermal spray deposition for the electro splitting of water for H<sub>2</sub> generation.

#### 5.4. Potential application of perovskites using thermal spray techniques

Not much work has been reported, but manufacturing of perovskite active catalysts using thermal spray coatings can be a novel approach.<sup>[206–208]</sup> Perovskites are  $\text{ABO}_3$  type materials existing in either oxide phase or the solid solution phase (where A is a rare-earth or alkaline earth element and B is a transition metal, with the ability to substitute into the A and B sites elements of varying valency).<sup>[209,210]</sup> Perovskites are semiconducting materials that can absorb and emit light for various applications in optoelectronics. In alkaline energy storage and conversion systems, perovskites are also attractive candidate materials, as such materials can have high structural stability, high ionic and electronic conductivities, good resistance against



electrolytic corrosion, high activities for both oxygen evolution and oxygen reduction reactions, electronegativity or ionic size to tune the structural, physical and electronic properties of the catalyst.<sup>[209]</sup> In solid electrolytes (e.g., oxygen ion-conducting (O-SOWEs) and proton conducting (H-SOWEs) which operates at high temperature) need to be dense to avoid gas transportation between a cathode and an anode as well as chemically and physically compatible with electrodes, application of perovskites can be useful.

Certain perovskites are known to be able to conduct protons at intermediate to high temperature ranges.<sup>[211–213]</sup> For example, the electrolyte materials in proton conducting (H-SOWEs) are perovskite-related structure (ABO<sub>3</sub>) oxides, where A = Ba, Sr, Ca; B = Ce, Zr. These materials can enable SOWEs to operate at a reduced temperature range (400–700 °C). To promote protonic conductivity it is common to substitute the B site with M<sup>3+</sup> ions, such as Y, Nd, Sm, Yb, In, Eu, Gd that form oxygen ion vacancies to increase the movement of protons.<sup>[214]</sup> It has been proved that BaCeO<sub>3</sub>- and BaZrO<sub>3</sub>-based electrolytes have better hydration capacity and higher protonic conductivity compared with Sr/CaCeO<sub>3</sub>- and Sr/CaZrO<sub>3</sub>-based oxides (Wang, Medvedev and Shao, 2018).<sup>[215]</sup> Also, for oxygen ion-conducting (O-SOWEs), there are some traditional electrolytes, such as stabilized zirconia, ceria-based oxides, doped LaGaO<sub>3</sub> and apatite-type structures with composition La<sub>10-x</sub>(SiO<sub>4</sub>)<sub>6</sub>O<sub>2±δ</sub> (note: x and δ mean the vacancies formed of the corresponding atom in the perovskite crystal lattice due to the introduction of the dopants).

Therefore, depending on the electrolyser types and catalyst layer requirements, some functional features of perovskite materials can help enhance electrolysis of water e.g., metal and non-metal doping can enhance visible spectrum activity, highly crystalline and small particle sizes can offer shorter migration distance for the charge carriers (leading to efficient charge separation). The addition of carbon can increase charge separation and visible-region activity. Introducing carbon can change the dispersion of charges leading to the migration of charges to the catalyst surface leading to higher evolution of hydrogen, due to the availability of free electrons Ag dopant can lead to efficient charge separation excited by the visible light photons and higher hydrogen evolution. Smaller particle sizes with higher crystallinity and surface area can lead to higher availability of sites for photocatalytic activity. Free electron surplus within the lattice could play a role in increasing the activity of the material.<sup>[210,216]</sup> While the incorporation of perovskite materials using thermal spray techniques is possible for electrolysis applications, but the practical issue remains with perovskite materials, such as its appropriateness (sprayable/flowable) for the specific thermal spray technique. Suspension or solution spraying (SPS, SPPS), as well as hybrid spraying is also possible, where the combinations of powder with suspension, powder with solution, and suspension with the solution can be deployed<sup>[20,178,217]</sup> to have desirable catalyst coatings.

## 5.5. Challenges in electrolysis modelling

Prior knowledge of properties of materials (such as mechanical, chemical, thermal, electrical, electronic, etc) is necessary to develop strategies for the structural design, material selection, and manufacturing of components in an electrolyser. Since thermal spray coatings are multi-layered structures with heterogeneous features consisting of materials or phases, therefore, various non-experimental modelling approaches (such as analytical, numerical, and computational) may be a cumbersome task. While there is a lack of such modelling-focused analysis, i.e., cross-property relations, their development serves as a useful tool in designing coated components with enhanced performance for electrolysis.

Various modelling approaches for electrolysers could help benchmarking various functionalities and should be validated against the experimental findings. As expected, various electrolysers are made of different components with their specific functions and operations. The materials, components, and processes happening in the electrolyser dictate the voltage value and its stability and thus affect the efficiency of the electrolyser. The electrocatalysts determine the reaction kinetics and an efficient catalyst could help lower the activation overpotentials for the OER and the HER. Therefore, it is important to understand the OER and HER activation barriers of different catalysts. As an example in PEM electrolyser, the porous structure of the catalyst layer (CL) and the porous transport layer (PTL) determines the flow and mass transport of gas and water, which are linked to the operational conditions. For example, a higher oxygen generation rate at high current density for a high hydrogen production rate could block the PTL for water to flow into the reaction sites at the CL. Moreover, the mass transport processes through the PTL and the flow channels (in the current collectors) could cause voltage instability and affect the electrolyser efficiency. Therefore, it is important to appreciate the gas-liquid flow and mass transport processes within the porous CL and PTL. The ohmic resistance in the membrane depends on the water saturation, as well as the polymer membrane properties. It is crucial to understand the ionic conductivity of the membrane, and the behaviour of the membrane under different operating conditions. Another phenomenon that could occur to affect the electrolyser performance and lifetime is hydrogen embrittlement of metal materials, which are common in all electrolyser types.

There is a need to use a holistic multiscale modelling approach to support materials and component design within the electrolysers, and provide fundamental understandings of the multiple physical and chemical processes. Depending on electrolyser types, atomic-scale density functional theory (DFT) and molecular dynamics (MD) simulations can be useful to understand hydrogen embrittlement and its effect on the properties of metals, which are important to the electrolyser lifetime. DFT simulations can be used to calculate the OER and HER activation barriers of promising and novel electrocatalysts and understand the effects of their electronic and atomic structures on the catalytic activities, which are crucial to electrolyser performance.<sup>[218–221]</sup> Molecular-level MD simulations

can be used to study both membranes (e.g., in PEM and AEM electrolyzers), derive important properties such as ionic conductivity and diffusion coefficient, and understand the membrane's behavior under different operating conditions.<sup>[222–226]</sup> Meso-scale models of the 3D porous electrodes (including CL and PTL) can also be developed based on the lattice Boltzmann method, to understand the multiphase flow and mass transport of gas and water in the electrode, and the effects on electrolyser performance, and to help design novel electrode structures to reduce mass transport resistance and improve electrolyser performance.<sup>[227–231]</sup> Finally, macro-scale modelling based on computational fluid dynamics (CFD) and finite element methods can be useful to simulate whole electrolyser cells, including different components, electrodes, membranes and current collectors, to predict electrolyser performance and optimise electrolyser components and operating conditions.<sup>[232–234]</sup>

The macro-scale multiphysics modelling of the hydrogen production requires correct representation of the fluidic, mechanical, thermal and electrochemical parts of the process to allow proper exploration of the vast multi-parametric space.<sup>[235,236]</sup> As for any multiphysics simulation, mesh independence, convergence tests, validation for each physical part of the problem separately and for the full models are required, including setting up a benchmark case, similar to simulations by Turek and Hron (2006)<sup>[237]</sup> in the fluid-structure interaction. A separate challenge in the area of multiphysics simulations is related to the use of existing design optimization solvers<sup>[238]</sup> and the development of the new design optimization techniques.

Multiphysics models can be distinguished by the type of coupling among the model components: decoupled processes, monolithic models, one-way coupled, two-way coupled, or models with a mixed type of coupling, when the system is complex and different elements are linked in a different manner. The challenge of a correct coupling is also in a careful selection of the solution steps for each computed physical process. The type and details of coupling in the model should be confirmed based on the systematic validation.

Apart from the modelling scales, simulation methods for fluids and structures in general can be grouped by the degree of representing the physics of the problem. The computational fluid dynamics (CFD) and finite element analysis (FEA) methodologies provide a detailed view on the physical processes and, therefore, are relatively independent from published experimental datasets in order to make predictions for an arbitrary set of input parameters. Following the range of models available for the fluids modelling, it is reasonable to expect in the future a development of modelling solutions for the hydrogen production of a phenomenological nature, where the actual physics of the problem is simplified up to the essential variables only, supported by a number of expressions or constants based on the available published data. Phenomenological models combine the advantages of reducing the model and input complexity and providing accurate results for selected characteristics.

Data driven artificial intelligence (AI) approaches are providing newer avenues for physics simplification and can be generally divided into the physics-informed neural networks, retaining the basic governing equations,<sup>[239]</sup> and the purely data-driven approaches working with the case parameters and the training-testing data only.<sup>[240]</sup> These models deliver highly accurate results in a timely manner and for any set of input parameters. However, these advantages are often accompanied by the demanding training and validation stages. The models based on neural networks or simplified physics (phenomenological) naturally have strong connections to specific datasets used for their development, improvement or training, so may not be fully reliable when used on a very different initial dataset or for extreme conditions.

At the current state of the art of the hydrogen production modelling, CFD- and FEA-based coupled multiphysics models can be considered as very flexible and advantageous for the purpose of accumulating more data on this complex phenomenon for challenging conditions,<sup>[234]</sup> such as high temperatures, high pressures, complex reactions, short time frames, etc.

## 5.6. Data analytics approach

It is clear that research has progressed significantly to improve catalysts performance through development of new candidate materials and/or using range of manufacturing/processing routes. However, further research is needed to achieve manufacturing thinner catalysts, higher efficiency, and durability. This will require the application of advanced material selection tools (e.g., material informatics) as well as advanced processing techniques. As extracted from Oerlikon Metco Thermal Spray Materials Guide (2018),<sup>[241]</sup> by Viswanathan et al. (2021)<sup>[86]</sup> in Figure 26, more broader approach could help in feedstock material selection and thermal spray techniques. The Figure 26 indicates that if energy is spent on powder manufacturing, means less energy can be spent on the coating process and vice-versa. This could be further analysed via data analytics (after extraction of data from all manufacturers of thermal spray grade feedstock materials), i.e., historical data gathering and analysis of various electrolyser devices from published literature followed by data classification (e.g., materials – coating/substrate and their properties, manufacturing techniques, process parameters, operating conditions, types of electrolyzers, electrolysis performance indicators, availability or materials, cost-effectiveness, stability at varying pH levels, corrosion conditions, life cycle, compactness, etc.).

As shown in Figure 27, such research should include the integration of historical data leading to the creation of a machine learning (ML) based predictive tool with the provision to investigate efficiencies at desirable operating conditions. This can then be followed by a sensitivity analysis of the catalyst's performance with respect to the manufacturing techniques and materials to identify optimal techniques for chosen electrolysis applications. It also needs to be investigated further, i.e., mitigating the degradation mechanism of catalysts during operation and maintaining the efficiencies.

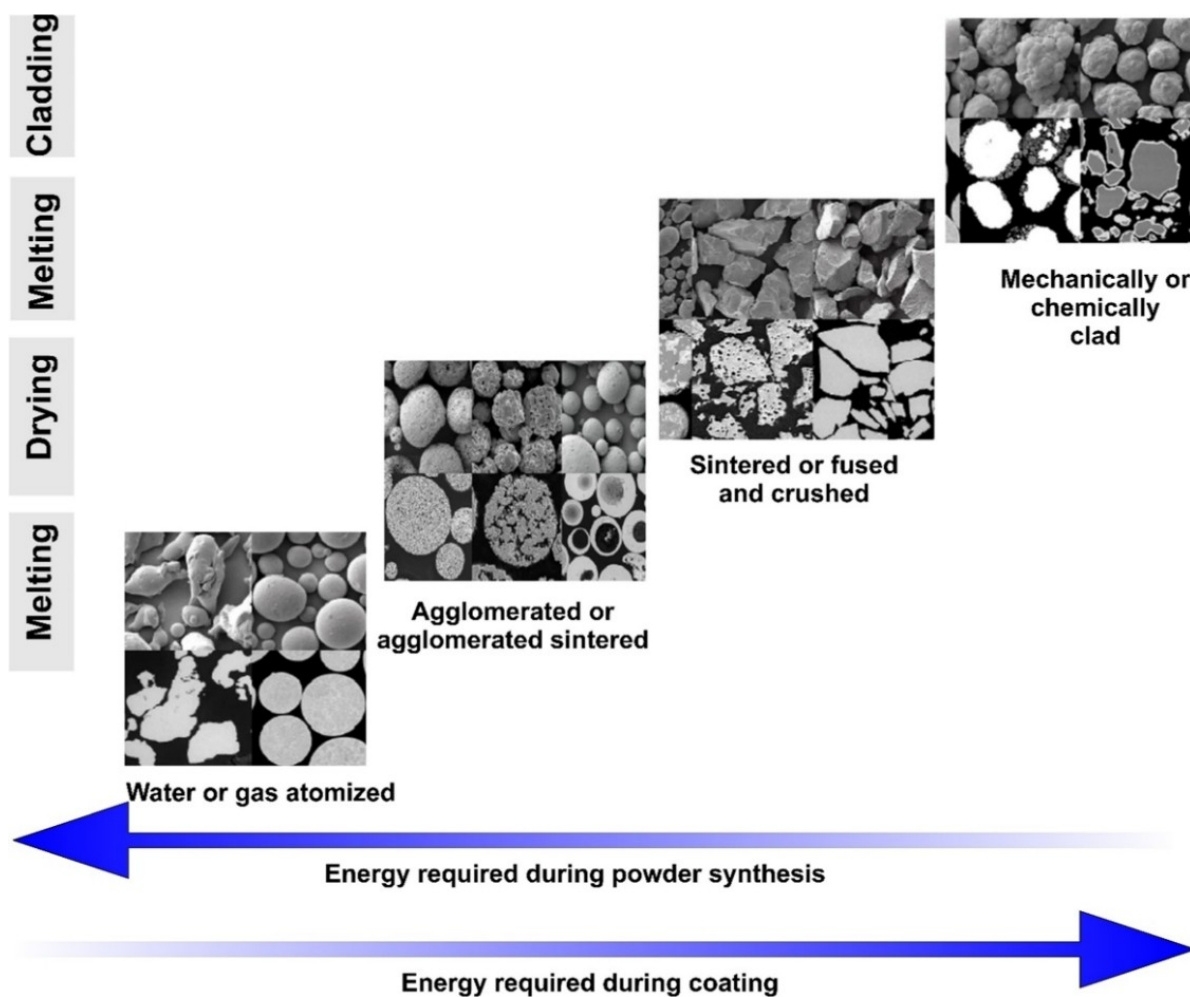


**Figure 26.** Relationship between energy required during feedstock powder synthesis (e.g., melting, drying, cladding processes) and during thermal spray coating (note: illustration are for 5  $\mu\text{m}$  to 200  $\mu\text{m}$  powder particle size range depending on the material and process (reproduced under the terms of the Creative Commons CC-BY license).<sup>[86]</sup> Copyright (2021), Springer Nature.

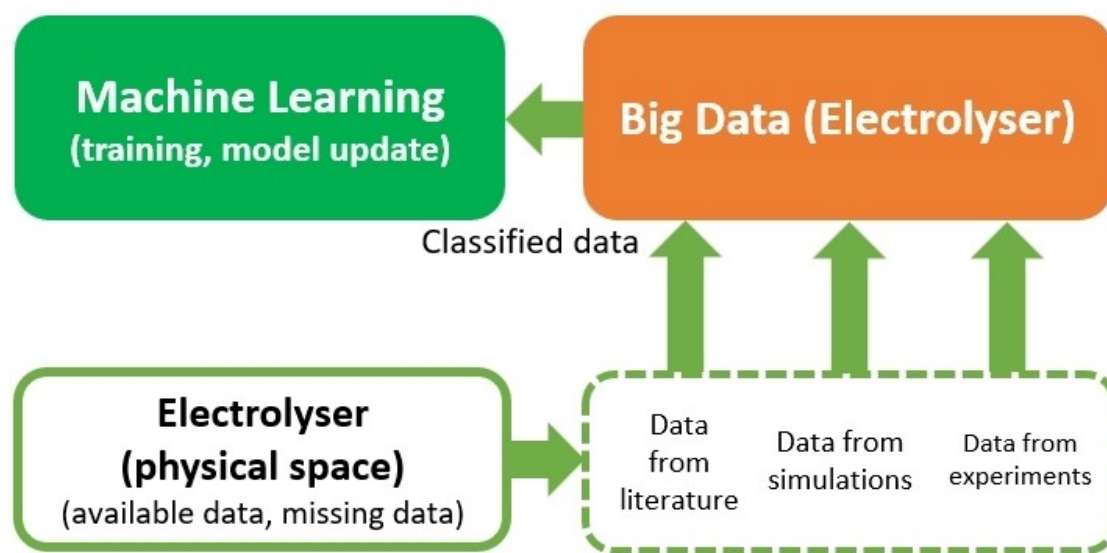


**Figure 27.** Data analytics approach in electrolysis (authors original image).



### 5.7. Degradation analysis considerations, challenges and opportunities

Efforts are being made to enhance the overall properties required for various components of electrolyzers, especially: (i) extended stability, (ii) compatibility with chemicals, (iii) minimising thermal expansion coefficient difference, (iv) lowering the internal electrical resistance and polarization at the interface between electrodes and electrolyte, and (v) enhancing mechanical strength of the supporting components. Considering various requirements, the development of appropriate coatings for key components for electrolyzers are very much required.

Failure investigations of electrolyzers have found deformation, fracture, delamination of the material due to the asymmetric material configuration, extension of a small defect which can be accidental during fabrication, and thermal, chemical, and mechanical stress generation during operations. These failures eventually degrade the performance of the cell over time and eventually lead to system failure. The development of characterisation and modelling tools for the analysis of electrolyzers is essential for the design process. However, these tools must also include coupling between the mechanical, fluid, thermal, electro-chemical, and structural behaviour. For thermo-mechanical and electro-chemical reasons, it is preferred to keep the coated layers as thin as possible, which implies that the cells are more susceptible to damage during production, assembly, and operation. Sensor-based instrumented mechanical testing and materials characterisation (e.g., elastic modulus, hardness, fracture toughness, adherence, etc.)<sup>[242–244]</sup> are required to optimise the support sections of the electrode/electrolyte/membrane/transport layer system while maintaining highly active areas.

Investigation into residual strain in catalysts (induced during thermal spray coating deposition) is needed to assure strong adherence with the substrate.<sup>[245–247]</sup> Since thermal energy from nuclear power and solar heat generators can enhance the electrolysis process (e.g., in solid oxide electrolyzers) and can produce more hydrogen per kWh of input energy, the investigation is needed to look into the residual strain of catalysts while testing at a range of temperatures, pressures, pH levels, mechanical loads, etc. Processes like these can also very well be studied using simulation based approaches involving continuum mechanics<sup>[248,249]</sup> and also molecular dynamics approaches.<sup>[250]</sup>

Some of the critical reviews stimulates knowledge related to the latest scientific strategies and industrial developments, as well as challenges encountered in the different domains of water electrolysis.<sup>[251,252]</sup> Despite the numerous challenges faced while developing critical and vital constituents in electrolyzers, there are many new research opportunities for scientists to develop new, highly efficient materials and manufacturing methods and endeavour to lower our greenhouse gas emissions.

## 6. Concluding remarks and prospects

A range of thermal spraying techniques have been used to fabricate layers (e.g., catalysts (anode/cathode), electrolyte, membrane, transport layer, and bipolar plates) for hydrogen production by splitting of water. In all such investigations, the spraying parameters and a number of spray passes were developed and optimized with varying levels of porosity, roughness, splats size and microstructures, largely to maximize apparent surface area of catalysts. Though with only a few examples, the application of modern suspension or solution based thermal spray techniques resulted in catalysts surface with broad surface microstructures (micrometre to nanometre) and enhanced specific surface areas. While exploring coating solutions for electrolysis, liquid feedstock based spraying appears more cognitive on account of fine sized splats, microstructure control, thin coating, suppressed grain growth, retention of starting phases etc. Nevertheless, the choice of solution precursor based spraying potentially stands to provide added advantage through the versatility in exploring range of coating chemistry and flexibility to deposit coatings with higher surface area. Solution precursor plasma spraying (SPPS) process opens up new avenues for developing compositionally complex functional oxide coatings and by means of hybridizing with powder injection system, allows composite metal/alloy/ceramic and ceramic films as well.

In most of these investigations, it was observed that thermally sprayed catalysts characteristics provide a large active surface area for the hydrogen evolution reaction. It has been demonstrated that thermally sprayed catalyst coatings with micrometric sized features promote the departure of the bubbles, and the nanometric sized microstructural features facilitate easier electron transfer by providing more reaction sites. Additionally, the catalysts could also exhibit hydrophilic behaviour which generally facilitates the separation of bubble from the surface as the electrolyte is more likely to replace the gas bubbles. Subsequently, the catalysts with optimized surface morphology and roughness (with the largest specific surface area) have exhibited the highest electrochemical performance for hydrogen evolution.

While fabricating catalysts for hydrogen production, it has been a common practice to enhance the electrocatalytic activity of the electrodes by using a complex mix of materials as well as enhancing the surface area (e.g., using wire mesh screen during spraying leading to blocks of coatings) to further enhance the active surface area. The changes in spray angle (normal and off angle) to the substrate can also help unique microstructures (i.e., providing a larger active electrode surface area) which lead to an increased rate of the hydrogen evolution reaction. Such a phenomenon also facilitates detachment of the hydrogen bubbles from the surface of the catalyst. Varied temperature, i.e., high temperature (in APS), leads to fully melted feedstock particles, relatively less temperature (in HVOF), leads to partially or un-melted feedstock particle, whereas near room temperature (i.e., cold spray), leads to minimal oxidation with highly deformed feedstock particles. Therefore, coatings with flattened particles (fully, partially, deformed) can be easily developed

which leads to different surface microstructures and roughness depending on spray techniques and process parameters. The spray techniques and process parameters could also lead to varied through-thickness residual stresses (e.g., compressive) which in turn could impact thermo-mechanical properties and electrocatalytic activities, but this aspect has never been investigated.

Except for a few examples, not much research has been carried to investigate the life cycle as well as long-term structural stability of the catalysts. As of now, electrolyser catalysts present some inherent challenges. Low mechanical strength, and electrode deterioration (corrosion, cracking, reduced residual strength), and the effect of high operating temperature (e.g., for solid oxide-based electrolysers) represents some of these inherent challenges. To summarise, almost any metallic, composite, cermet or ceramic materials that melt without decomposing can be used to produce a coating (e.g., thermal spray, cold spray). Typical coating thicknesses range from 0.05 to 0.5 mm. Thermal spray coating techniques can help spray nano-structured or micro-structured powder materials where a range of microstructure (e.g., porosity, crystallographic texture, phases, anisotropy, strains) can be controlled using appropriate process parameters. This review, therefore, indicates that a range of feedstock materials and thermal/cold spray coating techniques can play a key role in providing a scalable manufacturing route to current and next-generation catalyst for electrolysers. Also, to meet the specifications of current and future electrolysers, improved or new components based on selected materials and new surface designs with enhanced surface area (e.g., metasurface) are required. Looking into the feedstock materials used, potential feedstock material have although not been used, but there is no reason why they cannot be used.

There is also a need to develop a method or protocol in the field of materials used in all electrolysis types leading to the development of green hydrogen production informatics, for materials discovery. This should include electrolyser material data gathered from open access followed by data classification (i.e., numerical, categorical, time-series, text). Creating machine learning (ML) predictive tool is also important to analyse the sensitivity of the electrolyser performance with respect to materials, manufacturing, and electrolyser types. This can provide best possible combinations of potential candidate materials before experimental testing. This could be carried out by developing an algorithm that can read the data, create dependent and independent data sets based on associated features, splitting the data in training, and testing sets, training the model using the algorithm, evaluating the classifier, and choosing the classifier with the most accuracy. One can then investigate the relationship between materials and information by applying combinatorial chemistry, material property, manufacturing, structure-property relations, materials data management and product life management, leading to meta data generation to create value chain at each data points for future generation electrolysers. It is also crucial to optimise materials with good performance, low cost, and physical and chemical stability, including the need of rigorous modelling and simu-

lations to understand the principle of functional layers for enhanced hydrogen production by splitting water.

## Acknowledgements

The authors (NF, AP, MH, QC, BAH) acknowledges high temperature steam electrolysis related funding by the UKRI EPSRC via Grants No. EP/W033178/1 (METASIS). Authors (NF, AP, MH) acknowledges thermochemical electrolysis related funding by UK National Nuclear Laboratory (NNL) via gamechanger Grant No. GC 596 (THERMOSIS). Also, the author (BAH) acknowledge the funding support provided by the Leverhulme Trust Research Fellowship (LTRF2021\17131) related to redox hydrothermal reactor for production of green hydrogen. Additionally, the author (SG) acknowledge the funding support provided by the UKRI via Grants No. EP/S036180/1, EP/T001100/1 and EP/T024607/1, feasibility study award to LSBU from the UKRI National Interdisciplinary Circular Economy Hub (EP/V029746/1) and Transforming the Foundation Industries: a Network+ (EP/V026402/1), the Hubert Curien Partnership award 2022 from the British Council, Transforming the Partnership award from the Royal Academy of Engineering (TSP1332) and the Newton Fellowship award from the Royal Society (NIF\R1\191571).

## Conflict of Interest

The authors declare that they have no known competing financial interests or personal relationships that could have appeared to influence the work reported in this paper.

## Data Availability Statement

The data that support the findings of this study are available from the corresponding author upon reasonable request.

**Keywords:** catalysts · electrolyser · hydrogen production · renewable energy · thermal spray

- [1] Global Market Insights, Hydrogen Generation Market to hit \$160 billion by 2026, Says Global Market Insights, Inc. <https://www.globenewswire.com/en/news-release/2020/04/01/2009765/0/en/Hydrogen-Generation-Market-to-hit-160-billion-by-2026-Says-Global-Market-Insights-Inc.html> (accessed July 2021).
- [2] S. Z. Zhiznin, V. M. Timokhov, A. L. Gusev, *Int. J. Hydrogen Energy* **2020**, *45*(56), 31353–31366. <https://doi.org/10.1016/j.ijhydene.2020.08.260>.
- [3] IEA, Global electrolysis capacity becoming operational annually, 2014–2023, historical and announced, IEA, Paris <https://www.iea.org/data-and-statistics/charts/global-electrolysis-capacity-becoming-operational-annually-2014-2023-historical-and-announced> (accessed 10 July 2021).
- [4] IEA, Hydrogen, Paris, 2021. <https://www.iea.org/reports/hydrogen>.
- [5] S. Kiemel, T. Smolinka, F. Lehner, J. Full, A. Sauer, R. Mieke, *Int. J. Energy Res.* **2021**, *45*, 9914–9935. <https://doi.org/10.1002/er.6487>.
- [6] W. Qing, F. Liu, H. Yao, S. Sun, C. Chen, W. Zhang, *Adv. Colloid Interface Sci.* **2020**, *282*, 102207. <https://doi.org/10.1016/j.cis.2020.102207>.
- [7] A. Fardan, C. C. Berndt, R. Ahmed, *Surf. Coat. Technol.* **2021**, *409*, 126835. <https://doi.org/10.1016/j.surfcoat.2021.126835>.

- [8] R. Ahmed, O. Ali, C. C. Berndt, A. Fardan, *J. Therm. Spray Technol.* **2021**, *30*, 800–861. <https://doi.org/10.1007/s11666-021-01185-z>.
- [9] N. P. Padture, M. Gell, E. H. Jordan, *Science* **2002**, *296*, 280–284. <https://www.science.org/doi/10.1126/science.1068609>.
- [10] F. J. Hermanek, *Thermal spray terminology and company origins*, 1st ed.; ASM International: Materials Park, OH, USA, 5–11, **2001**.
- [11] P. L. Fauchais, J. V. R. Heberlein, M. I. Boulos, *Thermal Spray Fundamentals*, Springer, New York, USA **2014**. <https://doi.org/10.1007/978-0-387-68991-3>.
- [12] S. Kamnis, S. Gu, T. J. Lu, C. Chen, *Comput. Mater. Sci.* **2009**, *46*, 1038–1043. <https://doi.org/10.1016/j.commatsci.2009.05.009>.
- [13] E. Sadeghi, N. Markocsan, S. Joshi, *J. Therm. Spray Technol.* **2019**, *28*, 1749–1788. <https://doi.org/10.1007/s11666-019-00938-1>.
- [14] M. Oksa, E. Turunen, T. Suhonen, T. Varis, S.-P. Hannula, *Coating* **2011**, *1*, 17–52. <https://doi.org/10.3390/coatings1010017>.
- [15] A. S. M. Ang, C. C. Berndt, *Int. Mater. Rev.* **2014**, *59*, 179–223. <https://doi.org/10.1179/1743280414Y.0000000029>.
- [16] J. Karthikeyan, C. C. Berndt, S. Reddy, J.-Y. Wang, A. H. King, H. Herman, *J. Am. Ceram. Soc.* **2005**, *81*, 121–128. <https://doi.org/10.1111/j.1151-2916.1998.tb02303.x>.
- [17] V. Fournier, A. Quet, E. Meillot, H. Ageorges, *Surf. Coat. Technol.* **2021**, *406*, 126744. <https://doi.org/10.1016/j.surfcoat.2020.126744>.
- [18] L. Pawlowski, *Surf. Coat. Technol.* **2009**, *203*, 2807–2829. <https://doi.org/10.1016/j.surfcoat.2009.03.005>.
- [19] S. V. Joshi, G. Sivakumar, *J. Therm. Spray Technol.* **2015**, *24*, 1166–1186. <https://doi.org/10.1007/s11666-015-0262-y>.
- [20] S. Joshi, N. Markocsan, P. Nylén, G. Sivakumar, in *Handbook of Advanced Ceramics and Composites* (Eds: Y. Mahajan, J. Roy), Springer, Cham. **2020**, 1–42. [https://doi.org/10.1007/978-3-319-73255-8\\_48-1](https://doi.org/10.1007/978-3-319-73255-8_48-1).
- [21] P. Fauchais, A. Joulia, S. Goutier, C. Chazelas, M. Vardelle, A. Vardelle, S. Rossignol, *J. Phys. D* **2013**, *46*, 224015. <https://doi.org/10.1088/0022-3727/46/22/224015>.
- [22] N. P. Padture, K. W. Schlichting, T. Bhatia, A. Ozturk, B. Cetegen, E. H. Jordan, M. Gell, S. Jiang, T. D. Xiao, P. R. Strutt, E. Garcia, P. Miranzo, M. I. Osendi, *Acta Mater.* **2001**, *49*, 2251–2257. [https://doi.org/10.1016/S1359-6454\(01\)00130-6](https://doi.org/10.1016/S1359-6454(01)00130-6).
- [23] G. Bolelli, B. Bonferroni, V. Cannillo, R. Gadow, A. Killinger, L. Lusvarghi, J. Rauch, N. Stiegler, *Surf. Coat. Technol.* **2010**, *204*, 2657–2668. <https://doi.org/10.1016/j.surfcoat.2010.02.018>.
- [24] S. Björklund, S. Goel, S. Joshi, *Mater. Des.* **2018**, *142*, 56–65. <https://doi.org/10.1016/j.matdes.2018.01.002>.
- [25] S. Sampath, *J. Therm. Spray Technol.* **2010**, *19*, 921–949. <https://doi.org/10.1007/s11666-010-9475-2>.
- [26] N. H. Faisal, N. Sellami, F. Venturi, T. Hussain, T. Mallick, F. Muhammad-Sukki, A. Bishop, H. Upadhyaya, N. K. Katiyar, S. Goel, *Emergent Mater.* **2021**, *4*, 1619–1633. <https://link.springer.com/article/10.1007/s42247-021-00252-z>.
- [27] N. H. Faisal, R. Ahmed, S. P. Katikaneni, S. Souentie, M. F. A. Goosen, *J. Therm. Spray Technol.* **2015**, *24*, 1415–1428. <https://doi.org/10.1007/s11666-015-0315-2>.
- [28] M. D. Falco, G. Santoro, M. Capocelli, G. Caputo, A. Giaconia, *Int. J. Hydrogen Energy* **2021**, *46*, 10682–10696. <https://doi.org/10.1016/j.ijhydene.2020.12.172>.
- [29] J. Yates, R. Daiyan, R. Patterson, R. Egan, R. Amal, A. Ho-Baille, N. L. Chang, *Cell Rep. Phys. Sci.* **2020**, *1*, 100209. <https://doi.org/10.1016/j.xcrp.2020.100209>.
- [30] S. Ounnas, **2020**. Hydrogen Storage and Transportation. <https://www.subseauk.com/documents/documents2019/8%20-%20soffiane%20ounnas%20-%20xodus%20group.pdf> [accessed July 2021].
- [31] The Hydrogen Council. (2021). Hydrogen decarbonization pathways. January. [https://hydrogencouncil.com/wp-content/uploads/2021/01/Hydrogen-Council-Report\\_Decarbonization-Pathways\\_Executive-Summary.pdf](https://hydrogencouncil.com/wp-content/uploads/2021/01/Hydrogen-Council-Report_Decarbonization-Pathways_Executive-Summary.pdf).
- [32] Global Hydrogen Review, **2021**. <https://doi.org/10.1787/39351842-en>.
- [33] Element Energy Ltd, Hydrogen supply chain evidence base. Prepared by Element Energy Ltd for the Department for Business, Energy & Industrial Strategy. November **2018**.
- [34] S. Wang, A. Lu, C. J. Zhong, *Nano Convergence* **2021**, *8*, 4. <https://doi.org/10.1186/s40580-021-00254-x>.
- [35] A. Buttler, H. Spliethoff, *Renewable Sustainable Energy Rev.* **2018**, *82*, 2440–2454. <https://doi.org/10.1016/j.rser.2017.09.003>.
- [36] N. Tenhumberg, K. Bükler, *Chem. Ing. Tech.* **2020**, *92*, 1586–1595. <https://doi.org/10.1002/cite.202000090>.
- [37] H. A. Miller, K. Bouzek, J. Hnat, S. Loos, C. I. Bernäcker, T. Weißgärber, L. Röntzsch, J. Meier-Haack, *Sustain. Energy Fuels* **2020**, *4*, 2114–2133. <https://doi.org/10.1039/C9SE01240K>.
- [38] C. Santoro, A. Lavacchi, P. Mustarelli, V. D. Noto, L. Elbaz, D. R. Dekel, F. Frédéric Jaouen, *ChemSusChem* **2022**, e202200027. <https://doi.org/10.1002/cssc.202200027>.
- [39] J. D. Holladay, J. Hu, D. L. King, Y. Wang, *Catal. Today* **2009**, *139*, 244–260. <https://doi.org/10.1016/j.cattod.2008.08.039>.
- [40] S. S. Kumar, V. Himabindu, *Mater. Sci. Energy Technol.* **2019**, *2*, 442–454. <https://doi.org/10.1016/j.mset.2019.03.002>.
- [41] J. R. Varcoe, P. Atanassov, D. R. Dekel, A. M. Herring, M. A. Hickner, P. A. Kohl, A. R. Kucernak, W. E. Mustain, K. Nijmeijer, K. Scott, T. Xu, L. Zhuang, *Energy Environ. Sci.* **2014**, *7*, 3135–3191. <https://doi.org/10.1039/C4EE01303D>.
- [42] K. Zeng, D. Zhang, *Prog. Energy Combust. Sci.* **2010**, *36*, 307–326. <https://doi.org/10.1016/j.pecs.2009.11.002>.
- [43] I. Dincer, A. A. AlZahrani, in *Comprehensive Energy Systems*, Vol. 4 (Eds: I. Dincer), Elsevier **2018**, Ch. 4.25. <https://doi.org/10.1016/B978-0-12-809597-3.00442-9>.
- [44] Q. Cai, E. Luna-Ortiz, C. S. Adjiman, N. P. Brandon, *Fuel Cells* **2010**, *10*, 1114–1128. <https://doi.org/10.1002/face.200900211>.
- [45] M. A. Laguna-Bercero, *J. Power Sources* **2012**, *203*, 4–16. <https://doi.org/10.1016/j.jpowsour.2011.12.019>.
- [46] G. F. Naterer, S. Suppiah, M. A. Rosen, K. Gabriel, I. Dincer, O. Jianu, Z. Wang, E. B. Easton, B. M. Ikeda, G. Rizvi, I. Pioro, K. Pope, J. Mostaghimi, S. Lvov, Corpus ID: 201031462, **2019**. <https://research.library.mun.ca/13441/1/2015-IJHEB.pdf>.
- [47] X. L. Yan, R. Hino, *Nuclear Hydrogen Production Handbook*, CRC Press **2019**. <https://doi.org/10.1201/b10789>.
- [48] Solar thermochemical production of hydrogen—a review, A. Steinfeld, *Sol. Energy* **2005**, *78*, 603–615. <https://doi.org/10.1016/j.solener.2003.12.012>.
- [49] E. F. James, *Int. J. Hydrogen Energy* **2001**, *26*, 185–190. [https://doi.org/10.1016/S0360-3199\(00\)00062-8](https://doi.org/10.1016/S0360-3199(00)00062-8).
- [50] S. Z. Baykara, *Int. J. Hydrogen Energy* **2004**, *29*, 1451–1458. <https://doi.org/10.1016/j.ijhydene.2004.02.014>.
- [51] J. M. Norbeck, J. W. Heffel, T. D. Durbin, B. Tabbara, J. M. Bowden, M. C. Montani, Hydrogen fuel for surface transportation, Society of Automotive Engineers Inc., Warrendale, PA, **1996**, 548. <http://worldcat.org/isbn/1560916842>.
- [52] J. Xie, X. Wang, A. Li, F. Li, Y. Zhou, *Corros. Sci.* **2012**, *60*, 129–135. <https://doi.org/10.1016/j.corsci.2012.03.047>.
- [53] D. Wu, F. Mao, S. Wang, Z. Zhou, *J. Ceram. Process. Res.* **2013**, *14*, 677–681. <http://jcp.r.kbs-lab.co.kr/journal/download/pdf/1481>.
- [54] J. Sure, A. Shankar, S. Ramya, U. Mudali, *Ceram. Int.* **2012**, *38*, 2803–2812. <https://doi.org/10.1016/j.ceramint.2011.11.051>.
- [55] A. R. Kamali, D. J. Fray, *Carbon* **2013**, *56*, 121–131. <https://doi.org/10.1016/j.carbon.2012.12.076>.
- [56] K. Vignarooban, P. Pugazhendi, C. Tucker, D. Gervasio, A. Kannan, *Sol. Energy* **2014**, *103*, 62–69. <https://doi.org/10.1016/j.solener.2014.02.002>.
- [57] R. Sellers, W. Cheng, M. Anderson, K. Sridharan, C. Wang, T. Allen, Proceedings of ICAPP'12 (International Congress on Advances in Nuclear Power Plants), Paper 12189. Chicago: USA **2012**. <https://www.osti.gov/biblio/22107748-materials-corrosion-molten-lif-naf-kf-eutectic-salt-under-different-reduction-oxidation-conditions>.
- [58] E. Siantar, Study of the effect of molten CuCl immersion test on alloys with high Ni-content with and without surface coatings, Department of Automotive, Mechanical and Manufacturing Engineering, Master's Thesis, UOIT, Canada, **2012**. <https://ir.library.ontariotechu.ca/handle/10155/232>.
- [59] J. E. O'Brien, C. M. Stoots, J. S. Herring, M. G. McKellar, E. A. Harvego, M. S. Sohal, K. G. Condie, High temperature electrolysis for hydrogen production from nuclear energy – technology summary, U. S. Department of Energy National Laboratory, Idaho National Laboratory, INL/EXT-09-16140, **2010**. <https://indigitallibrary.inl.gov/sites/sti/sti/4480292.pdf>.
- [60] M. Roeb, M. Neises, N. Monnerie, F. Call, H. Simon, C. Sattler, M. Schmücker, R. Pitz-Paal, *Materials* **2012**, *5*, 2015–2054. <https://doi.org/10.3390/ma5112015>.
- [61] G. F. Naterer, I. Dincer, C. Zamfirescu, *Hydrogen Production from Nuclear Energy*, Vol. 8, Springer, London, **2013**. <https://www.springer.com/gp/book/9781447149378>.
- [62] D. Yadav, R. Banerjee, *Renewable Sustainable Energy Rev.* **2016**, *54*, 497–532. <https://doi.org/10.1016/j.rser.2015.10.026>.



- [63] G. F. Naterer, S. Suppiah, M. A. Rosen, K. Gabriel, I. Dincer, O. A. Jianu, Z. Wang, E. B. Easton, B. M. Ikeda, G. Rizvi, I. Pioro, K. Pope, J. Mostaghimi, S. N. Lvov, *Int. J. Hydrogen Energy* **2017**, *42*, 15708–15723. <https://doi.org/10.1016/j.ijhydene.2017.03.133>.
- [64] Z. Ping, W. Laijun, C. Songzhe, X. Jingming, *Renewable Sustainable Energy Rev.* **2018**, *81*, 1802–1812. <https://doi.org/10.1016/j.rser.2017.05.275>.
- [65] R. H. Carty, M. Mazumder, J. D. Schreider, J. B. Panborn, Thermochemical hydrogen production, Volume 1, Program summary. Final report Jan 1972–Dec 1980. United States. <https://www.osti.gov/biblio/6508184-thermochemical-hydrogen-production-volume-program-summary-final-report-jan-dec>.
- [66] K. F. Knoche, P. Schuster, T. Ritterbex, *Int. J. Hydrogen Energy* **1984**, *9*, 473–482. [https://doi.org/10.1016/0360-3199\(84\)90099-5](https://doi.org/10.1016/0360-3199(84)90099-5).
- [67] A. Farsi, I. Dincer, G. F. Naterer, *J. Cleaner Prod.* **2020**, *276*, 123833. <https://doi.org/10.1016/j.jclepro.2020.123833>.
- [68] L. Furatian, M. Mohseni, *J. Photochem. Photobiol. A* **2018**, *356*, 364–369. <https://doi.org/10.1016/j.jphtchem.2017.12.030>.
- [69] M. Penconi, F. Rossi, F. Ortica, F. Elisei, P. L. Gentili, *Sustainability* **2015**, *7*, 9310–9325. <https://doi.org/10.3390/su7079310>.
- [70] Y. Moriya, T. Takata, K. Domen, *Coord. Chem. Rev.* **2013**, *257*, 1957–1969. <https://doi.org/10.1016/j.ccr.2013.01.021>.
- [71] F. L. Toma, L. M. Berger, I. Shakhverdova, B. Leupolt, A. Potthoff, K. Oelschlägel, T. Meissner, J. A. I. Gomez, Y. Miguel, *J. Therm. Spray Technol.* **2014**, *23*, 1037–1053. <https://doi.org/10.1007/s11666-014-0090-5>.
- [72] A. Fujishima, K. Honda, *Nature* **1972**, *238*, 37–38. <https://www.nature.com/articles/238037a0>.
- [73] Y. Liu, J. Huang, X. Feng, H. Li, *J. Therm. Spray Technol.* **2021**, *30*, 1–24. <https://doi.org/10.1007/s11666-020-01118-2>.
- [74] C. A. Castro, A. Jurado, D. Sissa, S. A. Giraldo, *Int. J. Photoenergy* **2012**, article ID 261045. <https://doi.org/10.1155/2012/261045>.
- [75] A. Fujishima, T. N. Rao, D. A. Tryk, *J. Photochem. Photobiol. C* **2000**, *1*, 1–21. [https://doi.org/10.1016/S1389-5567\(00\)00002-2](https://doi.org/10.1016/S1389-5567(00)00002-2).
- [76] K. Hashimoto, H. Irie, A. Fujishima, *Jpn. J. Appl. Phys.* **2005**, *44*, 8269–8285. <https://iopscience.iop.org/article/10.1143/JJAP.44.8269>.
- [77] K. Nakata, A. Fujishima, *J. Photochem. Photobiol. C* **2012**, *13*, 169–189. <https://doi.org/10.1016/j.jphtchem.2012.06.001>.
- [78] M. G. Walter, E. L. Warren, J. R. McKone, S. W. Boettcher, Q. Mi, E. A. Santori, N. S. Lewis, *Chem. Rev.* **2010**, *110*, 6446–6473. <https://doi.org/10.1021/cr1002326>.
- [79] V. Etacheri, C. D. Valentin, J. Schneider, D. Bahnemann, S. C. Pillai, *J. Photochem. Photobiol. C* **2015**, *25*, 1–29. <https://doi.org/10.1016/j.jphtchem.2015.08.003>.
- [80] A. H. Navidpour, Y. Kalantari, M. Salehi, H. R. Salimijazi, M. Amirnasr, M. Rismanchian, M. A. Siahkali, *J. Therm. Spray Technol.* **2017**, *26*, 717–727. <https://doi.org/10.1007/s11666-017-0541-x>.
- [81] C. H. Liao, C. W. Huang, J. C. S. Wu, *Catalysts* **2012**, *2*, 490–516. <https://doi.org/10.3390/catal2040490>.
- [82] M. Huynh, T. Ozel, C. Liu, E. C. Lau, D. G. Nocera, *Chem. Sci.* **2017**, *8*, 4779–4794. <https://doi.org/10.1039/C7SC01239J>.
- [83] C. Hu, L. Zhang, J. Gong, *Energy Environ. Sci.* **2019**, *12*, 2620–2645. <https://doi.org/10.1039/C9EE01202H>.
- [84] J. Song, C. Wei, Z.-F. Huang, C. Liu, L. Zeng, X. Wang, Z. J. Xu, *Chem. Soc. Rev.* **2020**, *49*, 2196–2214. <https://doi.org/10.1039/C9CS00607A>.
- [85] A. I. Osman, N. Mehta, A. M. Elgarayh, M. Hefny, A. Al-Hinai, A. H. Al-Muhtaseb, D. W. Rooney, *Environ. Chem. Lett.* **2021**, *20*, 153–188. <https://doi.org/10.1007/s10311-021-01322-8>.
- [86] V. Viswanathan, N. K. Katiyar, G. Goel, A. Matthews, S. Goel, *Emergent Mater.* **2021**, *4*, 1515–1529. <https://doi.org/10.1007/s42247-021-00307-1>.
- [87] UK hydrogen strategy, **2021**, In Chemistry and Industry (London) (Vol. 85, Issue 9). [https://doi.org/10.1002/cind.859\\_6.x](https://doi.org/10.1002/cind.859_6.x).
- [88] 14040:2006, I. (n.d.). Environmental management – Life cycle assessment – Principles and framework. <https://www.iso.org/obp/ui/#iso:std:iso:14040:ed-2:v1:en>.
- [89] 14044:2006, I. (n.d.). Environmental management – Life cycle assessment – Principles and framework. <https://www.iso.org/obp/ui/#iso:std:iso:14044:ed-1:v1:en>.
- [90] S. H. Farjana, M. A. P. Mahmud, N. Huda, in *Life Cycle Assessment for Sustainable Mining* (Eds: S. H. Farjana, M. A. P. Mahmud, N. Huda), Elsevier **2021**, Ch. 1. <https://doi.org/https://doi.org/10.1016/B978-0-323-85451-1.00001-9>.
- [91] P. L. Spath, M. K. Mann, Life cycle assessment of renewable hydrogen production via wind/electrolysis, National Renewable Energy Laboratory, NREL/MP-560-35404, February, 1–13, **2004**. <https://www.nrel.gov/docs/fy04osti/35404.pdf>.
- [92] E. Cetinkaya, I. Dincer, G. F. Naterer, *Int. J. Hydrogen Energy* **2012**, *37*, 2071–2080. <https://doi.org/10.1016/j.ijhydene.2011.10.064>.
- [93] R. Bhandari, C. A. Trudewind, P. Zapp, *J. Cleaner Prod.* **2014**, *85*, 151–163. <https://doi.org/10.1016/j.jclepro.2013.07.048>.
- [94] V. Utgikar, T. Thiesen, *Int. J. Hydrogen Energy* **2006**, *31*, 939–944. <https://doi.org/10.1016/j.ijhydene.2005.07.001>.
- [95] A. Ozbilen, I. Dincer, M. A. Rosen, *J. Cleaner Prod.* **2012**, *33*, 202–216. <https://doi.org/10.1016/j.jclepro.2012.03.035>.
- [96] P. Lettenmeier, A. S. Gago, K. A. Friedrich, Protective coatings for low-cost bipolar plates and current collectors for proton exchange membrane electrolyzers for large scale energy storage from renewables, New Technologies in Protective Coatings, Carlos Giudice and Guadalupe Canosa, IntechOpen, (2017) DOI: 10.5772/intechopen.68528. Available from: <https://www.intechopen.com/books/new-technologies-in-protective-coatings/protective-coatings-for-low-cost-bipolar-plates-and-current-collectors-of-proton-exchange-membrane-e>.
- [97] A. S. Gago, S. A. Ansar, B. Saruhan, U. Schulz, P. Lettenmeier, N. A. Cañas, P. Gazdzicki, T. Morawietz, R. Hiesgen, J. Arnold, K. A. Friedrich, *J. Power Sources* **2016**, *307*, 815–825. <https://doi.org/10.1016/j.jpowsour.2015.12.071>.
- [98] P. Lettenmeier, R. Wang, R. Abouatallah, B. Saruhan, O. Freitag, P. Gazdzicki, T. Morawietz, R. Hiesgen, A. S. Gago, K. A. Friedrich, *Sci. Rep.* **2017**, *7*, 44035. <https://doi.org/10.1038/srep44035>.
- [99] L. Wang, T. Weissbach, R. Reissner, A. Ansar, A. S. Gago, S. Holdcroft, K. A. Friedrich, *ACS Appl. Energy Mater.* **2019**, *2*(11) 7903–7912. <https://doi.org/10.1021/acsaem.9b01392>.
- [100] F. Razmjooei, T. Morawietz, E. Taghizadeh, E. Hadjixenophontos, L. Mues, M. Gerle, B. D. Wood, C. Harms, A. S. Gago, S. A. Ansar, K. A. Friedrich, *Joule* **2021**, *5*, 1776–1799. <https://doi.org/10.1016/j.joule.2021.05.006>.
- [101] T. G. Coker, S. D. Argade, US4049841 A, **1977**. <https://patents.google.com/patent/US4049841A/en>.
- [102] D. E. Hall, *J. Appl. Electrochem.* **1984**, *14*, 107–115. <https://doi.org/10.1007/BF00611266>.
- [103] R. Henne, W. Schnurnberger, W. Weber, *Thin Solid Films* **1984**, *119*, 141–152. [https://doi.org/10.1016/0040-6090\(84\)90529-7](https://doi.org/10.1016/0040-6090(84)90529-7).
- [104] G. Schiller, V. Borck, *Int. J. Hydrogen Energy* **1992**, *17*, 261–273. [https://doi.org/10.1016/0360-3199\(92\)90001-D](https://doi.org/10.1016/0360-3199(92)90001-D).
- [105] G. Schiller, R. Henne, V. Borck, *J. Therm. Spray Technol.* **1995**, *4*, 185–194. <https://doi.org/10.1007/BF02646111>.
- [106] D. Mioussé, A. Lasia, V. Borck, *J. Appl. Electrochem.* **1995**, *25*, 592–602. <https://doi.org/10.1007/BF00573217>.
- [107] J. Fournier, D. Mioussé, J.-G. Legoux, *Int. J. Hydrogen Energy* **1999**, *24*, 519–528. [https://doi.org/10.1016/S0360-3199\(98\)00101-3](https://doi.org/10.1016/S0360-3199(98)00101-3).
- [108] E. Irissou, M. Blouin, L. Roué, J. Huot, R. Schulz, D. Guay, *J. Alloys Compd.* **2002**, *345*, 228–237. [https://doi.org/10.1016/S0925-8388\(02\)-00403-6](https://doi.org/10.1016/S0925-8388(02)-00403-6).
- [109] L. Birry, A. Lasia, *J. Appl. Electrochem.* **2004**, *34*, 735–749. <https://doi.org/10.1023/B:JACH.0000031161.26544.6a>.
- [110] A. Kellenberger, N. Vaszilcsin, W. Brandl, N. Duteanu, *Int. J. Hydrogen Energy* **2007**, *32*, 3258–3265. <https://doi.org/10.1016/j.ijhydene.2007.02.028>.
- [111] D. Chade, L. Berlouis, D. Infield, A. Cruden, P. T. Nielsen, T. Mathiesen, *Int. J. Hydrogen Energy* **2013**, *38*, 14380–14390. <https://doi.org/10.1016/j.ijhydene.2013.09.012>.
- [112] M. Aghasibeig, Engineered thermally sprayed electrodes for hydrogen production by alkaline water electrolysis, PhD thesis, Concordia University, **2015**. [https://spectrum.library.concordia.ca/id/eprint/980789/1/Aghasibeig\\_PhD\\_S2016.pdf](https://spectrum.library.concordia.ca/id/eprint/980789/1/Aghasibeig_PhD_S2016.pdf).
- [113] M. Aghasibeig, M. Mousavi, F. B. Ettouill, C. Moreau, R. Wuthrich, A. Dolatabadi, *J. Therm. Spray Technol.* **2014**, *23*, 220–226. <https://doi.org/10.1007/s11666-013-9997-5>.
- [114] M. Aghasibeig, C. Moreau, A. Dolatabadi, R. Wuthrich, *Surf. Coat. Technol.* **2016**, *285*, 68–76. <https://doi.org/10.1016/j.surfcoat.2015.11.025>.
- [115] J.-E. Kim, K.-K. Bae, C.-S. Park, S.-U. Jeong, K.-H. Baik, J.-W. Kim, Y.-H. Kim, K.-S. Kang, K.-B. Lee, *Data Brief* **2018**, *21*, 2059–2062. <https://doi.org/10.1016/j.dib.2018.10.167>.
- [116] J.-E. Kim, K.-K. Bae, C.-S. Park, S.-U. Jeong, K.-H. Baik, J.-W. Kim, K.-S. Kang, K.-B. Lee, Y.-H. Kim, *J. Ind. Eng. Chem.* **2019**, *70*, 160–168. <https://doi.org/10.1016/j.jiec.2018.10.010>.
- [117] R. Hino, H. Aita, K. Sekita, K. Haga, T. Iwata, Study on hydrogen production by high temperature electrolysis of steam, Department of

- Advanced Nuclear Heat Technology, Oarai Research Establishment, Japan Atomic Energy Research Institute, 97–064, 1997. <https://www.osti.gov/etdweb/servlets/purl/562087>.
- [118] A. Ansar, G. Schiller, O. Patz, J. B. Gregoire, Z. Ilhan, in *International Thermal Spray Conference 2008, ITSC*, 190–194, 2008. Verlag für Schweißen und verwandte Verfahren DVS-Verlag GmbH, Düsseldorf, Maastricht, The Netherlands. ISBN 978–3-87155-979-2. <https://core.ac.uk/download/pdf/11136048.pdf>.
- [119] G. Schiller, A. Ansar, M. Lang, O. Patz, *J. Appl. Electrochem.* **2009**, *39*, 293–301. <https://doi.org/10.1007/s10800-008-9672-6>.
- [120] M. Vardavoulias, P. Gkomoza, M. Arkas, D. K. Niakolas, S. G. Neophytides, *Coating* **2021**, *11*(6), 682. <https://doi.org/10.3390/coatings11060682>.
- [121] K. Azarbayjani, G. Rizvi, F. Foroutan, *Int. J. Hydrogen Energy* **2016**, *41*, 8394–8400. <https://doi.org/10.1016/j.ijhydene.2015.10.092>.
- [122] M. S. Azhar, Evaluation of the effects of molten CuCl on corrosion resistant coatings, Master's thesis, University of Ontario Institute of Technology, Canada, 2016. [https://ir.library.utoronto.ca/bitstream/10155/731/1/Azhar\\_Muhammad\\_Shuja.pdf](https://ir.library.utoronto.ca/bitstream/10155/731/1/Azhar_Muhammad_Shuja.pdf).
- [123] R. Dsouza, Investigation of copper deposition on steel in molten copper chloride, Master's thesis, University of Ontario Institute of Technology, Canada, 2018. [https://ir.library.utoronto.ca/bitstream/10155/920/1/Dsouza\\_Rion.pdf](https://ir.library.utoronto.ca/bitstream/10155/920/1/Dsouza_Rion.pdf).
- [124] G. F. Naterer, S. Suppiah, L. Stolberg, M. Lewis, Z. Wang, M. A. Rosen, I. Dincer, K. Gabriel, A. Odukoya, E. Secnik, E. B. Easton, V. Papangelakis, *Int. J. Hydrogen Energy* **2015**, *40*, 6283–6295. <https://doi.org/10.1016/j.ijhydene.2015.02.124>.
- [125] D. Chen, E. H. Jordan, M. Gell, *Surf. Coat. Technol.* **2008**, *202*, 6113–6119. <https://doi.org/10.1016/j.surfcoat.2008.07.017>.
- [126] G. Mauer, A. Guignard, R. Vaßen, *Surf. Coat. Technol.* **2013**, *220*, 40–43. <https://doi.org/10.1016/j.surfcoat.2012.08.042>.
- [127] C. Zhang, U. Chaudhary, S. Das, A. Godavarty, A. Agarwal, *J. Therm. Spray Technol.* **2013**, *22*, 1193–1200. <https://doi.org/10.1007/s11666-013-9964-1>.
- [128] S. Dosta, M. Robotti, S. Garcia-Segura, E. Brillas, I. G. Cano, J. M. Guilemany, *Appl. Catal. B* **2016**, *189*, 151–159. <https://doi.org/10.1016/j.apcatb.2016.02.048>.
- [129] F. Wang, X. Qian, X. Li, J. Ye, Z. Han, Y. Chen, G. Liu, J. Li, *Mater. Lett.* **2015**, *151*, 82–84. <https://doi.org/10.1016/j.matlet.2015.03.030>.
- [130] B. W. Robinson, C. J. Tighe, R. I. Gruar, A. Mills, I. P. Parkin, A. K. Tabecki, H. L. de Villiers Lovelock, J. A. Darr, *J. Mater. Chem. A* **2015**, *3*, 12680–12689. <https://doi.org/10.1039/C4TA05397D>.
- [131] R. Kumar, S. Govindarajan, K. S. K. J. Reddy, T. N. Rao, S. V. Joshi, S. Anandan, *ACS Appl. Mater. Interfaces* **2016**, *8*, 27642–27653. <https://doi.org/10.1021/acsami.6b07000>.
- [132] H. Khatibnezhad, F. Ambriz-Vargas, F. B. Ettouil, C. Moreau, *J. Eur. Ceram. Soc.* **2021**, *41*, 544–556. <https://doi.org/10.1016/j.jeurceramsoc.2020.08.017>.
- [133] R. Dom, G. Sivakumar, N. Y. Hebalkar, S. V. Joshi, P. H. Borse, *RSC Adv.* **2013**, *3*, 15217–15224. <https://doi.org/10.1039/C3RA42051E>.
- [134] J. G. Lee, D.-Y. Kim, J.-H. Lee, M.-W. Kim, S. An, H. S. Jo, C. Nervi, S. S. Al-Deyab, M. T. Swihart, S. S. Yoon, *ACS Appl. Mater. Interfaces* **2016**, *8*, 15406–15414. <https://doi.org/10.1021/acsami.6b03968>.
- [135] J. W. Schultze, M. Lohrengel, *Electrochim. Acta* **2000**, *45*, 2499–2513. [https://doi.org/10.1016/S0013-4686\(00\)00347-9](https://doi.org/10.1016/S0013-4686(00)00347-9).
- [136] P. Basnet, Y. Zhao, *Catal. Sci. Technol.* **2016**, *6*, 2228–2328. <https://doi.org/10.1039/C5CY01464F>.
- [137] C. Haisch, J. Schneider, M. Fleisch, H. Gutzmann, T. Klassenb, D. W. Bahnemann, *Dalton Trans.* **2017**, *46*, 12811–12823. <https://doi.org/10.1039/C7DT02063E>.
- [138] T.-G. Kim, B. Joshi, C.-W. Park, E. Samuel, M.-W. Kim, M. T. Swihart, S. S. Yoon, *J. Alloys Compd.* **2019**, *798*, 35–44. <https://doi.org/10.1016/j.jallcom.2019.05.255>.
- [139] K. Wathanyu, K. Tuchinda, S. Daopiset, S. Sirivisoot, *Surf. Coat. Technol.* **2022**, *445*, 128721. <https://doi.org/10.1016/j.surfcoat.2022.128721>.
- [140] P. Nehe, G. Sivakumar, S. Kumar, *Chem. Eng. J.* **2015**, *277*, 168–175. <https://doi.org/10.1016/j.cej.2015.04.121>.
- [141] F. Ghadami, A. S. R. Aghdam, *Thin Solid Films* **2019**, *678*, 42–52. <https://doi.org/10.1016/j.tsf.2019.02.019>.
- [142] A. R. Govande, A. Chandak, B. R. Sunil, R. Dumpala, *Int. J. Refract. Met. Hard Mater.* **2022**, *103*, 105772. <https://doi.org/10.1016/j.jirmhm.2021.105772>.
- [143] K. Yang, C. Chen, G. Xu, Z. Jiang, S. Zhang, X. Liu, *J. Mater. Res. Technol.* **2022**, *19*, 1906–1921. <https://doi.org/10.1016/j.jmrt.2022.05.181>.
- [144] R. Ghasemi, R. Shoja-Razavi, R. Mozafarinia, H. Jamali, *Ceram. Int.* **2013**, *39*, 9483–9490. <https://doi.org/10.1016/j.ceramint.2013.05.066>.
- [145] D. Wang, Z. Tian, L. Shen, Z. Liu, Y. Huang, *Ceram. Int.* **2014**, *40*, 8791–8799. <https://doi.org/10.1016/j.ceramint.2014.01.101>.
- [146] P.-C. Tsai, J.-H. Lee, C.-L. Chang, *Surf. Coat. Technol.* **2007**, *202*, 719–724. <https://doi.org/10.1016/j.surfcoat.2007.07.005>.
- [147] S. Joshi, P. Nylen, *Technologies* **2019**, *7*, 79. <https://doi.org/10.3390/technologies7040079>.
- [148] A. Milanti, V. Matikainen, H. Koivuluoto, G. Bolelle, L. Lusvardi, P. Vuoristo, *Surf. Coat. Technol.* **2015**, *277*, 81–90. <https://doi.org/10.1016/j.surfcoat.2015.07.018>.
- [149] A. Ganvir, S. Joshi, N. Markocsan, R. Vassen, *Mater. Des.* **2018**, *144*, 192–208. <https://doi.org/10.1016/j.matdes.2018.02.011>.
- [150] A. Ganvir, R. F. Calinas, N. Markocsan, N. Curry, S. Joshi, *J. Eur. Ceram. Soc.* **2019**, *39*, 470–481. <https://doi.org/10.1016/j.jeurceramsoc.2018.09.023>.
- [151] W. Fan, Y. Bai, *Ceram. Int.* **2016**, *42*, 14299–14312. <https://doi.org/10.1016/j.ceramint.2016.06.063>.
- [152] P. Fauchais, G. Montavon, R. S. Lima, B. R. Marple, *J. Phys. D* **2011**, *44*, 093001. <https://iopscience.iop.org/article/10.1088/0022-3727/44/9/093001>.
- [153] P. Fauchais, G. Montavon, *J. Therm. Spray Technol.* **2010**, *19*, 226–239. <https://doi.org/10.1007/s11666-009-9446-7>.
- [154] T. Bhatia, A. Ozturk, L. Xie, E. H. Jordan, B. M. Cetegen, M. Gell, X. Ma, N. P. Padture, *J. Mater. Res.* **2002**, *17*, 2363–2372. <https://doi.org/10.1557/JMR.2002.0346>.
- [155] R. Vaßen, D. Stöver, in *Advances in Ceramic Coatings and Ceramic-Metal Systems: Ceramic Engineering and Science Proceedings* (Eds: D. Zhu, K. Plucknett), John Wiley & Sons, Inc., **2005**, 2–10.
- [156] R. Vaßen, M. O. Jarligo, T. Steinke, D. E. Mack, D. Stöver, *Surf. Coat. Technol.* **2010**, *205*(4), 938–942. <https://doi.org/10.1016/j.surfcoat.2010.08.151>.
- [157] S. Mahade, N. Curry, S. Björklund, N. Markocsan, P. Nylén, *Surf. Coat. Technol.* **2015**, *283*, 329–336. <https://doi.org/10.1016/j.surfcoat.2015.11.009>.
- [158] A. Killinger, P. Müller, R. Gadow, *J. Therm. Spray Technol.* **2015**, *24*, 1130–1142. <https://doi.org/10.1007/s11666-015-0264-9>.
- [159] S. Goel, S. Björklund, N. Curry, U. Wiklund, S. Joshi, *Surf. Coat. Technol.* **2017**, *315*, 80–87. <https://doi.org/10.1016/j.surfcoat.2017.02.025>.
- [160] S. Mahade, K. Narayan, S. Govindarajan, S. Björklund, N. Curry, S. Joshi, *Materials* **2019**, *12*, 2344. <https://doi.org/10.3390/ma12152344>.
- [161] A. Ganvir, S. Björklund, Y. Yao, S. V. S. Vadali, U. Klement, S. Joshi, *Coating* **2019**, *9*, 171. <https://doi.org/10.3390/coatings9030171>.
- [162] R. Tummala, R. K. Guduru, P. S. Mohanty, *Mater. Res. Bull.* **2011**, *46*, 1276–1282. <https://doi.org/10.1016/j.materresbull.2011.03.028>.
- [163] D. Chen, E. H. Jordan, M. W. Renfro, M. Gell, *J. Am. Ceram. Soc.* **2009**, *92*, 268–271. <https://doi.org/10.1111/j.1551-2916.2008.02846.x>.
- [164] V. Viswanathan, R. Filmlalter, S. Patil, S. Deshpande, S. Seal, *J. Am. Ceram. Soc.* **2007**, *90*, 870–877. <https://doi.org/10.1111/j.1551-2916.2006.01463.x>.
- [165] Y. Wang, T. W. Coyle, *J. Fuel Cell Sci. Technol.* **2011**, *8*, 021005. <https://doi.org/10.1115/1.4002583>.
- [166] T. W. Coyle, Y. Wang, in *Thermal Spray 2007: Global Coating Solutions* (Eds: B. R. Marple, M. M. Hyland, Y.-C. Lau, C.-J. Li, R. S. Lima, G. Montavon), ASM International, Materials Park, Ohio, USA, **2007**, 699–704.
- [167] E. Garcia, Z. B. Zhang, T. W. Coyle, S. E. Hao, S. L. Mu, in *Thermal Spray 2007: Global Coating Solutions* (Eds: B. R. Marple, M. M. Hyland, Y.-C. Lau, C.-J. Li, R. S. Lima, G. Montavon), ASM International, Materials Park, Ohio, USA, **2007**, 650–654.
- [168] P. S. Mohanty, S. B. C. M. N. Anton, K. R. Guduru, US patent No. US20100323118 A1, **2010**. <https://patents.google.com/patent/US20100323118A1/en>.
- [169] V. Varadaraajan, B. C. Satishkumar, J. Nanda, P. Mohanty, *J. Power Sources* **2011**, *196*, 10704–10711. <https://doi.org/10.1016/j.jpowsour.2011.09.016>.
- [170] W. Duarte, S. Rossignol, M. Vardelle, *J. Therm. Spray Technol.* **2014**, *23*, 1425–1435. <https://doi.org/10.1007/s11666-014-0131-0>.
- [171] Y. Ma, X. Wang, X. You, J. Liu, J. Tian, X. Xu, H. Peng, W. Liu, C. Li, W. Zhou, P. Yuan, X. Chen, *ChemCatChem* **2014**, *6*, 3366–3376. <https://doi.org/10.1002/cctc.201402551>.
- [172] X. Fang, X. Zhang, Y. Guo, M. Chen, W. Liu, X. Xua, H. Peng, Z. Gao, X. Wang, C. Li, *Int. J. Hydrogen Energy* **2016**, *41*, 11141–11153. <https://doi.org/10.1016/j.ijhydene.2016.04.038>.

- [173] D. P. Minh, T. J. Siang, D.-V. N. Vo, T. S. Phan, C. Ridart, A. Nzihou, D. Grouset, in *Hydrogen Supply Chains (Design, Deployment and Operation)* (Eds: C. Azzaro-Pantel), Academic Press, 2018, Ch. 4. <https://doi.org/10.1016/B978-0-12-811197-0.00004-X>.
- [174] Y. Zhang, J. Xu, X. Xu, R. Xi, Y. Liu, X. Fang, *Catal. Today* 2020, 355, 518–528. <https://doi.org/10.1016/j.cattod.2019.06.060>.
- [175] X. Q. Ma, J. Roth, D. W. Gandy, G. J. Frederick, *J. Therm. Spray Technol.* 2006, 15, 670–675. <https://doi.org/10.1361/105996306X147090>.
- [176] M. Bai, H. Maher, Z. Pala, T. Hussain, *J. Eur. Ceram. Soc.* 2018, 38, 1878–1887. <https://doi.org/10.1016/j.jeurceramsoc.2017.10.026>.
- [177] J. Kilakoski, R. Trache, S. Björklund, S. Joshi, P. Vuoristo, *J. Therm. Spray Technol.* 2019, 28, 1933–1944. <https://doi.org/10.1007/s11666-019-00940-7>.
- [178] S. V. Joshi, G. Sivakumar, T. Raghuvveer, R. O. Dusane, *J. Therm. Spray Technol.* 2014, 23, 616–624. <https://doi.org/10.1007/s11666-014-0075-4>.
- [179] V. Testa, S. Morelli, G. Bolelli, L. Lusvardi, S. Björklund, S. Joshi, *Surf. Coat. Technol.* 2021, 425, 127682. <https://doi.org/10.1016/j.surfcoat.2021.127682>.
- [180] S. Mahade, A. Mulone, S. Björklund, U. Klement, S. Joshi, *Appl. Surf. Sci.* 2021, 570, 151227. <https://doi.org/10.1016/j.apsusc.2021.151227>.
- [181] A. Ganvir, A. R. Jahagirdar, A. Mulone, L. Örnfeldt, S. Björklund, U. Klement, S. Joshi, *J. Mater. Process. Technol.* 2021, 295, 117203. <https://doi.org/10.1016/j.jmatprotec.2021.117203>.
- [182] S. Mahade, A. Mulone, S. Björklund, U. Klement, S. Joshi, *J. Mater. Res. Technol.* 2021, 13, 498. <https://doi.org/10.1016/j.jmrt.2021.04.096>.
- [183] S. Mahade, L. Baïamonte, E. Sadeghimeresht, S. Björklund, F. Marra, S. Joshi, *Surf. Coat. Technol.* 2021, 412, 127015. <https://doi.org/10.1016/j.surfcoat.2021.127015>.
- [184] L. Li, P. Wang, Q. Shao, X. Huang, *Chem. Soc. Rev.* 2020, 49, 3072–3106. <https://doi.org/10.1039/D0CS00013B>.
- [185] L. M. Liz-Marzán, *Mater. Today* 2004, 7, 26–31. [https://doi.org/10.1016/S1369-7021\(04\)00080-X](https://doi.org/10.1016/S1369-7021(04)00080-X).
- [186] M. C. Tringides, M. Jalochoowski, E. Bauer, *Phys. Today* 2007, 60, 50–54. <https://doi.org/10.1063/1.2731973>.
- [187] X. Li, L. Liu, X. Ren, J. Gao, Y. Huang, B. Liu, *Sci. Adv.* 2020, 6, eabb6833. <https://www.science.org/doi/10.1126/sciadv.abb6833>.
- [188] T. Löffler, A. Ludwig, J. Rossmesl, W. Schuhmann, *Angew. Chem. Int. Ed.* 2021, 60, 26894–26903. <https://doi.org/10.1002/anie.202109212>.
- [189] N. K. Katiyar, K. Biswas, J.-W. Yeh, S. Sharma, S. C. Tiwary, *Nano Energy* 2021, 88, 106261. <https://doi.org/10.1016/j.nanoen.2021.106261>.
- [190] H. Schäfer, M. Chatenet, *ACS Energy Lett.* 2018, 3, 574–591. <https://doi.org/10.1021/acsenerylett.8b00024>.
- [191] A. Meghwal, A. Anupam, B. S. Murty, C. C. Berndt, R. S. Kottada, A. S. M. Ang, *J. Therm. Spray Technol.* 2020, 29, 857–893. <https://doi.org/10.1007/s11666-020-01047-0>.
- [192] Q. Lu, G. S. Hutchings, W. Yu, Y. Zhou, R. V. Forest, R. Tao, J. Rosen, B. T. Yonemoto, Z. Cao, H. Zheng, J. Q. Xiao, F. Jiao, J. G. Chen, *Nat. Commun.* 2015, 6, 6567. <https://doi.org/10.1038/ncomms7567>.
- [193] H.-J. Qiu, G. Fang, Y. Wen, P. Liu, G. Xie, X. Liu, S. Sun, *J. Mater. Chem. A* 2019, 7, 6499–6506. <https://doi.org/10.1039/C9TA00505F>.
- [194] A. Amiri, R. Shahbazian-Yassar, *J. Mater. Chem. A* 2021, 9, 782–823. <https://doi.org/10.1039/D0TA09578H>.
- [195] M. Fu, X. Ma, K. Zhao, X. Li, D. Su, *iScience* 2021, 24, 102177. <https://doi.org/10.1016/j.isci.2021.102177>.
- [196] Y. Sun, S. Dai, *Sci. Adv.* 2021, 7(20), eabg1600. <https://www.science.org/doi/10.1126/sciadv.abg1600>.
- [197] H. Zheng, G. Luo, A. Zhang, X. Lu, L. He, *ChemCatChem* 2021, 13, 806–817. <https://doi.org/10.1002/cctc.202001163>.
- [198] Y. Qiu, S. Thomas, M. A. Gibson, H. L. Fraser, N. Birbilis, *npj Mater. Degrad.* 2017, 1, 15. <https://doi.org/10.1038/s41529-017-0009-y>.
- [199] Z.-X. Cai, H. Gouo, Y. Ito, T. Tokunaga, M. Miyauchi, H. Abe, T. Fujita, *Chem. Sci.* 2021, 12, 11306–11315. <https://doi.org/10.1039/D1SC01981C>.
- [200] N. Kumar, C. S. Tiwary, K. Biswas, *J. Mater. Sci.* 2018, 53, 13411–13423. <https://doi.org/10.1007/s10853-018-2485-z>.
- [201] L. Sharma, N. K. Katiyar, A. Parui, R. Das, R. Kumar, C. S. Tiwary, A. K. Singh, A. Halder, K. Biswas, *Nano Res.* 2021, 15, 4799–4806. <https://doi.org/10.1007/s12274-021-3802-4>.
- [202] N. Kumar, K. Biswas, *Rev. Sci. Instrum.* 2015, 86, 083903–083908. <https://doi.org/10.1063/1.4929325>.
- [203] N. K. Katiyar, K. Biswas, C. S. Tiwary, L. D. Machado, R. K. Gupta, *Langmuir* 2019, 35, 2668–2673. <https://doi.org/10.1021/acs.langmuir.8b03401>.
- [204] N. K. Katiyar, K. Biswas, C. S. Tiwary, *Int. Mater. Rev.* 2020, 66, 493–532. <https://doi.org/10.1080/09506608.2020.1825175>.
- [205] Z. Jin, J. Lv, H. Jia, W. Liu, H. Li, Z. Chen, X. Lin, G. Xie, X. Liu, S. Sun, H.-J. Qiu, *Small* 2019, 15, 1904180. <https://doi.org/10.1002/sml.201904180>.
- [206] W. Ma, M. Jarligo, D. E. Mack, D. Pitzer, J. Malzbender, R. Vaßen, D. Stöver, *J. Therm. Spray Technol.* 2008, 17, 831–837. <https://doi.org/10.1007/s11666-008-9239-4>.
- [207] L. Wang, M. H. Habibi, J. I. Eldridge, S. M. Guo, *J. Eur. Ceram. Soc.* 2014, 34, 3941–3949. <https://doi.org/10.1016/j.jeurceramsoc.2014.05.015>.
- [208] Q. L. Li, X. Z. Cui, S. Q. Li, W.-H. Yang, C. Wang, Q. Cao, *J. Therm. Spray Technol.* 2015, 24, 136–143. <https://doi.org/10.1007/s11666-014-0158-2>.
- [209] J. Mefford, X. Rong, A. M. Abakumov, W. G. Hardin, S. Dai, A. M. Kolpak, K. P. Johnston, K. J. Stevenson, *Nat. Commun.* 2016, 7, 11053. <https://doi.org/10.1038/ncomms11053>.
- [210] S. Tasleem, M. Tahir, *Int. J. Hydrogen Energy* 2020, 45, 19078–19111. <https://doi.org/10.1016/j.ijhydene.2020.05.090>.
- [211] E. Vøllestad, R. Strandbakke, M. Tarach, D. Catalán-Martínez, M.-L. Fontaine, D. Beeaff, D. R. Clark, J. M. Serra, T. Norby, *Nat. Mater.* 2019, 18, 752–759. <https://doi.org/10.1038/s41563-019-0388-2>.
- [212] T. Murakami, J. R. Hester, M. Yashima, *J. Am. Chem. Soc.* 2020, 142, 11653–11657. <https://doi.org/10.1021/jacs.0c02403>.
- [213] M. Shiraiwa, T. Kido, K. Fujii, M. Yashima, *J. Mater. Chem. A* 2021, 9, 8607–8619. <https://doi.org/10.1039/D0TA11573H>.
- [214] S. Gopalan, A. V. Virkar, *J. Electrochem. Soc.* 1993, 140, 1060–5. <https://iopscience.iop.org/article/10.1149/1.2056197>.
- [215] W. Wang, D. Medvedev, Z. Shao, *Adv. Funct. Mater.* 2018, 28, 1802592. <https://doi.org/10.1002/adfm.201802592>.
- [216] H. Husin, C. Hung-Ming, S. Wei-Nien, P. Chun-Jern, C. Wei-Tsung, S. Hwo-Shuenn, H. Bing-Joe, *Appl. Catal. B* 2011, 102, 343–351. <https://doi.org/10.1016/j.apcatb.2010.12.024>.
- [217] S. Tailor, N. Vashishtha, A. Modi, S. C. Modi, *J. Therm. Spray Technol.* 2020, 29, 1134–1143. <https://doi.org/10.1007/s11666-020-01033-6>.
- [218] Y. Fukai, *The Metal-Hydrogen System: Basic Bulk Properties*, Springer Berlin, Heidelberg, 2005. <https://link.springer.com/book/10.1007/3-540-28883-X>.
- [219] G. Hachet, A. Metsue, A. Oudriss, X. Feaugas, *Int. J. Plast.* 2020, 129, 102667. <https://doi.org/10.1016/j.ijplas.2020.102667>.
- [220] C. Traisnel, A. Metsue, A. Oudriss, J. Bouhattate, X. Feaugas, *Comput. Mater. Sci.* 2021, 188, 110136. <https://doi.org/10.1016/j.commatsci.2020.110136>.
- [221] Y. Li, S. Rao, A. Hassaine, R. Ramakrishnan, D. Canoy, G. Salimi-Khorshidi, M. Mamouei, T. Lukasiewicz, K. Rahimi, *Sci. Rep.* 2021, 11, 22254. <https://doi.org/10.1038/s41598-021-01680-x>.
- [222] C. H. Park, T.-H. Kim, D. J. Kim, S. Y. Nam, *Int. J. Hydrogen Energy* 2017, 42, 20895–20903. <https://doi.org/10.1016/j.ijhydene.2017.05.146>.
- [223] Z. Rao, C. Zheng, F. Geng, *Comput. Mater. Sci.* 2018, 142, 122–128. <https://doi.org/10.1016/j.commatsci.2017.09.058>.
- [224] H. Kang, S. H. Kwon, R. Lawler, J. H. Lee, G. Doo, H.-T. Kim, S.-D. Yim, S. S. Jang, S. G. Lee, *J. Phys. Chem. C* 2020, 124, 21386. <https://doi.org/10.1021/acs.jpcc.0c03651>.
- [225] B. Gilois, F. Goujon, A. Fleury, A. Soldera, A. Ghoufi, *J. Membr. Sci.* 2020, 602, 117958. <https://doi.org/10.1016/j.memsci.2020.117958>.
- [226] B. Liu, B. Hu, J. Du, D. Cheng, H.-Y. Zang, X. Ge, H. Tan, Y. Wang, X. Duan, Z. Jin, W. Zhang, Y. Li, Z. Su, *Angew. Chem. Int. Ed.* 2021, 60, 6076–6085; *Angew. Chem.* 2021, 133, 6141–6150. <https://doi.org/10.1002/anie.202012079>.
- [227] D. Zhang, Q. Cai, S. Gu, *Electrochim. Acta* 2018, 262, 282–296. <https://doi.org/10.1016/j.electacta.2017.12.189>.
- [228] D. Zhang, Q. Cai, O. O. Taiwo, V. Yufit, N. P. Brandon, S. Gu, *Electrochim. Acta* 2018, 283, 1806–1819. <https://doi.org/10.1016/j.electacta.2018.07.027>.
- [229] D. Q. Liu, Z. Shadik, R. Lin, K. Qian, H. Li, K. K. Li, S. W. Wang, Q. P. Yu, M. Liu, S. Ganapathy, X. Y. Qin, Q.-H. Yang, M. Wagemaker, F. Y. Kang, X.-Q. Yang, B. H. Li, *Adv. Mater.* 2019, 31, 1806620. <https://doi.org/10.1002/adma.201806620>.
- [230] C. W. Wu, W. Zhang, X. Han, Y. X. Zhang, G. J. Ma, *J. Power Sources* 2020, 476, 228724. <https://doi.org/10.1016/j.jpowsour.2020.228724>.
- [231] D. Zhang, A. Forner-Cuenca, O. O. Taiwo, V. Yufit, F. R. Brushett, N. P. Brandon, S. Gu, Q. Cai, *J. Power Sources* 2020, 447, 227249. <https://doi.org/10.1016/j.jpowsour.2019.227249>.
- [232] M. Ishii, S. Kim, *Nucl. Sci. Eng.* 2004, 146, 257–273. <https://doi.org/10.13182/NSE01-69>.



- [233] M. Hossain, S. Z. Islam, P. Pollard, *Renewable Energy* **2013**, *51*, 404–418. <https://doi.org/10.1016/j.renene.2012.10.008>.
- [234] A. C. Olesen, S. H. Frensch, S. K. Kær, *Electrochim. Acta* **2019**, *293*, 476–495. <https://doi.org/10.1016/j.electacta.2018.10.008>.
- [235] S. S. Lafmejani, A. C. Olesen, S. K. Kær, *Int. J. Hydrogen Energy* **2017**, *42*, 16333–16344. <https://doi.org/10.1016/j.ijhydene.2017.05.079>.
- [236] X. Mao, W. Li, Y. Yuan, L. Yang, *Int. J. Hydrogen Energy* **2022**, *47*, 14469–14482. <https://doi.org/10.1016/j.ijhydene.2022.02.221>.
- [237] S. Turek, J. Hron, in *Fluid-Structure Interaction, Lecture Notes in Computational Science and Engineering*, vol 53 (Eds: H. J. Bungartz, M. Schäfer), Springer, Berlin, Heidelberg **2006**, 371–385. [https://doi.org/10.1007/3-540-34596-5\\_15](https://doi.org/10.1007/3-540-34596-5_15).
- [238] S. Xu, S. Timme, *Comput. Fluids* **2017**, *148*, 26–38. <https://doi.org/10.1016/j.compfluid.2017.02.012>.
- [239] M. Raissi, A. Yazdani, G. E. Karniadakis, **2018**, arXiv:1808.04327. <https://doi.org/10.48550/arXiv.1808.04327>.
- [240] C. E. Heaney, Z. Wolffs, J. A. Tómasson, L. Kahouadji, P. Salinas, A. Nicolle, C. C. Pain, *Phys. Fluids* **2022**, *34*, 055111. <https://doi.org/10.1063/5.0088070>.
- [241] Oerlikon Metco Thermal Spray Materials Guide, **2018**. <https://www.oerlikon.com/metco/en/products-services/materials/>.
- [242] N. H. Faisal, R. Ahmed, R. L. Reuben, *Int. Mater. Rev.* **2011**, *56*, 98–142. <https://www.tandfonline.com/doi/full/10.1179/1743280410Y.0000000004>.
- [243] A. Crawford, M. G. Droubi, N. H. Faisal, *J. Nondestruct. Eval.* **2018**, *37*, 33. <https://doi.org/10.1007/s10921-018-0488-y>.
- [244] S. Vanlanduit, M. Sorgente, A. R. Zadeh, A. Güemes, N. Faisal, in *Structural Health Monitoring Damage Detection Systems for Aerospace* (Eds: M. G. R. Sause, E. Jasiūnienė), Springer, Cham, Switzerland **2021**, Ch. 8. [https://doi.org/10.1007/978-3-030-72192-3\\_8](https://doi.org/10.1007/978-3-030-72192-3_8).
- [245] N. H. Faisal, R. Ahmed, A. K. Prathuru, S. P. Katikaneni, M. F. A. Goosen, S. Y. Zhang, *Exp. Mech.* **2018**, *58*, 585–603. <https://link.springer.com/article/10.1007/s11340-017-0298-7>.
- [246] N. H. Faisal, L. Mann, C. Duncan, E. Dunbar, M. Clayton, M. Frost, J. McConnachie, A. Fardan, R. Ahmed, *Surf. Coat. Technol.* **2019**, *357*, 497–514. <https://doi.org/10.1016/j.surfcoat.2018.10.053>.
- [247] N. H. Faisal, R. Ahmed, A. K. Prathuru, A. Paradowska, T. L. Lee, *Exp. Mech.* **2022**, *62*, 369–392. <https://doi.org/10.1007/s11340-021-00803-9>.
- [248] N. Khatri, B. M. Barkachary, B. Muneeswaran, R. Al-Sayegh, X. Luo, S. Goel, *Int. J. Extreme Manuf.* **2020**, *2*, 045102. <https://iopscience.iop.org/article/10.1088/2631-7990/abab4a>.
- [249] R. K. Mishra, S. Goel, H. Y. Nezhad, *Biomaterials and Polymers Horizon* **2022**, *1*, 1–14. <https://doi.org/10.37819/bph.001.01.0132>.
- [250] P. Fan, S. Goel, X. Luo, H. M. Upadhyaya, *Nanomanuf. Metrol.* **2022**, *5*, 39–49. <https://doi.org/10.1007/s41871-021-00109-3>.
- [251] M. Chatenet, B. G. Pollet, D. R. Dekel, F. Dionigi, J. Deseure, P. Millet, R. D. Braatz, M. Z. Bazant, M. Eikerling, I. Staffell, P. Balcombe, Y. Shao-Horn, H. Schäfer, *Chem. Soc. Rev.* **2022**, *51*, 4583–4762. <https://doi.org/10.1039/D0CS01079K>.
- [252] M. A. Khan, H. Zhao, W. Zou, Z. Chen, W. Cao, J. Fang, J. Xu, L. Zhang, J. Zhang, *Electrochem. Energy Rev.* **2018**, *1*, 483–530. <https://doi.org/10.1007/s41918-018-0014-z>.

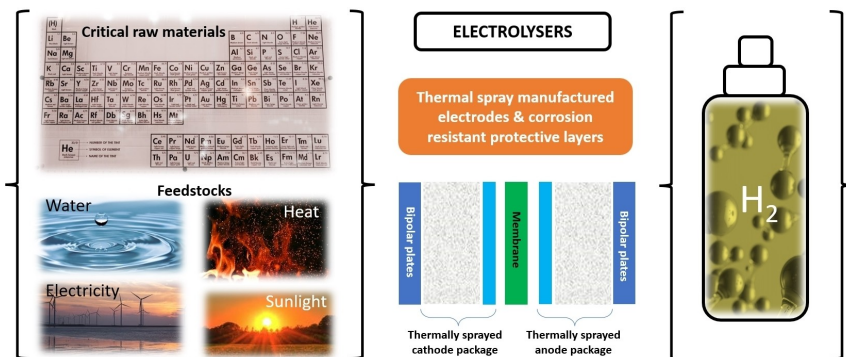
Manuscript received: August 25, 2022

Revised manuscript received: October 13, 2022

Accepted manuscript online: October 14, 2022

Version of record online: ■■■, ■■■■

## REVIEW



This is an extensive review on the application of thermally sprayed coatings with functional properties for electrolyzers. Such coatings are critical and vital constituents (as catalysts

(anode/cathode), solid electrolyte, and transport layer, including corrosion-prone parts such as bipolar plates) of the water splitting electrolysis process for hydrogen production.

Prof. N. H. Faisal\*, Dr. A. Prathuru, Dr. R. Ahmed, V. Rajendran, Prof. M. Hossain, Dr. V. Venkatachalapathy, Dr. N. K. Katiyar, J. Li, Y. Liu, Dr. Q. Cai, Dr. B. A. Horri, Dr. D. Thangana-dar, Dr. G. S. Sodhi, Dr. K. Patchigol-la, Dr. C. Fernandez, Prof. S. Joshi, Dr. S. Govindarajan, Dr. V. Kurushina, Dr. S. Katikaneni, Prof. S. Goel

1 – 54

**Application of Thermal Spray Coatings in Electrolyzers for Hydrogen Production: Advances, Challenges, and Opportunities**